Recursive bit-rate allocation using a convex optimization approach

Aniello Fiengo

ParisTech
INSTITUT DES SCIENCES ET TECHNOLOGIES
PARIS INSTITUTE OF TECHNOLOGY

TELECOM ParisTech

2016-ENST-0066

EDITE – ED 130

Doctorat ParisTech

T H È S E

pour obtenir le grade de docteur délivré par

Télécom ParisTech

Spécialité « Signal et Images »

présentée et soutenue publiquement par

Aniello FIENGO

le 7 novembre 2016

Allocation récursive débit distorsion avec une approche d'optimisation convexe

Recursive bit-rate allocation using a convex optimization approach

Directeur de thèse : **Béatrice PESQUET-POPESCU**
Co-encadrement de la thèse : **Marco CAGNAZZO**

Jury

M. Francois-Xavier COUDOUX, Professeur, Université de Valenciennes, Famars	Présidente
M. Benoit MACQ, Professeur, Université catholique de Louvain, Louvain	Rapporteur
M. Peter SCHELKENS, Professeur, Vrije Universiteit Brussel, Bruxelles	Rapporteur
M. Giovanni CHIERCHIA, Maître de Conférences, Université Paris-Est Marne-la-Vallée, Champs-sur-Marne	Esaminateur

THÈSE

Télécom ParisTech
Grande école de l'Institut Télécom - membre fondateur de ParisTech
46 rue Barrault — 75634 Paris Cedex 13 — Tél. +33 (0)1 45 81 77 77 — www.telecom-paristech.fr

To my family.
To the one who's missing.

Résumé

Introduction

Au cours de la dernière décennie, les progrès de la technologie de la vidéo numérique ont conduit à la création et au développement de nouvelles applications dans la communication vidéo, allant de la vidéoconférence et de la diffusion de contenu télévisuel en définition standard jusqu'à la télévision haute définition (HDTV/UHDTV) et applications pour la très haute qualité, telles que le cinéma numérique/l'imagerie numérique grand écran. Dans ce scénario, l'organisme de normalisation MPEG (Moving Picture Experts Group) sous l'autorité de l'ISO (International Organization for Standardization) et de la CEI (International Electrotechnical Commission), et le VCEG (Video Coding Experts Group) sous la IUT-T (International Telecommunication Union) ont développé des normes de codage vidéo qui répondent aux défis de la transmission de données audiovisuelles et des exigences croissantes pour une représentation efficace de la vidéo. La technologie de codage vidéo a été re-normalisée tous les ans, et la dernière norme de compression vidéo, connue sous le nom de High Efficiency Video Coding (HEVC) [SOHW12a], a été officiellement créée pour remplacer son prédécesseur H.264/MPEG-4 Advanced Video Coding (AVC) en janvier 2015 [WSBL03].

Dans ces normes, un rôle clé dans l'amélioration de la qualité visuelle des vidéos codées sur des canaux à capacité variables est joué par l'allocation de débit, qui est responsable de distribuer efficacement le budget de bits entre les images et les blocs de codage. Plus précisément, il représente une partie importante du module de contrôle de débit d'un codeur vidéo, qui comporte deux étapes: l'attribution de bits (BA), où le budget de bits total est effectivement affecté aux trames et unités de codage, et la sélection de quantification, où le paramètre de quantification (QP) est ajustée en fonction des bits attribués.

Cette thèse se concentre en particulier sur l'allocation de bits de niveau de cadre, dont le but est de parvenir à un compromis optimal entre le taux et la distorsion, sous une contrainte variant dans le temps imposé à l'un de ces variables. La répartition optimale du débit pour la vidéo est un problème non trivial, en raison de la dépendance au niveau du cadre induite par la compensation de mouvement. Pour contourner cette difficulté, on peut allouer le budget de bits indépendamment pour chaque trame, ce qui donne une formulation plus simple qui peut être abordée avec des méthodes numériques

standard, telles que l'optimisation Lagrangienne [SW98a] ou la programmation dynamique [OR98, MGL05, MXOW12a].

Étant donné la nature sous-optimale des approches image par image, un effort de recherche important a été fait au cours de la dernière décennie pour élargir le champ d'optimisation d'un cadre unique à un groupe de cadres (GOP). Une des premières tentatives dans ce sens a été faite par Ramchandran *et al.* [ROV94], qui a utilisé un cadre opérationnel de distorsion-débit pour rechercher la combinaison optimale de paramètres de quantification (QP) pour l'ensemble du GOP: une fois évalué tous les couples $(R_n(Q_1, Q_2, \ldots, Q_i), D_n(Q_1, Q_2, \ldots, Q_i))$ où $\{Q_n, D_n(Q_n), R_n(Q_n)\}$ se référer à la QP, la distorsion et le débit pour la trame n, la méthode effectue une recherche exhaustive du point R-D avec le coût Lagrangien minimum sous une contrainte de débit binaire total. Bien qu'elle ait été conçue pour l'allocation au niveau du cadre, cette méthode a été étendue à différents niveaux de codage, tels que des blocs dans le même cadre [YH00]. Bien que ces méthodes garantissent l'optimalité R-D, elles nécessitent d'évaluer un énorme ensemble de points pour chaque trame, ce qui rend la charge de calcul très élevée.

L'obstacle rencontré par les techniques basées sur la recherche est que le comportement R-D d'une trame résiduelle est inconnue avant le codage des images à partir de laquelle il a été prédit. Une approche possible pour contourner cette difficulté équivaut à estimer la distorsion de tels résidus sur la base de la version encodée de leurs référentiels [LO98, LCGK10, HKZK11]. Bien que l'optimalité n'est pas garantie (en raison de l'inexactitude du modèle), ces méthodes peuvent considérablement diminuer la complexité de calcul et produire des résultats prometteurs.

Dans ce contexte, une approche plus théorique remonte à Uz *et al.* [USC93], qui a proposé un modèle R-D récursif pour décrire la dépendance entre les cadres, et a abordé l'allocation de taux au niveau du cadre à partir d'une perspective lagrangienne. Ce modèle récursif a ensuite été étendu au niveau des pixels pour sélectionner de manière heuristique les paramètres de quantification optimale [VO10]. Plus récemment, une approche similaire a été utilisée pour formuler l'allocation des taux comme un problème d'optimisation non convexe, nécessitant ainsi une séquence d'approximations à résoudre [PAZ+13]; des solutions basées sur le modèle ont également été appliquées pour le filtrage wavelet basé sur le mouvement [ACAB07, CAAB04]. Le principe de l'approche récursive a également été utilisé dans le codage vidéo distribué (DVC) pour analyser la performance R-D des nouveaux schémas pour DVC multi-vues [MPP08].

D'autres travaux visent à minimiser la distorsion maximale des images codées (MINMAX), au lieu de la moyenne habituelle des distorsions (MINAVE), car le critère précédent pourrait conduire à certains avantages à la perception visuelle [HJH99]. Le critère MINMAX peut être optimisé à l'aide de la programmation dynamique [SMK99], des approches multi-passes [XCL06] ou des méthodes itératives ad hoc avec une complexité de codage plus faible [CSR+07]. Cependant, il n'est pas clair si le MINMAX est toujours un meilleur critère que le plus classique.

Les méthodes proposées dans la littérature pour faire face à la répartition des taux de niveau de la trame sont soit de nature théorique [USC93], exigeant computationnellement [ROV94], approximatif [PAZ+13], ou basée sur le critère MINMAX [CSR+07]. Dans cette thèse, nous proposons une solution efficace pour résoudre exactement le problème d'allocation de taux au niveau du cadre formulé avec le critère MINAVE. Notre approche est basée sur un modèle récursif R-D dans lequel la variance d'erreur d'une trame résiduelle est découplée en deux termes: la distorsion de la trame utilisée pour construire la prédiction et l'imprécision de l'estimation de mouvement. Notre méthode a été appliquée à l'encodeur vidéo H.264/AVC ainsi que l'encodeur vidéo HEVC, dans ses versions mono-vue et multi-vues.

Notions de fond

Dans le premier chapitre, nous présentons les concepts de base de la compression d'image et vidéo. D'abord, nous discutons de la nécessité et de la faisabilité de la compression d'image et vidéo, en introduisant la typologie différente de redondance typiquement présente dans un signal vidéo. Le paradigme de transformation est introduit ainsi que les bases du codage prédictif, et des métriques objectives pour l'évaluation de la distorsion sont présentées. Ensuite, nous donnons un résumé de l'évolution des normes de codage vidéo présentant H.264/AVC et expliquant en détail la dernière norme HEVC.

HEVC utilise une structure de codage appelée Coding Tree Unit (CTU) [HMK+10]: une image est divisée en CTU, chaque CTU peut être divisée en quatre Coding Units (CU), et chaque CU peut elle-aussi être divisée en quatre CU, et ainsi de suite jusqu'à arriver à une taille minimale autorisée de CU. Cette structure hiérarchique rend le codage plus adapté au contenu d'image avec la présence de tailles de bloc différentes dans la même image et est limité en définissant une taille de CTU maximale et un niveau de profondeur maximum. Le mode de codage spécifique est choisi au niveau CU entre quatre possibilités: mode Intra, mode Inter, mode Merge et mode Skip.

Chaque CU peut être divisée en Prediction Units (PU), qui sont les éléments élémentaires pour effectuer la prédiction. Le splitting de PU peut être asymétrique afin d'opérer une prédiction plus efficace; la Figure 1 montre les tailles de partition possibles. De plus, chaque CU peut être divisée en plusieurs Transform Units (TU), utilisées pour définir la taille de la transformée et de la quantification à appliquer, et qui sont organisées en une structure à quatre arbres. La taille d'une TU varie entre 4×4 et 32×32; dans le mode Intra, seules les partitions carrées sont disponibles, alors que dans le mode Inter les TU rectangulaires de taille 4×4, 16×4, 8×32 et 32×8 sont possibles.

HEVC soutiennent diverses méthodes de codage prédictif intra: deux modes non directionnels appelés Intra_Planar et Intra_DC et 33 modes directionnels appelés Intra_Angular [LBH+12]. Chaque mode prédit le PU actuel à partir des pixels de la rangée voisine au-dessus et de la colonne à gauche du PU courant. La Figure 2 montre les modes Intra utilisés

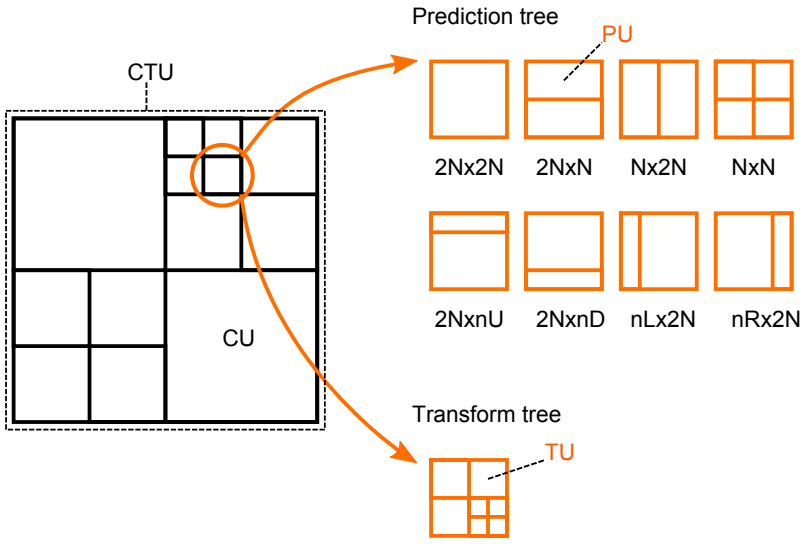

Figure 1: Structure de codage en arbres quaternaires dans HEVC

dans HEVC, ordonnés selon l'angle de direction. Intra_DC utilise une valeur moyenne d'échantillons de référence pour la prédiction, ce qui permet de coder efficacement des zones uniformes de l'image. Intra_Planar utilise une valeur moyenne de deux prédictions linéaires en utilisant quatre échantillons de coin et est conçu pour lisser la texture, ce qui empêche des discontinuités le long des limites de bloc.

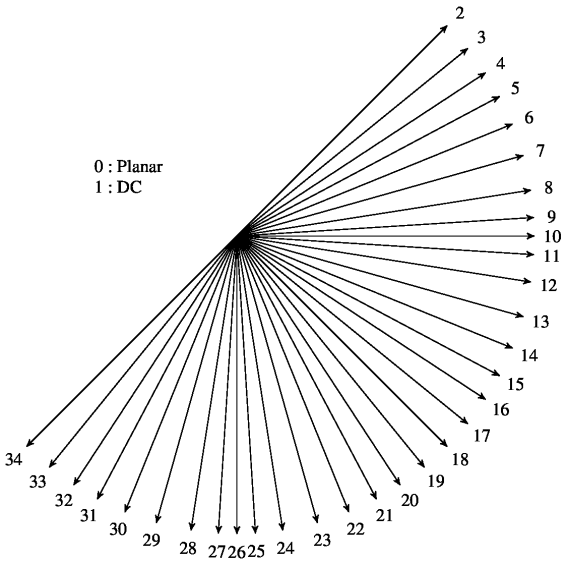

Figure 2: Modes Intra dans HEVC

Afin de réduire le nombre de bits utilisés pour signaler le mode Intra choisi pour la prédiction sur un PU, HEVC introduit l'outil Most Probable Mode (MPM). Si le meilleur mode Intra pour la PU actuelle correspond à l'un des candidats MPM, seuls 2 bits sont utilisés pour la signalisation: un indicateur signale l'utilisation d'un MPM et un second indique quel MPM candidat est utilisé.

Le mode de prédiction Inter évalue et transmet les MVs, tandis que ses deux variantes, Skip et Merge[HOB+12], obtiennent l'information de mouvement à partir de candidats spatiaux ou temporels (bloc voisin, spatialement ou temporellement respectivement), en exécutant des méthodes d'inférence de mouvement. Si un PU est encodé en mode Merge ou Skip, les seules informations transmises sont l'index du candidat sélectionné et, dans le cas du mode Skip, le signal résiduel est également omis.

Le processus de prédiction du MV dans HEVC s'appelle Advanced Motion Vector Prediction (AMVP) [LJPP08]: deux prédicteurs de vecteur de mouvement sont sélectionnés parmi un ensemble candidat de MV des PU couvertes par différentes positions voisines. La Figure 3 montre les 5 candidats spatiaux et 2 temporels. Les premiers candidats spatiaux sont dérivés de A_0 et A_1, un second de B_0, B_1 et B_2. Si les deux candidats sont identiques ou l'un des deux n'est pas disponible, un candidat temporel est dérivé de C_1 et C_2. Entre le MV et le MVP, seul un résiduel est envoyé, ainsi qu'un index indiquant lequel des deux candidats a été sélectionné.

En termes de compensation de mouvement, une précision d'un quart d'échantillon est utilisée pour les MV. L'interpolation des positions d'échantillons fractionnaires est effectuée en utilisant des filtres à base de DCT 7-tap et 8-tap. Similaire à H.264/AVC, le codage unipredictive et bipredictive est soutenu.

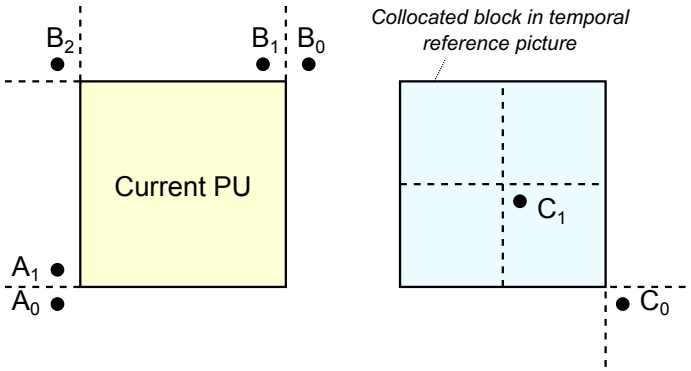

Figure 3: Candidats AMVP dans HEVC

Une extension multi-vues de HEVC, appelée MV-HEVC, a été finalisée en juillet 2014 [H2615], définie pour permettre le codage multi-vue avec des changements minimes à HEVC. Le point clé de l'extension multi-vues est la prédiction entre les vues, où une image dans la vue actuelle peut être prédite à partir de l'image de différentes vues au même instant de temps. Le mécanisme est similaire à la prédiction à compensation de mouvement, mais basé sur des images avec des points de vue différents plutôt que des instants de temps différents: un décalage de disparité basé sur bloc entre la vue courante et la vue de référence est déterminé et utilisé pour effectuer une prédiction compensée par disparité. La disparité est utilisée pour établir une correspondance entre des blocs dans des vues différentes et pour inférer les informations de mouvement d'une vue à une autre. Dans MV-HEVC, la prédiction inter-vue est réalisée d'une manière compatible avec le schème de prédiction

de mouvement de HEVC: la vue de base reconstruite est ajoutée aux listes d'images de référence des vues dépendantes.

Techniques débit-distorsion pour le codage vidéo

L'optimisation débit-distorsion (Rate-Distortion, R-D) est un outil important des encodeurs vidéo qui améliore significativement l'efficacité du codage en optimisant la quantité de distorsion par rapport à la quantité de données requise pour coder la vidéo. Pour assurer l'interopérabilité entre différents produits, dans les normes de codage vidéo, seules la syntaxe de flux de bits et le processus de décodage sont normalisés, mais des techniques d'optimisation débit-distorsion (RDO) ont été utilisées pendant le processus de normalisation afin d'évaluer l'amélioration potentielle de l'efficacité de codage fournie par un outil proposé pour inclusion dans la norme.

Dans le deuxième chapitre, nous introduisons les concepts de base de la théorie débit-distorsion et de la fonction débit-distorsion qui décrivent le compromis entre la quantité de données nécessaires pour coder la vidéo et la qualité obtenue. Ensuite, nous expliquons le concept d'optimisation débit-distorsion et comment les techniques RDO sont utilisées dans les encodeurs vidéo. Enfin, nous donnons quelques détails du module de contrôle de débit de HEVC qui utilise des techniques RDO.

La théorie débit-distorsion [Ber71] est une partie importante de la théorie de l'information, étudiée activement depuis 50 ans. A partir de l'œuvre de Claude Shannon [Sha48, Sha59], la théorie R-D est strictement liée au concept de codage de source ou de compression de source, en abordant le problème de représentation d'une source d'information avec le plus petit des bit possible pour une qualité de reproduction donnée [OR98].

Pour deux variables aléatoires X et Y, l'information mutuelle est définie comme:

$$I(X;Y) = H(X) - H(X|Y) \tag{1}$$

En considérant X comme signal de source, Y comme signal reçu par transmission sur canal et $d(x,y)$ comme fonction de distorsion, la fonction débit-distorsion est définie comme suit:

$$R(D) = \min_{p(y_j|x_j)} I(X;Y) \tag{2}$$

Où $R(D)$ est le taux réalisable à distorsion D. Pour une source donnée, la région débit-distorsion est une fermeture de paires débit-distorsion réalisables (R,D), et la fonction débit-distorsion est définie comme l'infimum de taux tels que, pour une distorsion donnée, le couple est dans la région débit-distorsion de la source.

Une solution analytique à ce problème de minimisation est souvent difficile à obtenir, et des limites supérieures et inférieures à ces fonctions sont utilisées dans des cas pratiques; on sait cependant que la fonction débit-distorsion de n'importe quelle source obéit à

certaines propriétés fondamentales: c'est une fonction convexe continue, monotoniquement décroissante. Selon la théorie de débit-distorsion, il n'existe pas de système de compression qui fonctionne mieux que la fonction R-D: plus un système de compression se rapproche de la borne inférieure, mieux il est performant. Dans de nombreux cas pratiques, le taux est limité par un budget de bits.

Dans le codage vidéo, puisque la quantification réduit le débit du signal compressé en échange d'une certaine distorsion, un problème typique d'optimisation R-D consiste à trouver l'étape de quantification appropriée q pour chaque coefficient de transformation qui minimise une mesure de distorsion D entre les échantillons originales et reconstruits, sous contrainte sur le budget de bits:

$$\min_{q} D(q) \quad \text{subject to} \quad R(q) \leq R_{budget}. \tag{3}$$

Ce problème peut être reformulé à l'aide du multiplicateur Lagrangien $\lambda \geq 0$ qui transforme le problème contraint en un non contraint:

$$\min_{q} J(q), \quad \text{where} \quad J(q) = D(q) + \lambda R(q) \tag{4}$$

où le coût Lagrangien J est minimisé pour une valeur particulière de λ et chacun q obtenu est une solution optimale [SW98a, WSJ$^+$03].

Une fois que nous avons défini la fonction débit-distorsion et introduit certains modèles de distorsion de taux utilisés dans le codage vidéo, nous définissons le problème de l'allocation de bits sous contrainte de budget de bits, concept fondamental d'optimisation débit-distorsion pour les codeurs vidéo. Compte tenu du nombre total de bits disponibles, ou budget, R_{budget}, l'objectif est de répartir le budget de bits entre les différentes unités de codage (macroblocs ou trames) en minimisant une certaine métrique de distorsion globale. Prenez en considération N unités de codage, chacune avec M choix de quantification disponibles. Pour chaque unité de codage i codée avec un quantificateur Q_i, nous définissons son taux $R_i(Q_i)$ et sa distorsion $D_i(Q_i)$ [OR98]. Le problème d'allocation de budget sous contrainte peut être énoncé comme trouver le quantificateur optimal $Q(i)$ pour chaque unité de codage i tel que

$$\sum_{i=1}^{N} R_i(Q_i) \leq R_{budget} \tag{5}$$

et certaines métriques $f\left(D_1(Q_1), D_2(Q_2), \ldots, D_N(Q_N)\right)$ sont minimisées.
Dans le codage vidéo différents types de métriques peuvent être utilisés. Par exemple, dans une approche de distorsion moyenne minimale (MMSE), nous avons

$$f\left(D_1(Q_1), D_2(Q_2), \ldots, D_N(Q_N)\right) = \sum_{i=1}^{N} D_i(Q_i). \tag{6}$$

Dans le problème minimax (MMAX) [SK97b, SK97a], la fonction de distorsion est

$$f\left(D_1(Q_1), D_2(Q_2), \ldots, D_N(Q_N)\right) = \max_{i\in\{1,\ldots,N\}} D_i(Q_i). \tag{7}$$

Un autre exemple est l'approche lexicographiquement optimale (MLEX) [D.T97], une extension de la solution minimax qui compare deux solutions en triant leurs indices de quantification et en considérant celui représenté par le plus petit nombre comme le meilleur dans le sens MLEX.

Dans le cas où le taux $R_i(Q_i)$ et la distorsion $D_i(Q_i)$ peuvent être mesurés indépendamment pour chaque unité de codage, la solution classique pour le problème d'allocation contrainte est basée sur la version discrète de l'optimisation Lagrangienne introduite par Everett [Eve63]. En disant que $R_i(Q_i)$ et $D_i(Q_i)$ sont mesurés indépendamment, nous voulons dire que les données R-D pour l'unité de codage i peuvent être calculées sans nécessiter l'encodage d'autres unités de codage. L'optimisation lagrangienne a été utilisée pour la première fois dans l'application de codage source [SG88, CL89, CLG89], dans l'allocation par tree-pruning et l'allocation contrainte par entropie [CL89, CLG89] et, depuis lors, par de nombreux auteurs [RV93, WG91, ORV94, CL97, KBSC92, LWC93, SB94].

L'idée de base de cette technique est de transformer le problème contraint en un non contraint afin de simplifier la résolution de celui-ci, en définissant une fonction de coût Lagrangienne $J_i(Q_i) = D_i(Q_i) + \lambda \cdot R_i(Q_i)$, où $\lambda \geq 0$ est le multiplicateur lagrangien. En choisissant un quantificateur plus grossier, le taux diminue et une distorsion augmente, avec un compromis entre les deux. Le multiplicateur de Lagrange permet de sélectionner le point de compromis spécifique: si $\lambda = 0$, la minimisation du coût Lagrangien équivaut à minimiser la distorsion; si λ est arbitrairement grand, minimiser J équivaut à minimiser le taux; les valeurs intermédiaires de λ déterminent les points de fonctionnement intermédiaires.

Pour résoudre le problème d'allocation restreinte, nous devons trouver un ensemble optimal de Q_i^* pour $i = 1, 2, \ldots, N$, de sorte que la minimisation de la distorsion totale dans la contrainte du budget total R_T:

$$\mathbf{Q}^* = (Q_1^*, Q_2^*, \ldots, Q_N^*) = \arg \min_{(Q_1,Q_2,\ldots,Q_N)} \sum_{i=1}^{N} D_i(Q_i) \tag{8}$$

avec la contrainte que $\sum_{i=1}^{N} R_i(Q_i) \leq R_{budget}$. En utilisant le multiplicateur lagrangien, nous transformons le problème en optimisation sans contrainte:

$$\mathbf{Q}^* = \arg \min_{(Q_1,Q_2,\ldots,Q_N)} \sum_{i=1}^{N} D_i(Q_i) + \lambda \sum_{i=1}^{N} R_i(Q_i). \tag{9}$$

De l'hypothèse de l'indépendance, on peut reformuler l'éq. 9 comme suit:

$$Q_i^* = \arg \min_{Q_i} \left[D_i(Q_i) + \lambda \cdot R_i(Q_i)\right]. \tag{10}$$

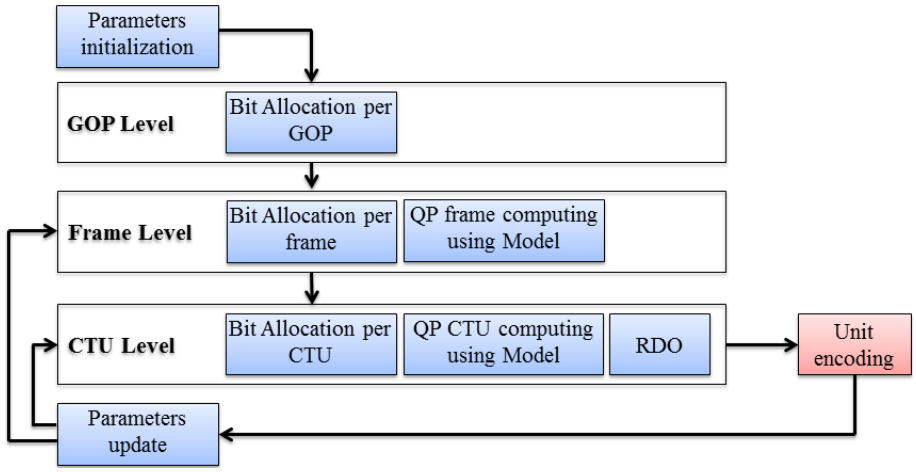

Figure 4: Contrôle de débit dans HEVC.

Le point de la courbe R-D qui minimise la fonction de coût J est, pour chaque unité de codage, le point de tangence de la ligne de pente absolue λ avec la coque convexe de la caractéristique R-D.

De nombreux scénarios pratiques impliquent des cadres de codage *dépendants*, c'est-à-dire où l'ensemble des points de fonctionnement R-D disponibles pour certaines unités de codage dépend du choix particulier du point R-D pour d'autres unités de codage, comme le montre la Figure 2.3. Ce problème, typique dans les schémas de codage basés sur la prédiction [USC93, ROV94], a été abordé par Ramchandran *et al.* [ROV94] en utilisant un cadre R-D opérationnel pour rechercher la combinaison optimale de QPs pour l'ensemble du GOP. Cependant, la recherche de paramètres nécessite d'évaluer un ensemble de points R-D pour chaque trame, ce qui rend la charge de calcul très élevée en raison du fait qu'un codage multi-pass est nécessaire.

Dans l'encodeur vidéo à l'état de l'art HEVC, la RDO est utilisé non seulement comme un schéma de sélection de mode, mais il est adopté dans le module de contrôle de débit. Le contrôle de débit est un outil non normatif, adopté pour ajuster le débit binaire de sortie et assurer une qualité visuelle élevée de la vidéo décodée dans des conditions de réseau limitées. Une tâche cruciale du contrôle de débit est de répartir de manière optimale le budget de bits dans la séquence, car cela affecte directement la distorsion visuelle des trames codées provenant de la quantification. A cet régard, le contrôle de débit de H.265/HEVC alloue le budget de bits à trois niveaux différents: le niveau GOP, le niveau de trame et le niveau d'unité de codage (CU), comme représenté sur la Figure 4.

Pour le niveau GOP, l'allocation de bits (BA) consiste en une affectation uniforme du budget de bits total pour la séquence sur les GOP, avec une fluctuation possible en fonction du nombre de trames restantes à encoder et des bits encore disponibles. Le BA au niveau de l'image fonctionne de manière similaire, avec un mécanisme de pondération pour varier l'affectation des bits pour chaque trame dans le GOP actuel en fonction de leur position

hiérarchique différente (une allocation non hiérarchique, tous les poids étant égaux à 1, est disponible). Au niveau de trame et au niveau de la CTU, après que le budget de bits a été alloué, le module de contrôle de débit calcule une QP optimale qui sera utilisée dans la quantification. Notre travail vise à remplacer le bloc BA mentionné, qui ne prend pas en compte les caractéristiques de séquence telles que la complexité de texture de la corrélation temporelle entre les trames pour l'affectation des bits, sans modifier les blocs responsables de la détermination QP, qui est exécutée avec le modèle R-λ [LLLZ12], ni le niveau de l'unité de l'arbre de codage (CTU).

Allocation de bit au niveau de trame

L'optimisation vise à sélectionner le meilleur élément d'un ensemble d'alternatives disponibles classées selon un critère donné. Dans le troisième chapitre nous introduisons une approche différente du problème d'optimisation basée sur les *algorithmes proximaux* différent de l'optimisation lagrangienne; en particulier, nous nous concentrons sur une sous-classe d'algorithme proximal, les *méthodes primal-dual*. Ces méthodes visent à résoudre le problème d'optimisation en résolvant simultanément un problème "primal", qui correspond à la tâche d'optimisation initiale, ainsi qu'une double formulation de ce problème, offrant des avantages computationnels importants grâce à leur aptitude à réaliser un fractionnement complet: chaque opérateur impliqué dans le problème est utilisé séparément et aucune inversion d'un opérateur linéaire n'est requise. En outre, les algorithmes d'optimisation dérivés des méthodes primal-dual peuvent être facilement parallélisé.

De nombreux problèmes de traitement des signaux impliquent de multiples objectifs à optimiser, conduisant à la généralisation (3.1):

$$\underset{x \in D}{\text{minimize}} \quad \{f_1(x), \ldots, f_R(x)\}, \tag{11}$$

où D désigne un ensemble de solutions réalisables, et $f_r : D \to \mathbb{R} \cup +\infty$ pour chaque $r \in \{1, \ldots, R\}$ sont les fonctions objectives. Une difficulté majeure qui se pose dans la résolution de ce problème multi-objectif découle du fait que certaines des fonctions ne sont généralement pas différentiables, excluant les techniques classiques d'optimisation lisse. Dans ce cas, une approche possible consiste à recourir à des approximations intelligentes pour lisser les fonctions non différentiables impliquées [Hub64, BTT89, HUL96, BNS13]. Une autre possibilité est, pour résoudre directement le problème non lisse initial, d'appliquer des méthodes de projection [YW82, CCC$^+$12], des méthodes de descente en coordonnées de bloc [Tse01] ou des méthodes de point intérieur [Wri97], mais elles imposent souvent des hypothèses restrictives sur le problème à résoudre. Une nouvelle classe d'algorithmes d'optimisation convexe efficaces, appelés *algorithmes proximaux*, vient d'émerger pour surmonter ces problèmes. Ils sont appelés proximal car chaque fonction non lisse dans (9) est impliquée par son opérateur de proximité et leur utilisation se répand rapidement grâce

à leur capacité à résoudre un large panel de problèmes d'optimisation convexe

Introduit dans les premiers travaux de Moreau [Mor65], *l'opérateur de proximité* représente un outil clé dans les méthodes proximales. L'opérateur de proximité d'une fonction convexe semi-continue inférieure $f \in \Gamma_0(\mathbb{R}^N)$, est défini comme

$$(\forall x \in \mathbb{R}^N) \qquad \operatorname{prox}_f(x) = \underset{u \in \mathbb{R}^N}{\arg\min} \ \frac{1}{2}\|u - x\|_2^2 + f(u). \tag{12}$$

L'opérateur de proximité peut être interprété comme une sorte d'étape implicite de sous-gradient pour la fonction f, car elle est caractérisée par l'inclusion

$$p = \operatorname{prox}_f(x) \quad \Leftrightarrow \quad p \in x - \partial f(p), \tag{13}$$

qui se réduit à

$$p = \operatorname{prox}_f(x) \quad \Leftrightarrow \quad p \in x - \nabla f(p). \tag{14}$$

si f est différentiable. Les opérateurs de proximité possèdent de nombreuses propriétés intéressantes qui les rendent très attrayants pour les algorithmes de minimisation itératifs [CCPW07, CP11c, BC11, PB14].

Les algorithmes proximaux peuvent être classés en méthodes *primal* [CP11c, PP12, ABDF10] et *primal-dual* [CP11a, CP12, Con13, KP15, Vu13, BnC11]. Les méthodes primal-dual, en particulier, procèdent en résolvant un problème primal, qui est la tâche d'optimisation initiale, ainsi qu'une formulation duale du problème. Ces méthodes sont en mesure de réaliser une division complète (chacun des opérateurs impliqués dans le problème est utilisé séparément), de sorte qu'aucune inversion d'un opérateur linéaire (ce qui est coûteux pour des problèmes à grande échelle) est nécessaire pendant l'optimisation et est facilement parallélisable. Un certain nombre de méthodes primal-dual peuvent être dérivées du *forward-backward* splitting [CCPVu14].

Ces techniques d'optimisation convexe sont utilisées pour résoudre le problème de l'attribution optimale de bits au niveau de trame pour HEVC. Nous présentons notre modèle récursif de taux de distorsion au niveau de trame, définissons le problème d'allocation de bits au niveau de trame et présentons une solution basée sur le fractionnement forward-backward et enfin nous présentons quelques résultats pour valider notre modèle R-D et évaluer l'efficacité de notre optimisation méthode.

La modélisation précise de la distorsion de débit (R-D) joue un rôle fondamental dans l'allocation optimale des bits. En raison des différentes caractéristiques des cadres, ainsi que des techniques sophistiquées de compression employées dans les algorithmes de codage, la modélisation analytique R-D reste un problème ouvert.

La première contribution de cette thèse est la proposition d'un modèle R-D approprié pour les trames d'un GOP capable de décrire des dépendances entre les distorsions des trames; nous avons utilisé les mêmes fondements théoriques que dans [USC93], mais nous

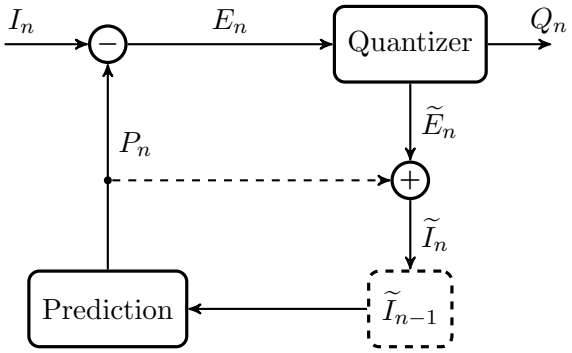

Figure 5: Encodeur vidéo hybride.

étendons le modèle R-D en laissant varier la décroissance exponentielle à chaque trame, ce qui nous permet de mieux représenter les non-stationnarités intrinsèques dans un groupe de trames (dans [USC93], il est explicitement requis que la décroissance exponentielle soit la même pour toutes les trames).

L'architecture générique d'un codeur vidéo hybride est présentée de façon synthétique dans la Fig. 5. Pour prendre en compte la dépendance temporelle entre les images, la séquence vidéo est organisée en un groupe d'images (GOP), que nous notons $I_0, \ldots, I_{N-1}$. La première trame I_0 est codée indépendamment en utilisant un schéma de quantification similaire à JPEG, tandis que les trames restantes $I_1, \ldots, I_{N-1}$ sont codées conjointement par un schéma de prédiction à compensation de mouvement.

Dans la configuration IPP...P, la trame I_n (avec $n = 1, \ldots, N-1$) est soustraite d'une prédiction P_n, donnant une trame résiduelle $E_n = I_n - P_n$ qui est envoyé au quantificateur. Ce dernier, avec des indices de quantification Q_n, produit le résidu de codage $\widetilde{E}_n$ qui sert à calculer la trame codée $\widetilde{I}_n = \widetilde{E}_n + P_n$, ce qui contribuera à la prédiction de la prochaine image.

La prédiction temporelle est basée sur l'estimation et la compensation de mouvement (ME et MC). La ME consiste à estimer le mouvement qui s'est produit entre la trame d'entrée I_n et la trame codée précédente $widetildeI_{n-1}$. Le résultat est un champ de vecteurs de mouvement $\mathbf{v}_n$ que sert à générer la prédiction, ce qui donne

$$P_n = f(\widetilde{I}_{n-1}, \mathbf{v}_n), \tag{15}$$

où f est la fonction de MC qui, dans sa forme la plus simple, traduit les blocs de $\widetilde{I}_{n-1}$ selon les vecteurs de mouvement dans $\mathbf{v}_n$.

Le contrôle de débit au niveau du cadre alloue le budget de bits dans un GOP en examinant le comportement R-D des différentes trames. Pour ce faire, une approche possible consiste à recourir à un modèle R-D paramétrique. Selon la théorie R-D [CT91],

la distorsion de la trame $\widetilde{I}_n$ codée à un taux élevé r_n lit

$$D_n = \mathbb{E}\left\{(I_n - \widetilde{I}_n)^2\right\} = \alpha_n \, \sigma_n^2 \, 2^{-2\,r_n}, \tag{16}$$

où $\alpha_n > 0$ est un paramètre libre, et σ_n^2 est la variance de la trame I_0 lorsque $n = 0$ pour le résidu E_n for $n \geq 1$. Le modèle R-D ci-dessus est avéré inexact dans le contexte du codage vidéo prédictif [HM02b], car la distorsion D_n dépend également de la trame $\widetilde{I}_{n-1}$ utilisée pour construire la prédiction compensée en mouvement.

Le cadre résiduel est factorisable en deux termes:

$$\begin{aligned} E_n &= I_n - P_n \\ &= \underbrace{\left[I_n - f(I_{n-1}, \mathbf{v})\right]}_{z_n} - \underbrace{\left[f(\widetilde{I}_{n-1}, \mathbf{v}) - f(I_{n-1}, \mathbf{v})\right]}_{q_n}, \end{aligned} \tag{17}$$

où z_n est l'erreur de prédiction de la frame *original* I_{n-1}, et q_n est l'erreur de quantification de la frame *encodé* $\widetilde{I}_{n-1}$. En supposant que z_n et q_n sont non corrélés, et $\mathbb{E}\{E_n\} = 0$, la variance du résiduel peut être décomposée comme

$$\sigma_n^2 = \underbrace{\mathbb{E}\left\{z_n^2\right\}}_{M_n} + \mathbb{E}\left\{q_n^2\right\}, \tag{18}$$

où M_n est l'erreur quadratique moyenne de l'estimation de mouvement. Le second terme est exactement la distorsion de $\widetilde{I}_{n-1}$, puisque

$$\begin{aligned} \mathbb{E}\left\{q_n^2\right\} &= \mathbb{E}\left\{\left[f(\widetilde{I}_{n-1}, \mathbf{v}) - f(I_{n-1}, \mathbf{v})\right]^2\right\} \\ &= \mathbb{E}\left\{\left[\widetilde{I}_{n-1} - I_{n-1}\right]^2\right\} \\ &= D_{n-1}, \end{aligned} \tag{19}$$

sous l'hypothèse d'une stationnarité à sens large. Par conséquent, le comportement R-D d'une trame I_n peut être modélisé comme [USC93]

$$D_n = \alpha_n \, (M_n + D_{n-1}) \, 2^{-2\,r_n}, \tag{20}$$

où, pour $n = 0$, M_0 indique la variance de I_0 et $D_{-1} = 0$. Par conséquent, pour $n \geq 1$, la distorsion D_n est contrôlée par deux termes: le taux r_n utilisé pour coder $\widetilde{I}_n$, et la distorsion D_{n-1} de sa référence encodée $\widetilde{I}_{n-1}$, conduisant à un modèle récursif R-D.

Afin de mieux représenter le fait que le comportement R-D dans un GOP peut changer d'un cadre à un autre, nous modélisons la fonction R-D d'un cadre I_n comme suit

$$D_n = \alpha_n \, (M_n + D_{n-1}) \, e^{-\beta_n \, r_n}, \tag{21}$$

où (α_n, β_n) sont des paramètres à estimer dans le GOP.

Le point clé du modèle ci-dessus est que la distorsion D_n dépend en fait de toutes les trames impliquées dans la chaîne de prédictions menant à I_n. Cela peut être clairement démontré par le principe d'induction, qui conduit à

$$\begin{aligned} D_n &= \alpha_n \left(M_n + D_{n-1}\right) e^{-\beta_n r_n} \\ &= \alpha_n \left(M_n + \alpha_{n-1}(M_{n-1} + D_{n-2}) e^{-\beta_{n-1} r_{n-1}}\right) e^{-\beta_n r_n} \\ &\dots \\ &= \sum_{\ell=0}^{n} \alpha^{(\ell,n)} M_\ell \, e^{-\sum_{j=\ell}^{n} \beta_j r_j}, \end{aligned} \tag{22}$$

où $\alpha^{(\ell,n)} = \prod_{j=\ell}^{n} \alpha_j$. Puisque nous avons une somme d'exponentiels composée d'une transformation linéaire, on peut conclure que la distorsion D_n est une fonction convexe de taux $r_0, \dots, r_n$.

L'estimation des paramètres du modèle est effectuée par des encodages multiples des séquences à différentes valeurs de paramètre de quantification (QP). Pour chaque trame, nous avons enregistré les valeurs de D et R produites à la sortie du codeur et, après une transformation logarithmique de D, nous avons estimé les paramètres du modèle en recourant à une régression linéaire. Le paramètre $(M_n)_{0 \le n \le N-1}$, qui représente la prédiction de mouvement, est extrapolée à partir d'une version modifiée du codeur. Pour évaluer davantage la précision de la relation R-D, la métrique R^2 [DF99] est utilisé pour mesurer le degré de variation des données d'un modèle donné:

$$R^2 = 1 - \frac{\sum_i (X_i - \hat{X}_i)^2}{\sum_i (X_i - \bar{X})^2}, \tag{23}$$

où X_i et $\hat{X}_i$ sont les valeurs réelles et estimées d'un point de données, et $\bar{X}$ est la moyenne de tous les points de données. Plus la valeur de R^2 est proche de 1, plus le modèle est précis. Nous avons comparé le modèle proposé en (21) au modèle R-D classique (20) et au modèle proposé dans [PAZ+13]. Le Tableau 1 montre les valeurs R^2 associées à la fonction R-D pour différentes séquences. Comme le montre le tableau, pour toutes les séquences d'essai, le modèle proposé donne des valeurs R^2 plus élevées qui indiquent une précision plus élevée.

La répartition optimale des taux consiste à trouver le vecteur de taux $r = (r_0, \dots, r_{N-1})$ qui minimise la distorsion globale tout en maintenant le taux total sous un budget donné $\eta > 0$, c'est-à-dire

$$\underset{r \in [0,+\infty[^N}{\text{minimize}} \quad \sum_{n=0}^{N-1} D_n(r_0, \dots, r_n) \qquad \text{s. t.} \qquad \sum_{n=0}^{N-1} r_n \le \eta. \tag{24}$$

En utilisant la fonction de distorsion proposée dans l'éq (22), la formulation ci-dessus se

Sequence	R^2 *with* (21)	R^2 *with* (20)	R^2 *with* [PAZ+13]
BasketballDrive	0.992	0.986	0.937
BQTerrace	0.998	0.921	0.727
Cactus	0.999	0.922	0.913
Kimono1	0.999	0.941	0.972
ParkScene	0.999	0.947	0.963
BasketballDrill	0.974	0.940	0.970
BQMall	0.999	0.916	0.975
RaceHorses (832x480)	0.998	0.952	0.934
BlowingBubbles	0.999	0.937	0.916
BQSquare	0.997	0.903	0.925
RaceHorses(416x240)	0.991	0.963	0.893

Table 1: Précision d'estimation de distorsion pour différentes séquences évaluées par R^2

résume à un problème d'optimisation convexe qui peut être *efficacement* et *exactement* résolu par les algorithmes proximaux primal-dual.

Pour obtenir un aperçu de la solution du Problème (24), on peut introduire un vecteur $u = (u_{n\ell})_{0\leq n\leq N-1, 0\leq \ell\leq n}$ défini comme

$$u_{n\ell} = -\sum_{j=\ell}^{n} \beta_j r_j, \tag{25}$$

ce qui nous permet d'exprimer la distorsion globale comme une somme séparable d'exponentiels

$$\varphi(u) = \sum_{n=0}^{N-1} \sum_{\ell=0}^{n} \alpha^{(n,\ell)}\, M_\ell\, e^{u_{n\ell}}. \tag{26}$$

Par conséquent, le Problem (24) peut être reformulé comme suit

$$\underset{r\in\mathbb{R}^N}{\text{minimize}} \quad \varphi(\mathsf{L}r) + \iota_C, \tag{27}$$

où $\mathsf{L}\colon \mathbb{R}^N \mapsto \mathbb{R}^{\frac{N(N+1)}{2}}$ est l'opérateur linéaire qui mappe le vecteur $r \in \mathbb{R}^N$ dans le vecteur $u \in \mathbb{R}^{\frac{N(N+1)}{2}}$ défini dans (25), $C \subset \mathbb{R}^N$ est l'ensemble convexe fermé non vide défini comme

$$C = \big\{ r \in [0, +\infty[^N \;\big|\; \sum_{n=0}^{N-1} r_n \leq \eta \big\}, \tag{28}$$

et ι_C désigne la fonction indicatrice de C, égale à 0 si $r \in C$ et $+\infty$ sinon, afin d'appliquer la contrainte budgétaire binaire.

Pour la résolution du Problème (27), nous utilisons l'algorithme Forward-Backward Primal-Dual, qui consiste à itérer les étapes suivantes pour une initialisation donnée

Algorithm 1 FBPD [Con13] pour résolution du Problème (27)

Inputs : $\eta, (\alpha_n, \beta_n, M_n)_{0 \leq n \leq N-1}$
Output : r
Initialization
$\quad$ select $r^{[0]} \in \mathbb{R}^N$ and $u^{[0]} \in \mathbb{R}^{\frac{N(N+1)}{2}}$
$\quad$ set $\tau > 0$ and $\gamma > 0$ such that $\tau\gamma\|\mathsf{L}\|^2 \leq 1$
For $i = 0, 1, \ldots$
$\quad r^{[i+1]} = P_C\big(r^{[i]} - \tau\,\mathsf{L}^\top u^{[i]}\big)$
$\quad u^{[i+1]} = \mathrm{prox}_{\gamma\varphi^*}\Big(u^{[i]} + \gamma\,\mathsf{L}\big(2r^{[i+1]} - r^{[i]}\big)\Big)$

$(r^{[0]}, u^{[0]})$:

$$(\forall i \in \mathbb{N}) \quad \left\lfloor \begin{array}{l} r^{[i+1]} = \mathrm{prox}_{\tau\iota_C}\Big(r^{[i]} - \tau\mathsf{L}^\top u^{[i]}\Big) \\ u^{[i+1]} = \mathrm{prox}_{\gamma\varphi^*}\Big(u^{[i]} + \gamma\,\mathsf{L}\big(2r^{[i+1]} - r^{[i]}\big)\Big) \end{array} \right. \tag{29}$$

où $\tau > 0$ et $\gamma > 0$ sont deux paramètres algorithmiques, tandis que φ^* désigne le conjugué convexe de la fonction φ.

Le principal avantage des opérateurs de proximité est que les fonctions à optimiser n'ont pas besoin d'être différentiables. Ceci nous permet d'imposer la contrainte C définie dans l'éq. (28) grâce à sa fonction indicatrice, puisque l'opérateur de proximité de ι_C coÃ¯ncide avec la *projection orthogonale* sur C.

Par conséquent, les itérations dans (29) conduisent à l'Algorithme 1, qui est garanti à converger vers une solution au Problem (27) pour un choix approprié de τ et γ [Con13], et peut être efficacement mis en œuvre sur les architectures multicœurs et GPGPU [GCPP12].

Afin d'évaluer la validité de notre méthode d'allocation de taux, nous l'avons comparée avec l'algorithme de contrôle de taux de H.264/AVC [SWL03]. Pour les séquences *akiyo, coastguard, eric, football, foreman* et *hall*, La Figure 6 montre à gauche les taux attribués par la méthode proposée (ligne rouge pleine) et par H.264/AVC (ligne bleue pointillée), en fonction du numéro de trame, tandis que sur la droite les distorsions correspondantes; en particulier, pour H.264/AVC on montre la distorsion produite codant les séquences avec le contrôle de débit activé, alors que pour notre méthode la distorsion est simplement évaluée à partir de notre modèle R-D en utilisant les taux alloués. Comme on peut voir sur les figures, l'allocation des taux de la méthode proposée est très différente de la référence, en particulier pour les trames I. En outre, notre répartition des taux est plus uniforme au sein du GOP. C'est un résultat important, car souvent l'encodeur H.264/AVC montre un comportement gourmand sous-optimal: il alloue la plus grande partie du budget de bits aux premières trames du GOP et donc il court rapidement des bits pour le reste GOP, provoquant une augmentation de la distorsion globale. Ces résultats montrent que la distorsion obtenue avec la méthode proposée est toujours inférieure à celle obtenue par

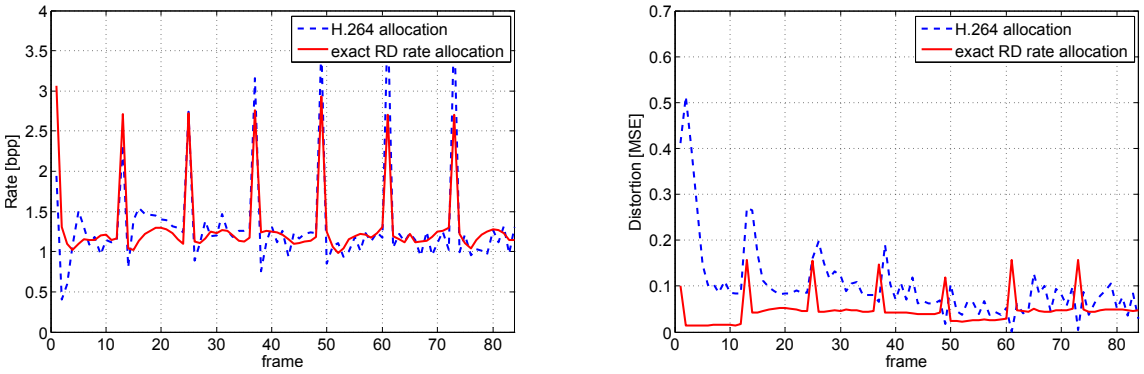

(a) Taux vs numéros d'image

(b) Distorsion vs numéros d'image

Figure 6: Séquence *akiyo*

l'algorithme de contrôle de débit.

Résultats expérimentaux

Dans le quatrième chapitre nous présentons quelques résultats expérimentaux qui montrent l'efficacité de la méthode proposée: nous intégrons notre méthode dans l'encodeur H.265/HEVC et comparons les performances de R-D de notre approche avec le module de contrôle de débit de H.265/HEVC et la méthode de Ramchandran [ROV94].

Nous avons incorporé notre méthode dans l'implémentation de référence de l'encodeur HEVC (*HM.13 RExt-6.0*), qui est capable de coder uniquement la composante Luma d'une séquence vidéo, afin d'évaluer avec précision la validité de notre modèle R-D et évaluer facilement les performances globales.

Dans nos expériences, nous avons utilisé plusieurs séquences de classe A, B, C, D et E des *Common Test Conditions* de HEVC [Bos13], présentant des caractéristiques significativement différentes en termes de scènes lisses et complexes et de mouvements lents et rapides. La configuration du codeur est réglée comme suit: I-P-P-P comme structure de GOP avec une seule cadre de référence (chaque trame P dans un GOP dépend uniquement de la précédente), afin d'avoir la meilleure correspondance avec le modèle R-D proposé; la plage de recherche maximale pour l'estimation de mouvement est fixée à 64. Quatre target bit rates différents sont sélectionnés pour chaque séquence afin de couvrir une plage PSNR de 35 dB à 42 dB. Le cadre expérimental est composé de trois étapes, comme le montre la Figure 7.

Afin d'évaluer la validité de notre méthode d'allocation de débit, nous l'avons comparée au système de contrôle de taux R-λ mis en œuvre dans le logiciel de référence de HEVC. Bjontegaard Δ bitrate (BDBR) et Bjontegaard Δ PSNR (BDPSNR)[Bjo01] sont déployés pour mesurer la performance moyenne sur les quatre débits cibles pour chaque séquence. Pour BDPSNR, un nombre positif indique un gain PSNR réalisé par notre méthode au

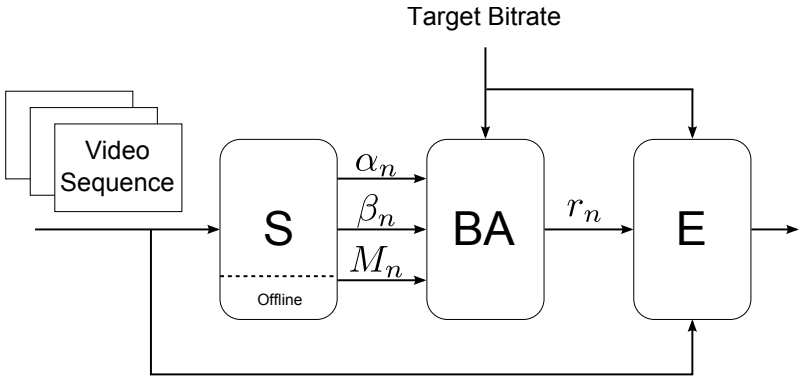

Figure 7: Organigramme de la méthode proposée: estimation des paramètres (block **S**), allocation des bits (block **BA**), et encodage vidéo (block **E**).

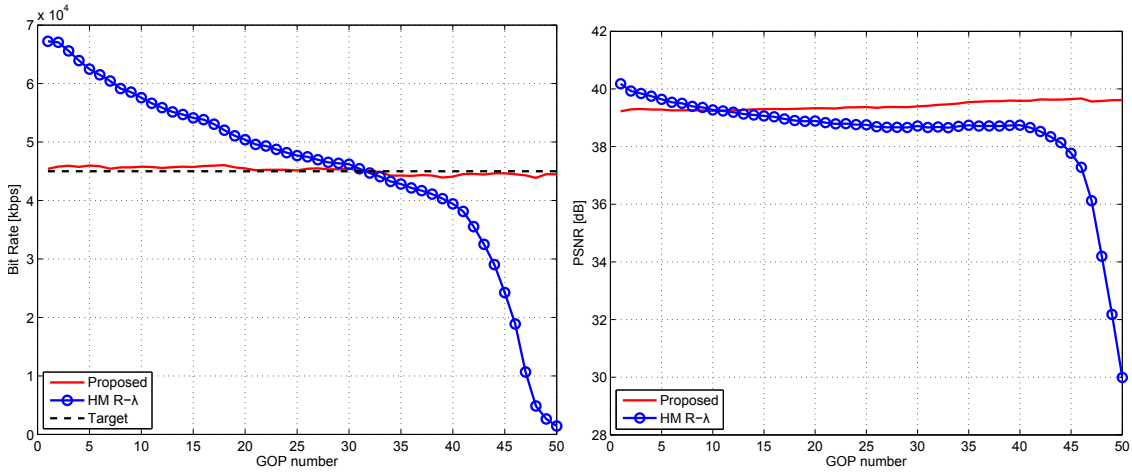

Figure 8: Taux vs numéros de GOP (gauche) et PSNR vs numéros de GOP (droit) pour la séquence *Cactus*.

même débit; pour BDBR, un nombre négatif dans le tableau indique une réduction de taux obtenue à la même qualité PSNR. Le Tableau 2 présente la performance débit-distorsion de HM R-λ et notre schéma pour chaque séquence, ainsi que les résultats moyens pour chaque classe. Comme le montre le tableau, notre méthode surpasse l'encodeur classique en termes de PSNR moyen pour toutes les séquences vidéo à différents débits; en particulier, nous avons un gros gain pour toutes les séquences de classe B avec un maximum de 1.32 dB en termes de Δ PSNR et une réduction de débit de 30.73 %.

Un autre avantage de la méthode proposée sur HM R-λ est une meilleure stabilité en termes de débit. Comme montré dans la Figure 8, HM R-λ produit de fortes fluctuations autour du taux cible sur les GOPs, alors que notre méthode est beaucoup plus stable, atteignant le débit cible pour chaque GOP. Ces fluctuations ont un impact important sur la *qualité subjective* des séquences vidéo, qui diminuent considérablement pour les derniers GOPs, comme le montrent les graphiques de droite de la Figure 8. De plus, Figures 9 and 10 illustrent certains résultats qualitatifs subjectifs de la méthode proposée et du

Sequence	BDPSNR (dB)	BDBR (%)	av. BDPSNR (dB)	av. BDBR (%)
SteamLocomotiveTrain	0.62	-18.62	0.41	-8.68
NebutaFestival	0.50	-5.97		
PeopleOnStreet	0.45	-8.74		
Traffic	0.10	-1.41		
BasketballDrive	1.02	-28.00	0.93	-24.85
BQTerrace	1.01	-26.47		
Cactus	0.89	-30.73		
Kimono1	0.82	-21.21		
ParkScene	0.93	-17.84		
BasketballDrill	0.41	-9.06	0.49	-10.77
BQMall	0.59	-12.06		
PartyScene	0.43	-9.54		
RaceHorses (832x480)	0.55	-12.41		
BasketballPass	0.12	-1.89	0.74	-11.32
BlowingBubbles	0.99	-15.25		
BQSquare	1.32	-19.80		
RaceHorses (416x240)	0.52	-8.35		
FourPeople	0.43	-6.87	0.23	-5.86
KristenAndSara	0.22	-6.79		
vidyo1	0.17	-6.34		
vidyo3	0.23	-4.83		
vidyo4	0.12	-4.48		

Table 2: Métriques de Bjontegaard de la technique proposée par rapport à HM R-λ sur diverses séquences.

(a) Méthode proposée. (b) HM R-λ.

Figure 9: Qualité subjective de la séquence *Cactus* à 10 Mbps puor la frame No. 90.

(a) Méthode proposée. (b) HM R-λ.

Figure 10: Qualité subjective de la séquence *Cactus* à 10 Mbps puor la frame No. 198.

contrôle des taux de HEVC. Pour chaque séquence, les images du sommet correspondent à notre méthode, alors que celles du bas correspondent à HM R-λ. Ces figures présentent le cadre No. 90 et le cadre No. 198 pour les séquences *Cactus* et *ParkScene* pour les deux méthodes, et donnent un exemple visuel des fluctuations de qualité signalées dans la Figure 8, montrant une qualité visuelle constante pour notre méthode sur toute la séquence, tandis que la perte de qualité de HM entraîne des artefacts de blocage sévères.

Nous comparons également notre méthode avec la technique d'allocation de bits proposée par Ramchandran *et al.* [ROV94]; L'optimalité de cette méthode est garantie par le fait qu'elle choisit la combinaison de quantificateurs avec le coût Lagrangien minimum parmi toutes les combinaisons possibles. Dans[ROV94], deux *condition d'élagage* impliquées par la propriété monotonicité des courbes R-D, qui sont prouvées ne pas affecter l'optimalité de la solution, sont introduites afin d'alléger la charge de calcul, et des *heuristiques suboptimales* sont proposés pour obtenir une réduction supplémentaire de la complexité en échange de une perte de performance. Nous comparons notre méthode à cette solution sous-optimale, mais faisable, en termes de performance R-D et de temps d'exécution.

La première étape pour implémenter [ROV94] était la phase de *génération de données*: pour générer la R-D, nous avons encodé chaque séquence avec toutes les combinaisons de QP possibles le long des trames. La complexité de cette phase est clairement exponentielle

Sequence	BDPSNR (dB)	BDBR (%)	av. BDPSNR (dB)	av. BDBR (%)
SteamLocomotiveTrain	-0.38	7.49	-0.19	6.10
NebutaFestival	0.51	-5.41		
PeopleOnStreet	-0.17	3.35		
Traffic	-0.72	18.96		
BasketballDrive	-0.01	0.16	-0.18	5.01
BQTerrace	-0.30	6.44		
Cactus	-0.16	6.01		
Kimono1	-0.03	0.77		
ParkScene	-0.40	12.00		
BasketballDrill	-0.79	18.96	-0.55	12.86
BQMall	-0.74	17.75		
RaceHorses (832x480)	-0.10	1.88		
BasketballPass	-0.68	12.36	-0.66	11.13
BlowingBubbles	-0.61	11.54		
BQSquare	-0.97	14.81		
RaceHorses (416x240)	-0.40	5.79		

Table 3: Comparaison des performances de [ROV94] et de la méthode de méthode proposée en utilisant les métriques de Bjontegaard.

avec le nombre de trames, et il est possible de calculer le nombre d'opérations de codage par séquence comme $\sum_{n=1}^{N} q^n = \frac{q^{N+1}-1}{q-1}$, où N est le nombre de trames codées, et q est le nombre de QP utilisé. Afin d'avoir un temps d'encodage raisonnable, on choisit $N = 4$ et $q = 9$, en utilisant les QPs 20, 22, 25, 27, 30, 32, 35, 37, 40; encore une fois, nous avons utilisé comme codeurHM.13 RExt-6.0 avec la commande de débit désactivée, et une configuration I-P-P-P.

Pour chaque séquence, nous avons défini un ensemble de valeurs λ, et pour chacune d'elles nous avons sélectionné le chemin optimal, c'est-à-dire la combinaison de QPs, avec le coût Lagrangien minimum; parmi tous les points R-D optimaux, nous avons sélectionné quatre avec un PSNR dans la plage de 35 dB $\sim$ 42 dB, et utilisé les valeurs de débit relatives comme *target bit rates* pour notre méthode.

Le Tableau 3 présente la performance R-D de l'heuristique sous-optimale de [ROV94] et de notre méthode en termes de BDBR and BDPSNR, montrant que notre méthode fonctionne légèrement pire que [ROV94], avec une différence en termes de débit inférieur à 7% pour plusieurs séquences, et une différence moyenne de 9%. La seule exception, représentée par la sequence *NebutaFestival*, est expliquée par le fait que notre méthode exploite toute l'allocation de débit possible, tandis que pour [ROV94] nous choisissons un sous-ensemble de QPs possibles, qui est assez grand pour toutes les autres expériences, à l'exception de ce cas. De plus, nous avons comparé les temps d'exécution de ces méthodes. Le Tableau 4 présente une comparaison des temps d'exécution entre notre

méthode et celle de [ROV94]. Le temps global de notre méthode est donné par la somme de trois contributions: l'estimation des paramètres (90% du temps global), l'algorithme d'optimisation convexe (une petite fraction du temps global) et l'encodage vidéo (environ les 10% du temps global). Le temps global de [ROV94] est donné par la somme de deux contributions: la génération des données (99% du temps total) et la recherche du meilleur point R-D. Ces temps dépendent de la valeur λ choisie: un λ plus petit implique l'élagage d'un plus grand nombre de points R-D (moins d'opérations de codage à effectuer), ce qui entraîne un temps plus faible. Le Tableau 4 montre que la méthode dans [ROV94] nécessite au moins quatre fois le temps requis par notre méthode, avec une différence de deux ordre de grandeur dans le pire des cas et un ratio moyen de 91.

Sequence	*Setup Time (s)*			*Execution Time (s)*				*Global Time (s)*		
	Proposed	Method in [ROV94]		*Proposed*		Method in [ROV94]		*Proposed*	Method in [ROV94]	
	S	*Max*	*Min*	BA + E		*Max*	*Min*	S+BA+E	*Max*	*Min*
SteamLocomotiveTrain	9579	1470060	37355	0.03	193.518	61.631	1.511	9773	1470122	37356
NebutaFestival	14359	2051171	52867	0.04	1198.331	63.194	1.628	15557	2051234	52869
PeopleOnStreet	8643	1462725	27515	0.03	387.052	106.361	1.566	9030	1462831	27516
Traffic	6897	1225989	22674	0.04	289.185	110.398	1.939	7186	1226099	22676
BasketballDrive	4424	968370	12904	0.12	286.642	150.672	3.921	4711	968521	12908
BQTerrace	4830	941150	18827	0.05	350.262	125.125	1.408	5180	941275	18828
Cactus	4759	932963	17079	0.05	358.504	158.755	1.359	5118	933122	17080
Kimono1	3652	600207	10151	0.03	359.219	132.866	1.183	4011	600340	10152
ParkScene	4318	822478	14018	0.05	462.142	170.827	1.430	4780	822649	14019
BasketballDrill	785	103651	2276	0.04	48.079	86.823	1.516	833	103738	2278
BQMall	886	178867	2893	0.05	54.164	220.521	1.525	940	179088	2895
RaceHorses (832x480)	1008	149803	1858	0.04	91.317	105.121	1.530	1099	149908	1860
BasketballPass	149	38520	578	0.04	15.412	191.807	1.597	164	38712	580
BlowingBubbles	248	69695	994	0.04	24.602	180.332	1.676	273	69875	996
BQSquare	251	55029	962	0.05	22.731	169.733	1.718	274	55199	964
RaceHorses (416x240)	241	58712	972	0.05	28.290	161.830	1.780	269	58874	974

Table 4: Comparaison des temps globaux. Pour notre méthode, les valeurs temporelles concernent l'estimation des paramètres (S), l'algorithme d'optimisation convexe (BA) et l'encodage vidéo (E). Pour la méthode dans [ROV94], les temps concernent un grand λ (Max) et un petit λ (Min).

En résumé, notre méthode présente un fort gain par rapport au système de contrôle débit de HM R-λ avec une meilleure stabilité en termes de débit, alors que la petite perte de la méthode dans [ROV94] est largement compensée par un temps d'exécution beaucoup plus rapide.

Les résultats présentés pour H.264/AVC et HEVC montrent clairement l'efficacité et la polyvalence de notre modèle R-D récursif utilisé en combinaison avec la méthode d'optimisation proposée. La dernière partie de ce travail de thèse a été l'application de la méthode proposée dans le contexte du codage vidéo multi-vue. La répartition optimale des débits est une tâche difficile à accomplir dans le codage vidéo multi-visuel, car avec la dépendance entre les trames induites par la compensation de mouvement, la dépendance entre différentes vues doit être considérée.

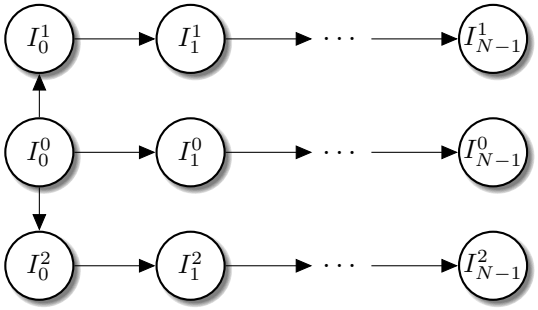

Figure 11: Graphique de dépendance utilisé.

Tout d'abord, nous généralisons notre approche en considérant le scénario où la dépendance entre les images peut être représentée comme le graphique représenté dans la Figure 11, où I_n^k désigne la n-ième image de la vue k, avec $k = 0$ étant la vue centrale et $k \geq 1$ les vues latérales. Deuxièmement, nous intégrons l'algorithme proposé dans l'encodeur MV-HEVC, afin de comparer la performance R-D de notre approche avec le contrôle de débit de MV-HEVC. Le cadre expérimental partage la même structure de celui développé pour l'encodeur vidéo HEVC.

Pour évaluer la validité de notre méthode d'allocation de débit, nous l'avons comparée avec l'algorithme de contrôle de taux standard de MV-HEVC. Le Tableau 5 montre la performance débit-distorsion de notre méthode comparée à MV-HEVC évaluée avec les métriques de Bjontegaard [Bjo01]. Pour chaque séquence, une valeur moyenne sur les trois vues du gain en termes de Bjontegaard bitrate (BDBR) et Bjontegaard PSNR (BDPSNR) est présentée. Les résultats indiquent que notre méthode fournit une économie de débit moyenne de 20% par rapport à la norme MV-HEVC avec un gain moyen de 0.70 dB en termes de PSNR. En termes d'exactitude d'allocation, la différence entre le débit cible et le débit atteint est pour chaque séquence inférieure à 10%, avec une valeur moyenne parmi toutes les séquences de 7.5%.

Sequence	BDPSNR (dB)	BDBR (%)
Balloons	1.20	-21.52
Kendo	0.35	-7.86
Newspaper_CC	0.65	-23.35
Undo_Dancer	0.49	-12.88
GT_Fly	0.83	-20.34
Poznan_Hall2	0.59	-34.72
Poznan_Street	0.82	-23.61
Average	0.70	-20.61

Table 5: Gain moyen de PSNR et économies de débit par rapport à l'extension directe HEVC multi-vues (MV-HEVC).

Conclusions et travaux futurs

Le but de cette thèse était de développer une méthode optimale d'allocation des bits au niveau du cadre. Les méthodes existantes mises en œuvre dans les codecs vidéo modernes tels que H.264/AVC et H.265/HEVC, sont basées sur des formules heuristiques simples qui tiennent compte de paramètres tels que le nombre de trames dans un GOP, les bits encore disponibles et l'occupation du tampon. Ces méthodes ne tiennent pas compte des caractéristiques des séquences et de la dépendance entre trames consécutives, résultant, comme indiqué dans le chapitre précédent, de fortes fluctuations du débit autour du débit cible assigné qui ont un impact énorme sur la qualité visuelle de la séquence codée, qui diminuent dramatiquement pour les derniers GOP codés.

Notre méthode est basée sur un modèle R-D précis pour les trames d'un GOP capable de décrire des dépendances entre les distorsions des trames. Ce modèle R-D nous a permis de formuler le problème d'allocation de bits comme un problème d'optimisation convexe qui a été résolu, de manière précise et efficace, en utilisant des techniques d'optimisation convexe. La méthode a été intégrée avec succès dans l'encodeur vidéo HEVC et adaptée au scénario multi-vues pour être utilisée dans MV-HEVC.

Un modèle R-D récursif pour les trames d'un GOP a été proposé. Nous avons étendu le modèle R-D classique proposé dans [USC93] en laissant varier la décroissance exponentielle à chaque trame. La distorsion de chaque trame à l'intérieur d'un GOP est exprimée en fonction du débit utilisée pour coder la trame, et nous sommes en mesure de prendre en compte les dépendances entre les trames en utilisant l'erreur d'estimation de mouvement, et les caractéristiques de texture de la séquence en utilisant la variance de la trame et deux paramètres de modèle α et β qui modifient la décroissance exponentielle du modèle d'origine. La précision du modèle proposé a été vérifiée sur la base de la métrique R^2, qui a été conçue pour mesurer quantitativement le degré d'écart par rapport à un modèle

donné, montrant une performance de montage élevée, supérieure aux autres modèles R-D pris en considération.

Un algorithme efficace basé sur la moderne optimisation convexe a été proposé. Le modèle R-D proposé nous a permis de formuler le problème d'allocation au niveau du cadre comme un problème d'optimisation convexe et, parmi les solutions de minimisation possibles, un algorithme Forward-Backward Primal-Dual a été développé en collaboration avec le Dr. Giovanni Chierchia. La complexité de l'algorithme n'est pas affectée par le nombre total de trames dans une séquence vidéo, grâce au fait qu'il est implémenté de sorte que le processus d'optimisation fonctionne en parallèle sur les GOPs. Un premier ensemble d'expériences réalisées sur l'encodeur vidéo H.264/AVC a montré comment l'attribution de débit de la méthode proposée est très différente de la référence, en particulier pour les trames I, et plus uniforme au sein du GOP, en évitant le comportement sous-optimal gourmand de H.264/AVC qui alloue la plus grande partie du budget de bits aux premières trames du GOP et par conséquent il court rapidement des bits pour les trames restantes, provoquant une augmentation de la distorsion globale.

La méthode proposé a été appliqué à l'encodeur vidéo à l'état de l'art HEVC. Le module de contrôle de débit de *HM.13 RExt-6.0* a été modifié afin d'intégrer l'algorithme d'allocation de bits basé sur l'optimisation convexe et les résultats ont été comparés au contrôle de taux standard R-λ de HEVC en termes de Bjontegaard bitrate and Bjontegaard PSNR. Les expériences ont prouvé que notre méthode surpasse l'encodeur classique pour toutes les séquences vidéo à différents débits avec un gain maximum de 1.32 dB en termes de Δ PSNR et une réduction de débit maximum de 30.7%, fournissant une meilleure stabilité en termes du débit, atteignant le débit cible pour chaque GOP et fournissant une qualité visuelle constante sur toute la séquence, tandis que les fluctuations autour du débit cible sur les GOP présentées par HM ont eu comme conséquence une perte de qualité sévère pour les derniers GOP de chaque séquence.

Nous avons également comparé notre méthode avec la technique d'allocation de bits proposée dans [ROV94] et basée sur une recherche exhaustive de la la solution avec le coût Lagrangien minimum parmi toutes les combinaisons de quantification possibles. Comme prévu, la recherche exhaustive a surpassé notre solution en termes de Δ PSNR, mais la perte en performance est contrebalancé par une complexité beaucoup plus faible, avec un temps d'exécution entre quatre fois et cent fois plus court.

Enfin, notre méthode a été adaptée au scénario multi-vues et mise en œuvre dans MV-HEVC. Les résultats obtenus ont démontré que notre modèle R-D analytique permet de décrire avec précision les dépendances temporelles et inter-vues dans un groupe de trames, obtenant de meilleurs résultats au sens R-D que le contrôle de débit standard dans MV-HEVC.

Des perspectives intéressantes peuvent être proposées pour poursuivre le travail effectué dans cette thèse. La méthode proposée a été prouvée pour obtenir de meilleurs résultats que le contrôle débit standard, mais a été développée pour une structure de codage très

spécifique, avec un seul cadre de référence. Nous sommes conscients de l'importance de considérer un nombre de références égal à $K > 1$. Notre idée est de généraliser l'erreur de prédiction introduisant un poids $\omega_{n,n-1}$ qui prend en considération le pourcentage de blocs de trame n prévu à partir du cadre $n - i$.

Le problème d'une structure de prédiction différente comprenant des trames bi-prédictives est actuellement à l'étude. Considérant une structure I-B-P-B-P avec une alternance de trames B, en positions paires à l'intérieur d'un GOP, qui dépendent de la trame précédente et suivante, et des trames P, en positions impaires, qui ne dépendent que de la trame P (ou I) précédente. On peut dériver une expression récursive pour la distorsion d'une trame générique, différente pour les valeurs paires ou impaires de k.

Au cours des dernières années, de nombreux programmes d'observation terrestre par satellite ont été déployés dans le but de détecter les changements, de surveiller systématiquement les cultures, avoir conscience rapide de la situation, de surveiller les activités et ainsi de suite. Dans le contexte de l'acquisition d'images multi-spectrales, une quantité énorme de données doit être stockée, et HEVC, avec ses excellentes performances débit-distorsion, pourrait représenter un outil de compression très efficace même s'il ait été conçu pour un type de données totalement différent.

Etant donné que les satellites ont typiquement quelques jours de **temps de révision** (temps écoulé entre les observations d'un même point sur terre par un seul satellite), il est raisonnable de s'attendre une forte corrélation temporelle entre des images consécutives de la même scène, similaire à celle des signaux vidéo naturels, en plus de la corrélation inter-bandes. Notre idée est de décrire ces dépendances temporelles et inter-bandes en utilisant notre modèle R-D récursif au niveau de trame afin d'améliorer la compression réalisable avec HEVC appliquée à ces différents types de signaux, qui peuvent être assimilés à des séquences vidéo multi-vues.

Abstract

Optimal rate allocation is among the most challenging tasks to perform in the context of predictive video coding, because of the dependencies between frames induced by motion compensation. Several techniques have been proposed in the literature to select the coding parameters that achieve an optimal trade-off between rate and distortion, and many conventional coding schemes tend to make these choices frame by frame. However, it is widely recognized that, from a rate-distortion standpoint, the optimal choice for a single frame may be potentially suboptimal for encoding the remaining frames, and an optimization that jointly takes into consideration the dependencies between frames may yield a significant bit reduction.

In this context, we propose an efficient solution to exactly solve the frame-level bit allocation problem. First, we derive an analytical rate-distortion model that explicitly takes into account the dependencies between frames. The proposed approach allows us to formulate the frame-level optimal rate allocation as a convex optimization problem.

Among the many approaches proposed in the literature to solve this class of problems, we resort here to proximal algorithms, which can handle a wide class of convex optimization problems involving non-smooth penalizations and hard constraints. In particular, we employ the primal-dual M+LFBF algorithm, which guarantees the convergence (under weak conditions) in a reasonable time even for large-scale problems, offers robustness to numerical errors and its structure makes it suitable for parallel implementations. Within this framework, we are able to achieve the exact solution in limited time (even for large-size problems).

This technique was integrated into the recent HEVC encoder, and tested on several standard sequences. Experiments indicate that the proposed rate allocation ensures a better performance than the standard HEVC rate control.

We also extended our work to multi-view video coding, generalizing our approach in order to accommodate the more intricate prediction schemes used in MV coding. Again, the technique was integrated in the MV-HEVC encoder, and we compared the R-D performance of our approach with the standard MV-HEVC rate control. The results of our experiments, conducted on different standard test sequences, demonstrate the effectiveness of our proposition.

Keywords: Video coding, MV video coding, rate distortion, convex optimization, bit allocation.

Table of Contents

List of Figures

List of Tables

Introduction

Context and Motivation

In the last decade, progress in digital video technology led to the generation and development of new applications in video communication, ranging from video conferencing and broadcasting of standard-definition TV content up to high-definition television (HDTV/UHDTV) and very-high-quality applications, such as digital cinema/large-screen digital imagery. In this scenario, standardization bodies called the Moving Picture Experts Group (MPEG) under the authority of the International Organization for Standardization (ISO) and the International Electrotechnical Commission (IEC) and the Video Coding Experts Group (VCEG) under International Telecommunication Union (IUT-T) have been developing video coding standards that respond to audiovisual data transmission challenges and the increasing requirements for efficient representation of video. Several successive have been presented over the years obtaining improvements in functionality and rate-distortion performance, and the latest video compression standard, known as High Efficiency Video Coding (HEVC) [SOHW12a], has been formally established to substitute its predecessor H.264/MPEG-4 Advanced Video Coding (AVC) in January 2015 [WSBL03].

In these standards, a key role in improving the visual quality of encoded videos over capacity varying channels is played by the rate allocation, which is responsible to efficiently distribute the bit budget among frames and coding blocks. More specifically it represents an important part of the rate control module of a video encoder, which involves two steps: *bit allocation (BA)*, where the total bit budget is actually allocated to frames and coding units, and *quantization selection*, where the quantization parameter (QP) is adjusted in function of the allocated bits.

This thesis focuses in particular on the frame level bit allocation, whose goal is to achieve an optimal trade-off between rate and distortion, under a time-varying constraint imposed to one of such variables. The optimal rate allocation for video is a non-trivial problem, because of the frame-level dependency induced by motion compensation. In order to circumvent this difficulty, one can allocate the bit budget independently for each frame, yielding a simpler formulation that can be tackled with standard numerical methods, such as Lagrangian optimization [SW98a] or dynamic programming [OR98, MGL05, MXOW12a].

Given the suboptimal nature of frame-by-frame approaches, a substantial research

effort has been made in the last decade to enlarge the optimization scope from a single frame to a group of frames (GOP). One of the first attempts in this sense was made by Ramchandran *et al.* [ROV94], who used an operational R-D framework to search the optimal combination of quantization parameters (QP) for the whole GOP: once evaluated all the couples $(R_n(Q_1, Q_2, \ldots, Q_i), D_n(Q_1, Q_2, \ldots, Q_i))$, where $\{Q_n, D_n(Q_n), R_n(Q_n)\}$ refer to QP, distortion, and bit rate for frame n, the method performs an exhaustive search of the R-D point with the minimum Lagrangian cost under a total bit rate constraint. Although it was conceived for the allocation at frame level, this method has been extended to different coding levels, such as blocks within the same frame [YH00]. While these methods guarantee the R-D optimality, they require to evaluate a huge set of points for each frame, making the computational burden very high.

The obstacle encountered by search-based techniques is that the R-D behaviour of a residual frame is unknown before encoding the frames from which it was predicted. A possible approach to circumvent this difficulty amounts to estimating the distortion of such residuals on the basis of the encoded version of their reference frames [LO98, LCGK10, HKZK11]. Although the optimality is not guaranteed (due to the inaccuracy of the model), these methods can greatly decrease the computational complexity and yield promising results.

Within this context, a more theoretical approach dates back to Uz *et al.* [USC93], who proposed a recursive R-D model to describe the dependency between frames, and approached the frame-level rate allocation from a Lagrangian perspective. This recursive model was later extended at pixel level for heuristically selecting the optimal quantization parameters [VO10]. More recently, a similar approach was used to formulate the rate allocation as a non-convex optimization problem, thus requiring a sequence of approximations to be solved [PAZ+13]; model-based solutions were also applied for wavelet motion-based filtering [ACAB07, CAAB04]. The principle behind the recursive approach was also used in distributed video coding (DVC) to analyse the R-D performance of new schemes for multi-view DVC [MPP08].

Some other works focus on minimizing the maximum distortion of encoded frames (MINMAX), instead of the usual average of distortions (MINAVE), as the former criterion might lead to some benefits to the visual perception [HJH99]. The MINMAX criterion can be optimized through dynamic programming [SMK99], multi-pass approaches [XCL06], or ad-hoc iterative methods with lower encoding complexity [CSR+07]. However, it is not clear whether the MINMAX is always a better criterion than the more classical one.

Contributions

The methods proposed in the literature to deal with the frame-level rate allocation are either theoretical in nature [USC93], computationally demanding [ROV94], approximated [PAZ+13], or based on the MINMAX criterion [CSR+07]. In this thesis, we propose an

efficient solution to exactly solve the frame-level rate allocation problem formulated with the MINAVE criterion. Our approach is based on a recursive R-D model in which the error variance of a residual frame is decoupled in two terms: the distortion of the frame used to build the prediction, and the inaccuracy of motion estimation. Our method was applied to H.264/AVC video encoder as well as HEVC video encoder, in its single view and multi-view versions. An encoding framework has been developed, based on:

- An accurate R-D model for the frames of a GOP able to describe dependencies between the distortions of the frames; we used the same theoretical foundations as in [USC93], but we extend the R-D model by letting the exponential decay vary at each frame, allowing us to better represent the intrinsic non-stationarities in a group of frames. With this model we express the distortion of each frame inside a GOP as a function of the rate used to encode the frame, and we are able to take into account the dependencies between the frames using the motion estimation error, and the texture characteristics of the sequence using the variance of the frame and two model parameters α and β which change the exponential decay of [USC93]. This model allow us to formulate the frame-level allocation problem as a convex optimization problem and use convex optimization techniques to solve it in an accurate and efficient way.

- An efficient algorithm based on modern convex optimization [CP11c, Con13, CP12, Vu13, KP15, CPPPP14], in order to find the optimal solution in limited time even for hundreds of frames. The algorithm was developed in collaboration with Dr. Giovanni Chierchia, whose work on proximal algorithms represented an important base for this thesis. An interesting feature of the algorithm is that its complexity is not affected by the total number of frames in a video sequence, thanks to the fact that it is implemented so that the optimization process works in parallel over the GOPs.

- A modified version of the video encoder, whose rate control module is able to accept as inputs the solutions of the convex optimization algorithm, *i.e.* a vector containing the optimal rate for each frame, and uses the allocated rates for the quantization parameter selection.

We verified the accuracy of the R-D model proposed for the single-view case on typical H.264/AVC and HEVC sequences. The model was adapted to the multi-view scenario in order to take into account the inter-frame dependencies; the minimization algorithm was modified as well. We compared our method to the standard rate control of the considered encoders and, in the single-view case, we compared our results to an exhaustive search method presented in [ROV94]. Our experiments indicate that the optimal rate allocation, when supported by an accurate R-D model, attains better results in terms of Δ PSNR and % bit rate than the standard rate control in HEVC. Moreover, the comparison with

the exhaustive search method showed an average loss of 9% in terms of bit rate, which is widely compensated by an execution time that is two hundred times faster.

Structure of the manuscript

This manuscript is composed of four distinct parts, corresponding to just as many chapters. In the first chapter background notions on video coding are reported. Then the second chapter introduces the basic concepts of rate distortion optimization (RDO) for video coding. The third chapter presents the basic concepts of convex optimization based on proximal algorithms and our recursive frame-level rate-distortion model. The fourth chapter presents our experimental results. More precisely, the manuscript is organized as follows:

- In Chapter 1 some background notions related to video compression are presented, including the concept of hybrid video coder and objective metrics for the evaluation of the distortion. Then follows a summary of the evolution of video coding standards and finally a detailed description of the two latest standards H.264/AVC and HEVC, as well as the HEVC multi-view extension.

- In Chapter 2 we define the rate-distortion function and introduce some rate-distortion models used in video coding. Then we define the problem of bit allocation under a bit-budget constraint and present the Lagrangian optimization as a possible solution to the minimization problem. We explain the concept of rate-distortion optimization and how RDO techniques are used in video encoders. Finally, we give some details of rate-control module of HEVC which uses RDO techniques.

- In Chapter 3 we introduce the basic concepts of convex optimization based on proximal algorithms, presenting the proximal operator and introducing the forward-backward splitting, in order to address the problem of optimal frame-level bit allocation for HEVC. Then we present our recursive frame-level rate-distortion model, define the bit allocation problem at frame level and present a solution based on the forward-backward spitting. Finally, we present some results to validate our R-D model and asses the effectiveness of our optimization method.

- Chapter 4 presents the results to validate our convex optimization algorithm for frame level bit allocation on the HEVC platform. Our method is compared to the standard R-λ rate control scheme of HEVC, and the bit allocation method in [ROV94] which performs an exhaustive research among all the possible R-D operating points. Finally, we present the results obtained by adapting our method to the multi-view scenario integrating our rate allocation algorithm to MV-HEVC.

This manuscript ends with a summary of the proposed method and the associated results, as well as some perspectives for future work.

Chapter 1

Background notions

Contents

The target of this thesis is to propose a novel framework to perform optimal bit rate allocation for video coding using convex optimization techniques. Consequently, we begin this manuscript with the fundamentals of video coding. In this chapter, we introduce the basic concepts of image and video compression. First we discuss the necessity and the

feasibility of image and video compression. The transform paradigm is introduced as well as the basics of predictive coding, and objective metric for the evaluation of the distortion are presented. Then we give a summary of the evolution of video coding standards and finally the latest two standards, H.264/AVC and HEVC, are explained in details.

1.1 Basic concepts of video coding

Video signals contain information in three dimensions, referred to as *spatial* and *temporal* domains. In particular, given the three-dimensional signal $I_k(m, n)$, the pair (m, n) defines the space, and k the time; a single image $I_k(m, n)$ is called frame. The human visual system is able to form, transmit and analyse $10 - 12$ separate images per second and perceive them individually [RM00], and an illusion of continuity can be created by showing more than 12 frames per second (fps). This principle is the base of the video sequence representation and is the reason for using a rate of capture of 15 to 30 images per second; this rate is referred to as frame rate f.

An uncompressed digital video sequence requires a very large amount of data to be stored and transmitted. For a single monochromatic digital still image with N rows, M columns and B bits of grey level resolution, the storage required is NMB bits; for a trichromatic image composed by Red (R), Green (G) and Blue (B) components this quantity increases three times, and a 512×512 image at 8 bits requires nearly a megabyte of digital storage space; considering the additional third dimension with a frame-rate of 30 fps, a 512×512×8×3 color video sequence occupies 23.6 megabytes for each second, requiring ~ 85 gigabytes for a 2-hour long digital film.

Therefore in practice it is necessary to compress video, *i.e.* to reduce the number of bits used in its representation. Traditional video coding techniques focus on eliminating the redundant elements of a video sequence in order to obtain the best reduction with an acceptable loss in quality [Bov00]. In particular, video compression feasibility rests with two types of redundancies, *i.e.* statistical redundancy and psycho-visual redundancy.

1.1.1 Statistical redundancy

Statistical redundancy can be classified into two types: *spatial* redundancy and *temporal* redundancy [SS08], as shown in Figure 1.1.

- Spatial redundancy is concerned with the statistical correlation between pixels within a frame. Within an image frame, except for the edge regions, most of the intensity values change continuously from pixel to pixel, resulting in a very high correlation along a row or a column. As a result, the intensity value of a pixel can be predicted from the neighbouring ones, meaning that it is not necessary to represent each pixel in a frame independently.

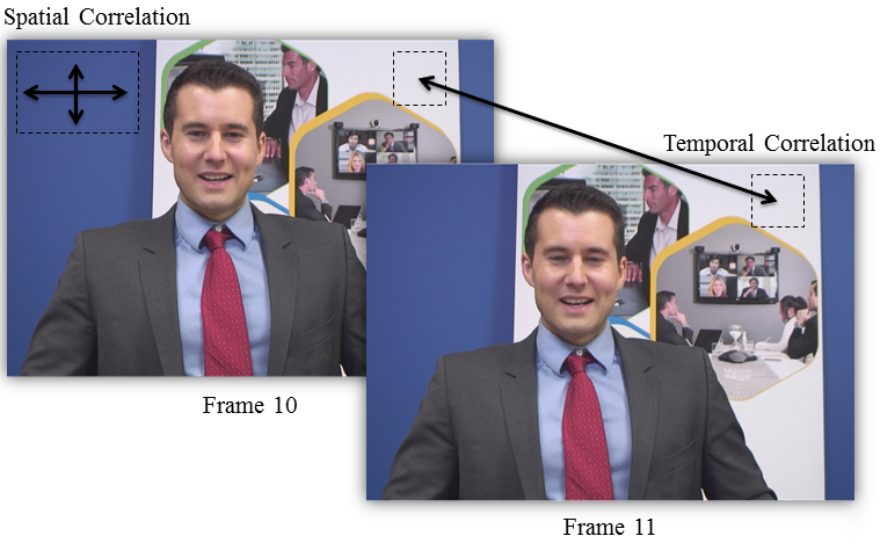

Figure 1.1: Spatial and temporal redundancy

- Temporal redundancy, or inter-frame redundancy, represents the statistical correlation between pixels from consecutive frames in a video sequence. For a temporal image sequence, taken by a fixed camera, with a short time interval between two consecutive pictures, it is easy to imagine that the similarity between two neighbouring frames is strong, producing a high inter-frame correlation. As a result, it is possible to predict a frame from its neighbouring ones along the temporal dimension.

1.1.2 Pshychovisual redundancy

The human visual system (HVS) is unable to respond with equal sensitivity to all incoming visual information; some pieces of information may be more relevant than others. The knowledge of which type of information are more or less important to the HVS have led to techniques able to eliminate or reduce psycho-visual redundancy. Some aspects of the HVS are briefly discussed in this section. They are luminance masking, texture masking, frequency masking, temporal masking, and color masking.

- Luminance masking states that the sensitivity of the eye to a stimulus depends on the intensity of another stimulus simultaneously present. In particular, contrast sensitivity is a measure of the ability to discern between luminances of different levels in a static image, and many contrast sensitivity functions have been presented in the literature [Wat87, LF80].

- Texture masking states that the discrimination threshold increases with increasing picture details [CBL72, NP77, Lim90, Mit96], *i.e.* the human eye is more sensitive to noise in smooth regions than in textured regions of a frame.

- Frequency masking states that the discrimination threshold increases with frequency

increase, *i.e.* the HVS is less sensitive to the high-frequency content [CBL72]. Transform coding, discussed in 1.2.3, relying on frequency masking, uses a discrete cosine transform (DCT) to drop some high-frequency coefficients with small magnitudes achieving data compression without loss of visual quality.

- Temporal masking states that the HVS is not able to immediately adapt itself to the scene when the scene changes abruptly, and during the transition it is not sensitive to details. The masking effect takes place before the abrupt change, in which case is called backward temporal masking, as well as after the scene change, and it is referred to forward temporal masking [Mit96] This effect has to be taken into consideration when allocating data in video coding.

- Colour masking is related to the sensitivity of HVS to the visible light. In particular, HVS is much more sensitive to the luminance, which is concerned with the perceived brightness, than to chrominance, which is related to the perception of the dominant wavelength of a color (hue) and its purity (saturation) [VNB67, Mul85]. This implies that, in video coding, data compression can be obtained by allocating more bits to the luminance component than to the chrominance, using of full resolution for the intensity component, and a sub-sampling both horizontally and vertically for the two chrominance components.

1.2 Transform coding paradigm

is a class of data compression algorithms that allows the original data to be perfectly reconstructed from the compressed data. By contrast, lossy compression permits reconstruction only of an approximation of the original data

As discussed above, compression of a video is necessary in order to reduce the amount of data necessary for the storage and the transmission, and can be achieved using lossless techniques, which allow the original data to be perfectly reconstructed from the compressed data, or lossy techniques, which permit reconstruction only of an approximation of the original data. We can define the compression rate as:

$$\text{Compression Ratio} = \frac{\text{Uncompressed Size}}{\text{Compressed Size}}. \tag{1.1}$$

Lossless compression [RS01] is not very efficient, achieving a compression ratio of $3 - 4$. However, lossless compression techniques are used in video encoder, in addition to lossy techniques, in order to remove statistical redundancy from data.

Lossy compression [Sal07] is necessary in order to achieve a high compression ratio required for digital videos, being able to reduce both statistical and psycho-visual redundancy without affecting the viewer's perception of visual quality in a significant way. Visual

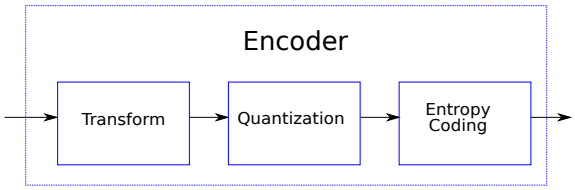

Figure 1.2: Lossy compression scheme

quality is, therefore, an important factor in image and video compression, and quality measures play an important role in visual communications.

Consider a generic image processing system, where $f(m,n)$ is the input, and $g(m,n)$ is the output of the system; in the specific case of video compression system, the input is the original image $I_k(m,n)$ and the output is the decoded one $\widehat{I}_k(m,n)$. In evaluating the quality of $g(m,n)$, we define the following functions:

- Error Function
$$e(m,n) = f(m,n) - g(m,n) \tag{1.2}$$

- Mean Absolute Difference (MAD)
$$\text{MAD} = \frac{1}{MN}\sum_{n=1}^{N}\sum_{m=1}^{M}|e(m,n)| \tag{1.3}$$
where M and N are horizontal and vertical dimension of the image,

- Mean Square Error (MSE):
$$\text{MSE} = \frac{1}{MN}\sum_{n=1}^{N}\sum_{m=1}^{M}e(m,n)^2 \tag{1.4}$$

- Peak Signal-to-Noise Ratio (PSNR)
$$\text{PSNR} = 10\log_{10}\left(\frac{(s^L-1)^2}{\text{MSE}}\right) \tag{1.5}$$
where L indicates the bit depth.

A typical lossy image compression scheme is shown in Figure 1.2: the encoder consists of a linear transform operation, a quantization and a variable length coder (VLC) [Bov00]. The transformation decorrelates the data, the quantization reduces the required bit rate and the VLC performs a lossless coding to reduce statistical redundancy. We separately describe each block in the following sections.

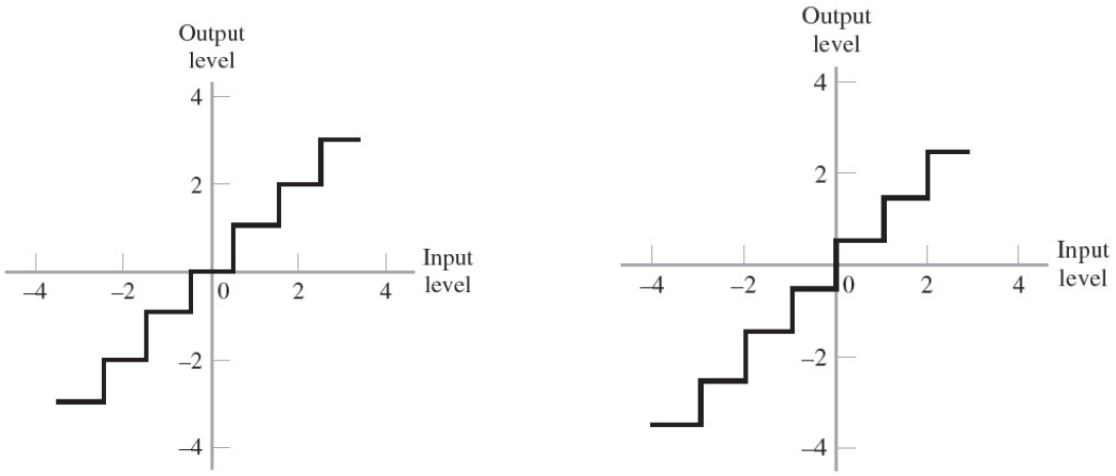

(a) Mid-tread quantization

(b) Mid-riser quantization

Figure 1.3: Input-output characteristic of uniform quantizers

1.2.1 Quantization

Quantization is a non-linear irreversible process of converting a continuous-valued signal into a discrete-valued signal which has a discrete range. This process has the purpose of reducing the necessary rate for the data representation, and is the core of all lossy compression algorithms. The difference between an input value and its quantized quantized value is referred to as quantization error, that can be evaluated objectively or subjectively depending on the application [GG92]. In general, quantization is a mapping from a set S to a discrete subset C of cardinality N.

$$Q : x \in S \to C = \{y_1, \ldots, y_N\} \tag{1.6}$$

The set S is divided into regions R_i for $i = 1, \ldots, N$, where $\cup_{i=1}^{N} = S$ and $S_i \cap S_j = \emptyset$. A region R_i is defined as

$$R_i = \{x \in S : Q(x) = y_i\} \tag{1.7}$$

If N is a power of 2, the number of bits required for each symbol of C is $R = \log_2 N$. If $x \in R_i$, the reconstructed value y_i is associated to x. The quantization can be seen as a cascade of two operations: an encoding operation, where the value $x \in R_i$ is mapped to the index of the region i to which it is associated; a decoding operation where the index i is mapped to the reconstruction value y_i. If all the regions R_i are intervals of the same amplitude and y_i is the center of the region R_i, the quantization is called uniform. Figure 1.3 shows the input-output characteristic of a uniform quantizer:the end points of the interval are called decision levels, the output of the quantization is referred to as the reconstruction level, the length of the interval is called the step size of the quantizer and denoted by δ. In particular, Figure 1.3 shows two typical examples of uniform quantizers:

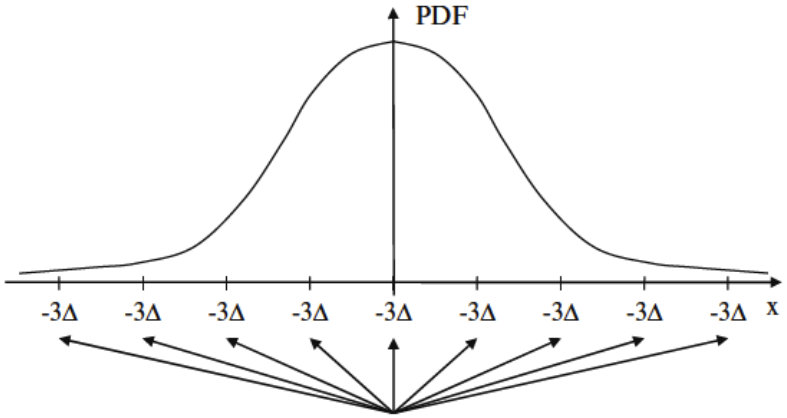

(a) Resources are uniformly allocated for a uniform quantizer

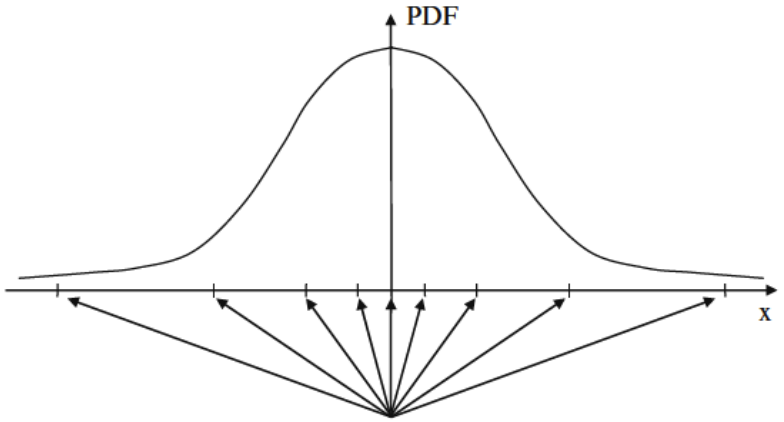

(b) Resources are nonuniformly allocated for a nonuniform quantizer

Figure 1.4: Quantization resources are under-utilized by the uniform quantizer (a) in the tail areas and over-utilized in the head area of the PDF. These resources are re-distributed in the nonuniform quantizer (b)

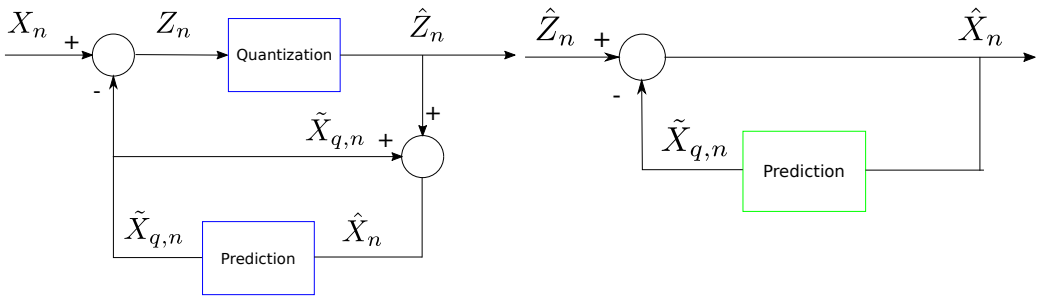

(a) Encoder (b) Decoder

Figure 1.5: Predictive coding

mid-tread and mid-riser. Mid-tread quantizers have a reconstruction level that is exactly zero, as shown in Figure 1.3(a), while mid-riser quantizers have a decision level that is exactly zero, as shown in Figure 1.3(b)[GG92].

Uniform quantization is the best choice for uniformly distributed signal, otherwise a quantizer with classification intervals of different sizes has to be used. In this case, called non-uniform quantization, optimal regions and optimal reconstruction values can be evaluated according to the statistic of the input signal x; an example of non-uniform quantizer is shown in Figure 1.4. An iterative procedure to perform those choices is the Lloyd-Max algorithm [Llo82], which gives optimal reconstruction values and optimal regions according to the statistics of the input signal X. As shown in Figure 1.4(b), the less probable range of values is coarsely quantized than the most probable region. In this case, considering that the source can be modelled as a random variable X and the distortion is defined as $D = \mathbb{E}[|X - \widehat{X}|^2]$, at high resolution it is possible approximate D as

$$D = h_X \sigma_X^2 2^{-2R}$$

where σ_X^2 is the variance of X, h_X is a shape factor that depends on the probability density function (pdf) of X, and R is the number of bit used for the quantization.

1.2.2 Predictive coding

Rather than encoding a signal directly, differential coding techniques, also known as predictive coding, encodes the difference between the signal and its prediction. As discussed in Section 1.1.1, video signals present a large amount statistical correlation, and by exploiting the spatial and/or the temporal correlation between pixels in the prediction, the predictive coding represents a very efficient choice in the context of compression. Consider a discrete random process X_n, let $\widetilde{X}_n$ be the prediction of X_n, *i.e.* a function of the M previous samples:

$$\widetilde{X}_n = f\left(X_{n-1}, X_{n-2}, \ldots, X_{n-M}\right), \tag{1.8}$$

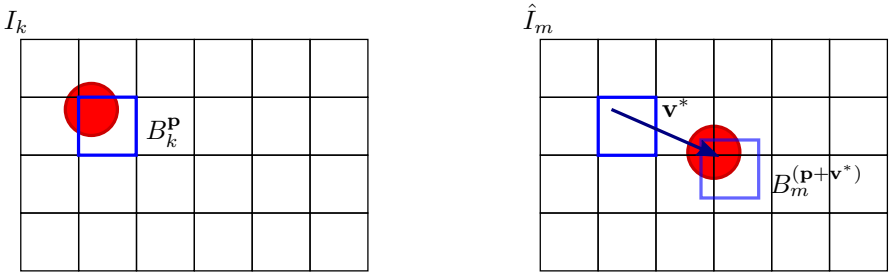

Figure 1.6: Motion estimation and compensation.

the principle of prediction is to quantize Z_n instead of X_N, where

$$Z_n \triangleq X_n - \tilde{X}_n \tag{1.9}$$

Defining $\widetilde{Z}_n$ and $\widetilde{X}_n$ as the reconstructed values of Z_n and X_n, we obtain that

$$\mathbb{E}\left[|X_n - \widehat{X}_n|^2\right] = \mathbb{E}\left[|X_n - \widetilde{X}_n + \widetilde{X}_n - \widehat{X}_n|^2\right] = \mathbb{E}\left[|Z_n - \widehat{Z}_n|^2\right] \tag{1.10}$$

This way, it is possible to reduce the distortion of X_n by quantizing Z_n: the the variables X_n are correlated with each other, the more the variance of the prediction error Z_n is smaller than the one of X_n. Figure 1.5 shows the prediction scheme at the encoder (a) and at the decoder (b). In order to have the same prediction at both sides, instead of considering $\tilde{X}_n$, we consider

$$\widetilde{X}_{q,n} = f\left(\widehat{X}_{n-1}, \widehat{X}_{n-2}, \ldots, \widehat{X}_{n-M}\right). \tag{1.11}$$

Motion estimation and compensation

Motion estimation and compensation are simple differential coding techniques used to exploit the temporal redundancy of video signals. The current frame I_k is predicted from a previously transmitted neighbouring frame $\widehat{I}_m$ by estimating and compensating the objects' motion [Bov00, PPCD14]. If the two frames are very similar, it is more efficient in terms of R-D performance to send the estimated motion vectors and the prediction error. First of all, the frame I_k is divided into blocks of size M×M, then the current macroblock $B_k^{\mathbf{p}}$ in position $\mathbf{p}$ is predicted from another macroblock of frame $\widehat{I}_m$; a vector $\mathbf{v}$ that models the movement of a block from position $\mathbf{p}$ to position $\mathbf{p}+\mathbf{v}$ and called *motion vector* (MV) is created. Formally, the optimal motion vector $\mathbf{v}^*$ in the search window W is:

$$\mathbf{v}^* = \arg\min_{\mathbf{v}\in W} d(\mathbf{v}) \ . \tag{1.12}$$

where $d(\mathbf{v})$ is a cost function

$$d(\mathbf{v}) = d\left(B_k^{\mathbf{p}}, B_m^{(\mathbf{p}+\mathbf{v})}\right). \tag{1.13}$$

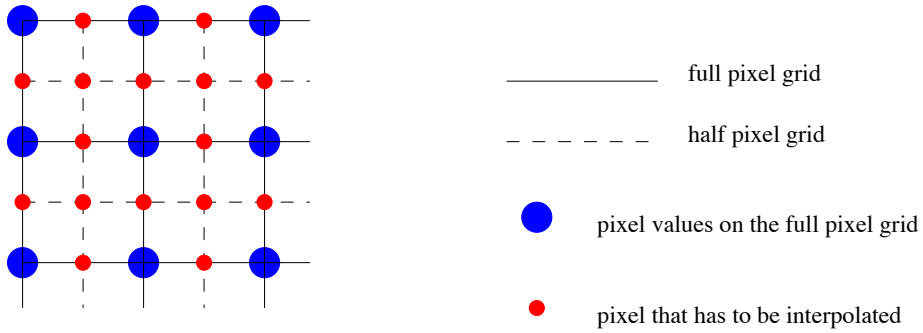

Figure 1.7: There is no pixel value at the half-pixel locations: interpolation is required to produce the pixel values at the half-pixel positions.

The movement calculated for all the block of a frame constitutes the motion estimated in a frame. This motion vector field is sent to the decoder which, using the motion vector $\mathbf{p}$, can produce the prediction of I_k from the reconstructed frame $\widehat{I}_m$; this operation is called motion compensation (MC). Figure 1.6 shows an example of motion estimation and compensation.

Motion estimation with sub-pixel precision

In video sequences, an object often moves to a position that is not on the grid but between the pixels, while the motion estimation introduced in the previous section is restricted to only integer pixel accuracy. As shown in Figure 1.7, an interpolation is required since there is no pixel value at the half-pixel locations. In order to implement the motion estimation with $1/N$-pixel precision, the image $\overline{I}_m$ has to be created from an expansion of the reconstructed reference image $\widehat{I}_m$ by a factor N. For each block of the frame I_k, a research is performed to find the most similar to it in the frame $\overline{I}_m$, and the obtained vector that describes the displacement is divided by N.

1.2.3 Transform

The first step of the chain shown in Figure 1.2 is the transform. The basic idea of transform coding (TC) is that the transformed version of the image is less correlated and the energy is compacted in the transform domain, so that a few quantized non-zero coefficients have to be encoded. A meaningful interpretation of TC considers the original image to be a weighted sum of basis images, where the weights are the transform coefficients. These weights, which are essentially a measure of the correlation between the original image and the corresponding basis image, are less correlated than the image pixels, and have a great disparity in variance distribution. The weights with large energy are finely quantized, the weights with small energy are coarsely quantized, while the majority of weights are insignificant and discarded. Since the quantized non-zero coefficients have a very nonuniform probability distribution, variable-length codes can be used, achieving a high coding efficiency.

Several linear, reversible, unitary transforms have been utilized in TC, including discrete Karhunen-Loeve transform (KLT) [Kar47, Loé48], the Discrete-Fourier transform (DFT) [CT65], the Walsh transform [Wal23], the Hadamard transform [Had93] and the Discrete-Cosine transform (DCT) [ANR74]. The KLT represents the optimal transform, able to decorrelate produce uncorrelated transform coefficients, and to compact most of the energy in a small fraction of the coefficients. However, KLT can not be used in practice since it requires the calculation of the image block covariance matrix for every transformed image block, for which no fast algorithm exists. In practice, the best choice among the other transforms is the DCT: it is not data dependent,it results very close to the optimum KLT in terms of energy compaction, and it can be implemented with a fast algorithm. Moreover, it has been found to be efficient not only for coding still images, but also for coding residual images in predictive coding, resulting a valuable tool for video compression.

1.2.4 Lossless coding

As shown in Figure 1.2, the last step of a lossy compression scheme is lossless coding, also called entropy coding. Given a random variable X with an alphabet of cardinality M, the entropy of X is defined as

$$H(X) = -\sum_{i=1}^{M} p_i \log_2(p_i) \tag{1.14}$$

where $p_i = Pr(X_k = x_i)$. The Shannon source coding theorem establishes that a sequence of N i.i.d. random variables X_k with entropy $H(X)$ can be compressed into more than $NH(X)$ bits with negligible risk of information loss, as $N \to \infty$. Lossless coding attempts to minimize the average number of bit per symbol getting close to the theoretical limit of the entropy. This is usually achieved by using variable length codewords, where shorter codewords are assigned to most probable symbols. Huffman coding [Huf52], arithmetic coding [HV92] and Lempel-Ziv (LZ) [ZL77] are the commonly used coding schemes.

1.3 Video coding standard evolution

The VCEG (Video Coding Expert Group) of the ITU-T (International Telecommunication Union) and the MPEG (Moving Picture Expert Group) formed by ISO (International Standard Organization) and IEC (International Electrotechnical Commission) are the two major international standardization organizations, responsible for standardization of H.261 [Lio91] and H.263 [CEGK98] the former, MPEG-1 [ISO] and MPEG-4 [Ric04] the latter. The two groups collaborated to produce, in 1994, H.262/MPEG-2 [Has97] and formed the Joint Video Team (JVT) in 2001 to develop H.264/MPEG-4 AVC [SOHW12b] and, in 2010 the Joint Video Team on Video Coding (JCT-VC) for the development of H.265 also known as High Efficiency Video Coding (HEVC) [SSB14].

The very first of the H.26x standard is H.261. The standard is based on the so called

block-based hybrid video coding approach with the introduction of the concept of macroblock (MB) as basic processing unit and inter-picture prediction to reduce temporal redundancy. MPEG-1, designed by MPEG for low-resolution applications, is based on motion compensated transform coding and the main coding tool are the conversion to YUV space color with UV sub-sampling, 8×8 DCT transform for spatial de-correlation, bi-directional inter-prediction and sub-pixel precision motion estimation and compensation. Used by many digital cable and satellite TV services, MPEG-1 was replaced by H.262/MPEG-2 and used for both transmission media and digital storage media such as DVD. Motion compensation with blocks of 16×16 and scalability tools are introduced.

H.263, standardized in 1993 by VCEG, was developed for video conferencing at low bit-rate in the mobile wireless communication scenario. It is based on H.261 and adopts a hybrid inter-picture prediction with 16×16/8×8 block based motion compensation and 8×8 DCT. MPEG-4 standardization started in 1998 with the intent to deal with multimedia content in object-based, interactive and non-linear way. New coding tools are introduced, such as object and shape coding, face modelling, wavelet-based still image coding and scalable video coding.

H.264/MPEG-4 AVC and HEVC are the last video coding standard, whose first version was published in 2003 and 2013, respectively. The following sections give some more details about both standards.

1.4 H.264/AVC standard

Developed by the JVT of the ISO/IEC and ITU-T VCEG as a coding standard of high coding efficiency, H.264/AVC can save about 50 % bit rate compared with the prior coding standards under the same reconstructed picture quality [WSJ+03]. Released in 2003 [Joi09], the main goals of the standardization effort have been enhanced compression performance and provision of a "network friendly" video representation addressing "conversational" applications, such as video telephony, and "non-conversational" applications, such as storage, broadcast of streaming [STL04]. An overview of the main technical features of H.264/AVC is provided.

1.4.1 Coding structure

H.264/AVC is designed, as well as all prior ITU-T and ISO/IEC JTC1 video standards since H.261 [Int90], following the block-based hybrid video coding approach depicted in Figure 1.8. YCbCr is the color space used by H.264/AVC, where the colors representation is separated into three components: the luma component Y represents the brightness, the two chroma components Cb and Cr represent the extent to which the color deviates form gray toward blue and red respectively. Because the HVS is more sensitive to luma than chroma, as already stated in Section 1.1.2, a sub-sampling of the chroma component is

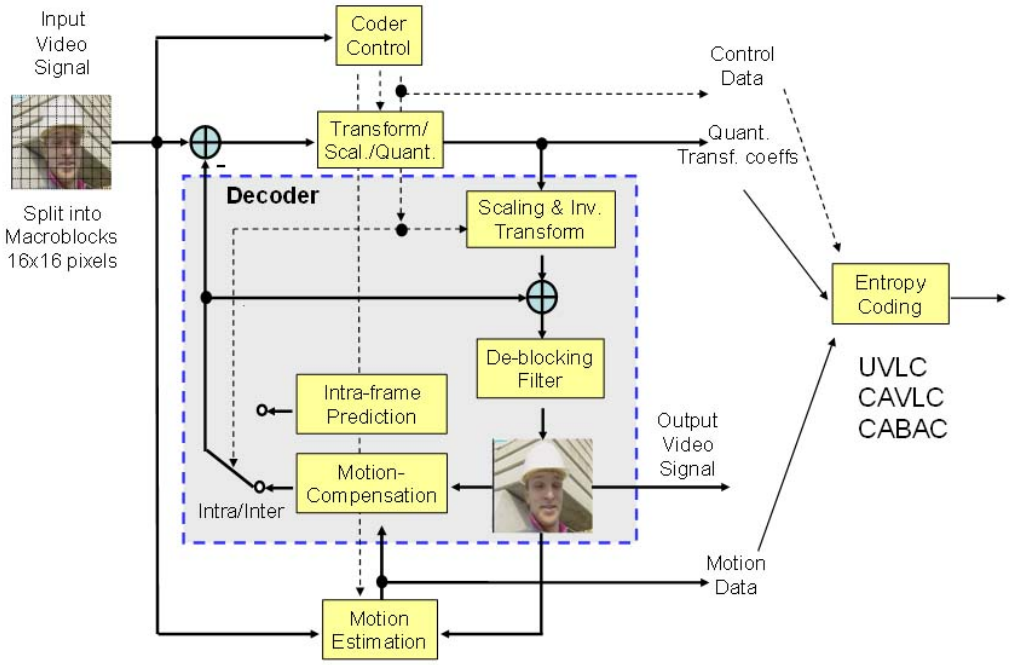

Figure 1.8: Basic coding structure for H.264/AVC for a macroblock

applied to reduce the color information. The color structure is denoted by 4:2:0 in which the chroma signals are sub-sampled by 2 in both horizontal and vertical dimensions, and each sample is encoded with 8 bits of precision. Macroblocks are the building blocks of the standard: each encoded picture is represented in block-shaped units of associated luma and chroma samples called macroblocks. Each MB covers a square area of 16×16 samples of the luma component and 8×8 samples of the two chroma components used in the color space representation [WSBL03]. Different frames are organized into group of

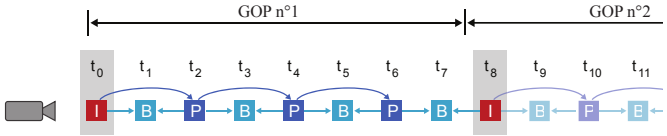

Figure 1.9: Example of a GOP

pictures (GOP), as shown in Figure 1.9. A picture can be split into one ore several slices: a slice is a sequence of macroblocks processed in the order of a raster scan.Each slice can be coded using different coding types:

- I slice: all the macroblocks are coded using intra-frame prediction, *i.e.* spatial prediction without reference to the content of some other picture
- P slice: in addition to intra prediction, some macroblocks can be coded using inter-frame temporal prediction from past slices; skip mode, where no information is sent for the macroblock, is also available

- B slice: all the coding types presented for P slice are available and some macroblocks can be coded using inter prediction from future slices and from average of past and future slices.

Lagrangian rate distortion optimization (RDO) method is used to select the coding mode with highest coding efficiency [LJ03]: the encoder selects the mode that minimizes the cost function $J = D + \lambda R$, where a large value of λ gives more emphasis to the rate R than to the distortion D. Lagrangian RDO will be explained in more details in Chapter 2.

1.4.2 Intra-frame prediction

Intra-frame spatial prediction may be performed for 16×16 luma MB, denoted as INTRA_16×16, and 4×4 luma sub-block, denoted as INTRA_4×4.

INTRA_16×16 is well suited for relatively homogeneous image areas. For each 16×16 MB, one of four prediction modes can be utilized, as shown in Figure 1.10:

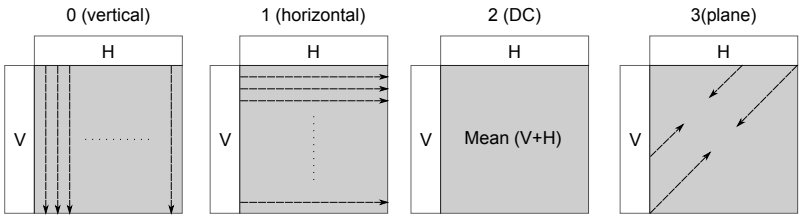

Figure 1.10: Intra-prediction modes for a 16×16 luma block defined in H.264/AVC

- Mode 0 (vertical): extrapolation from upper samples (H)
- Mode 1 (horizontal): extrapolation from left samples (V)
- Mode 2 (DC): mean of upper and left-hand samples (H+V).
- Mode 4 (Plane): a linear "plane" function is fitted to the upper and left-hand samples H and V. This works well in areas of smoothly-varying luminance.

INTRA_4×4 is more suited for for coding parts of a picture with significant details. Each 4×4 block is predicted from spatially neighbouring samples labelled A-M in Figure 1.11, according to nine different modes, as shown in the figure. Since chroma is usually smooth over large areas, chroma samples of a MB are predicted using similar prediction technique as for the luma component in INTRA_4×4.

1.4.3 Inter-frame prediction

Inter-prediction is designed to exploit temporal correlation between frames, and is supported by both P and B slices. The substantial difference is that, while P slices could use one only prediction form past frames, B slices could also use from future frames. Inter-prediction

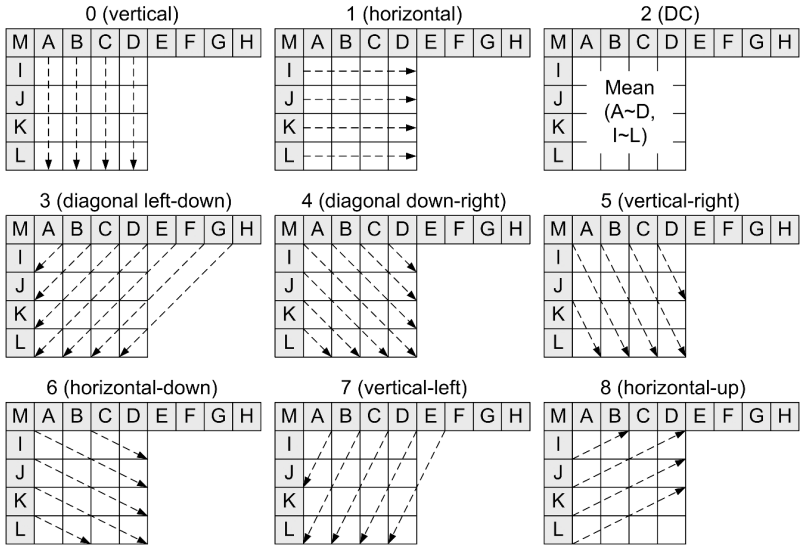

Figure 1.11: Intra-prediction modes for a 4×4 luma block defined in H.264/AVC

in H.264/AVC uses a variable size motion compensation: each 16×16 luma MB can be partitioned into blocks of different sizes. Partitions with block sizes of 16×16, 16×8, 8×16, 8×8 samples are supported; furthermore, each 8×8 can be sub-partitioned into partitions of 8×4, 4×8 or 4×4 luma samples. Figure 1.12 illustrate the partitioning.

Multiple reference frames can be used in a weighted fashion [FG03].The use of multiple reference frames may improve coding *occlusion areas*, where prediction from the previous frame result inaccurate.

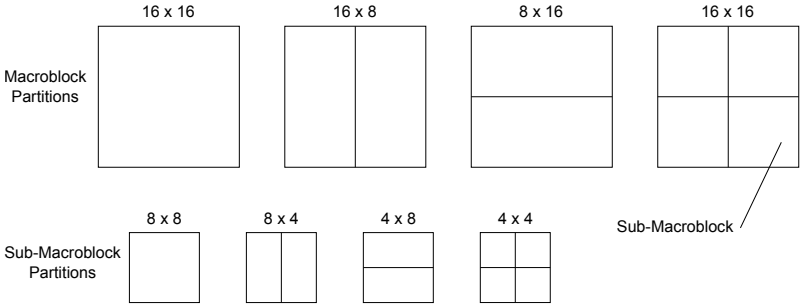

Figure 1.12: Segmentations of the macroblock for motion compensation

1.4.4 Transform and entropy coding

Similar to previous standards, H.264/AVC utilizes transform coding of the prediction residuals, with two main differences. First of all, the transform is applied to 4×4 blocks instead of 8×8 blocks, resulting in a reduction of ringing artefacts (spurious signals near sharp transitions). The encoder is also able to use 8×8 blocks for the transform in order to compress more efficiently highly correlated regions; an adaptive selection between the 4×4 and 8×8 transform block size is implemented in the encoder. Secondly, instead of a 4×4

DCT, a separable integer transform with similar properties as a DCT is used, resulting in an inverse transform defined by exact integer operations, avoiding inverse-transform mismatches. After the inverse transform at the decoder, a deblocking filter is added [LJL+03]: it consists in an adaptive low pass filter which reduces *blocking artefacts* by smoothing the block transitions.

H.264/AVC includes two different entropy coding techniques: context-adaptive variable length coding (CAVLC) [Joi09] and context-adaptive binary arithmetic coding (CABAC) [MSW03]. The first one is an adaptive variant of Huffman coding targeted at applications that require a simpler entropy decoder. The second one is based on arithmetic coding techniques: instead of encoding each symbol separately, it encodes an entire message in a single number between 0.0 and 1.0. CABAC achieves higher compression ratios than CAVALC, but it requires a greater computational effort for the decoding.

1.5 HEVC

The High Efficiency Video Coding (HEVC) standard is the most recent joint video project of the ITU-T video coding expert group and the ISO/IEC VCEG and ISO/IEC MPEG standardization organizations, working together in a partnership known as the Joint Collaborative Team on Video Coding (JCT-VC). The main goal of HEVC is to provide high coding efficiency for ultra high definition (UHD) content. Compared to the previous H.264/AVC, the new standard performs a 50% bit rate reduction for equal perceptual video quality[OSS+12]. HEVC is based on the same block-based hybrid video coding approach of its predecessors, and shares the same main structure of H.264/AVC with some differences. The main differences between the two standards are explained below.

1.5.1 Coding structure

The core structure in previous standards was the macroblok, a 16×16 block of luma samples and, in the usual 4:2:0 color sampling, two corresponding 4×4 blocks of chroma samples. HEVC uses an analogous structure called coding tree unit (CTU) [HMK+10] a picture is divided into CTUs, each CTU can be split into four coding units (CU), each CU can be further split into four CUs, and so on. This hierarchical block structure makes the encoding more adapted to the image content with the presence of different block sizes within the same image, and is limited by setting a maximum CTU size and a maximum depth level. The specific coding mode is chosen at CU level among four possibilities: Intra mode, Inter mode, Merge mode and Skip mode (further details in following sections).

Each CU can be divided into prediction units (PUs), which are the elementary elements to perform prediction. PU spitting can be asymmetrical in order to operate a more efficient prediction; Figure 1.13 shows the possible partition sizes. Furthermore, each CU can be partitioned into multiple transform units (TUs), used to define the size of the transform

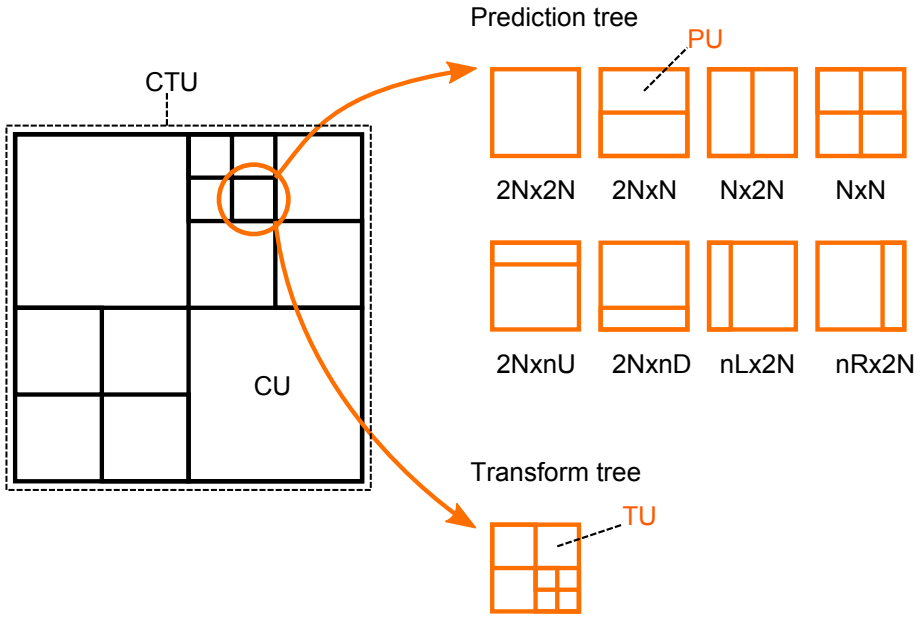

Figure 1.13: Quadtree structure of a CTU and possible partition shapes

and quantization to be applied, and which are organized in a quad-tree structure. The size of a TU varies between 4×4 and 32×32; in Intra mode, only square partitions are available, while in Inter mode rectangular TUs of size 4×4, 16×4, 8×32 and 32×8 are possible.

1.5.2 Intra-frame prediction

HEVC support various intra-picture predictive coding methods: two non-directional modes referred as Intra_Planar and Intra_DC, and 33 directional modes referred as Intra_Angular [LBH+12]. Each mode predicts the current PU from pixels of the neighbouring row above and column left of the current PU. Figure 1.14 shows the Intra modes used in HEVC, ordered according to the direction angle. Intra_DC uses an average value of reference samples for the prediction, resulting efficient to code uniform areas of the image. Intra_Planar uses an average value of two linear predictions using four corner samples and is adapted to smooth texture, preventing discontinuities along the block boundaries.

In order to reduce the number of bits used for signalling the Intra mode chosen for the prediction on a PU, HEVC considers two most probable modes (MPMs). If the best Intra mode for the current PU matches one of the MPM candidates, only 2 bits are used for signalling: one flag signals the use of an MPM and a second one signals which MPM candidate is used.

1.5.3 Inter-frame prediction

The Inter prediction-mode evaluates and transmits MVs, while its two variants, Skip and Merge [HOB+12], obtain the motion information from spatial or temporal candidates

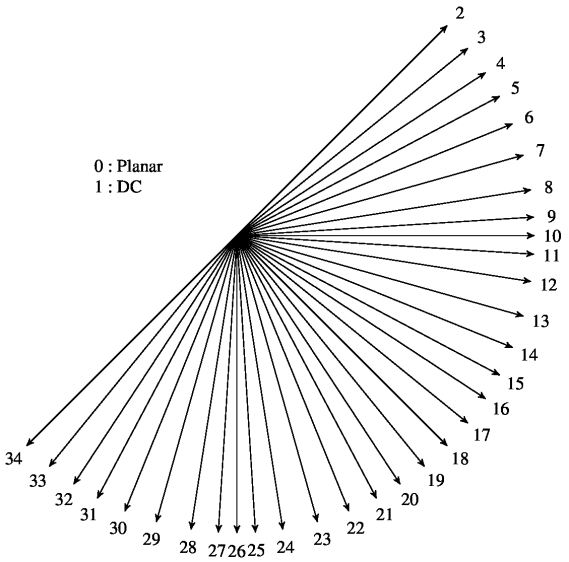

Figure 1.14: Intra modes in HEVC

(neighbouring block, spatially or temporally respectively), performing motion inference methods. If a PU is encoded in either Merge or Skip mode, the only transmitted information is the index of the selected candidate and, in the case of Skip mode, the residual signal is also omitted.

For the Inter mode, the advanced motion vector prediction (AMVP) [LJPP08]: two motion vector predictor are selected among an AMVP candidate set of MVs of the PUs covered by different neighbouring positions. Figure 1.15 shows the 5 spatial and 2 temporal candidates. The first spatial candidates is derived from A_0 and A_1, a second one from B_0, B_1 and B_2. If the two candidates are identical or one of the two is unavailable, a temporal candidate is derived from C_1 and C_2. Between the MV and the MVP, only one residual is sent, along with a index to signal which of the two candidates was selected.

In terms of motion compensation, quarter-sample precision is used for the MVs. Interpolation of fractional-sample positions is performed using 7-tap and 8-tap DCT-based filters. Similar to H.264/AVC, uni-predictive and bi-predictive coding is supported.

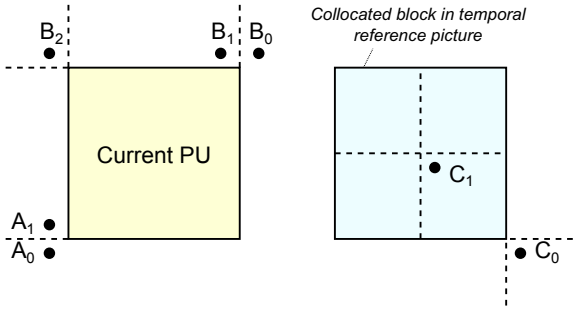

Figure 1.15: AMVP candidates in HEVC

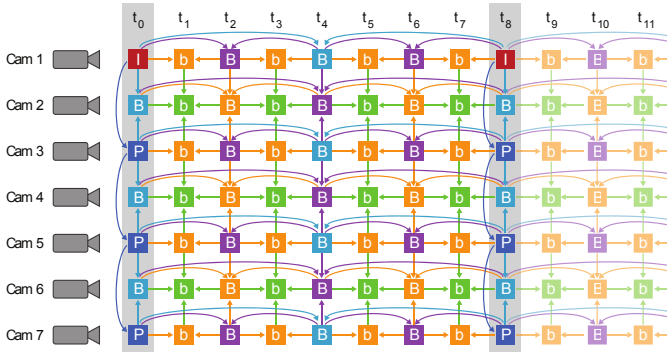

Figure 1.16: Multiview coding structure

1.5.4 Transform and entropy coding

HEVC relies on transform coding of the prediction error residual in a similar manner as his predecessor. As mentioned in Section 1.5.1, the residual block is partitioned into multiple square TBs. The basic transform is an approximated version of DCT, but an alternative integer transform based on the discrete sine transform (DST) has been implemented for 4×4 luma residual blocks for intra-picture prediction modes. RDO is performed in order to find the best combination of transform size and intra-prediction mode.

HEVC uses uniform reconstruction quantization (URQ) controlled by a quantization parameter (QP), with quantization scaling matrices supported for various block sizes. The QP ranges from 0 to 51, and is used to determine the quantization step used for the transformed coefficients according to the following relationship:

$$q = 2^{\frac{QP-4}{6}}. \tag{1.15}$$

Only one entropy coding method is specified in HEVC rather than two as in H.264/AVC, which is a faster version of CABAC entropy coding with a substantially less number of contexts. Similarly to H.264/AVC, deblocking filter is used, with the only difference that it is only applied to the edges that are aligned on a 8×8 sample grid, instead of a 4×4 sample grid.

1.5.5 Multi-view extension of High Efficiency Video Coding

In multi-view video (MVV) a single scene is shot simultaneously by N cameras arranged in different spatial positions [CPD13]. The resulting set of N 2D signals, called multi-view video, is very costly in terms of bitrate and needs to be efficiently compressed. In order to do so, the strong correlation between views should be exploited. Figure 1.16 shows a typical multi-view coding structure, where one of the views, denoted as base view, is coded independently of the other views, using only temporal prediction.

A multi-view extension of HEVC, referred to as MV-HEVC, was finalized in July 2014 [H2615], defined to allow multi-view coding with minimal changes to HEVC. The

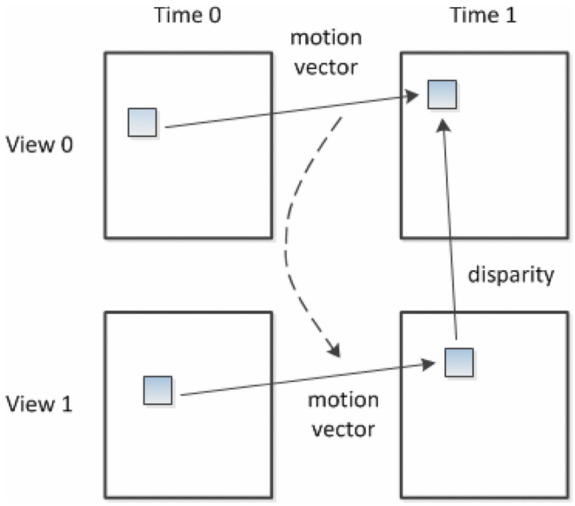

Figure 1.17: Motion prediction between views

key point of the multi-view extension is inter-view prediction, where a picture in the current view can be predicted from picture of different views at the same time instant. The mechanism is similar to the motion-compensated prediction, but based on pictures with different viewpoints rather than different time instants: a block-based disparity shift between current view and reference view is determined and used to perform a disparity-compensated prediction. Disparity is used to establish a correspondence between blocks in different views and to infer the motion information from one view to another. Figure 1.17 shows motion prediction between views: the motion vector of view 0 is used to infer the motion vector of view 1. In MV-HEVC, the inter-view prediction is realized in a way that is compatible with HEVC motion prediction scheme: the reconstructed base view is added to the reference picture lists of the dependent views.

Illumination changes between different views, caused by cameras non calibrated in color transfer or by lighting effects, may affect the inter-view prediction. In order to improve the coding efficiency for blocks predicted from inter-view reference pictures, illumination compensation (IC) was introduced [LJS+12]. Two parameters a and b are used to correct the inter-view prediction signal: instead of computing the residual r between the current PU coded with disparity-compensate prediction $\mathrm{PU}_{\mathrm{cur}}$ and its reference $\mathrm{PU}_{\mathrm{ref}}$ as $\mathrm{PU}_{\mathrm{cur}} - \mathrm{PU}_{\mathrm{ref}}$, it would be computed as:

$$\mathrm{PU}_{\mathrm{cur}} - (a \cdot \mathrm{PU}_{\mathrm{ref}} + b). \tag{1.16}$$

The two model parameters a and b are computed using reconstructed neighbour samples and they are not transmitted in the bit stream; a flag is used in order to communicate whether IC is applied or not.

.

Chapter 2

Rate-Distortion Techniques for Video Coding

Contents

The rate-distortion optimization is an important tool of video encoders that significantly improves coding efficiency by optimizing the amount of distortion against the amount of data required to encode the video. In order to ensure the interoperability between different products, in video coding standards only the bit-stream syntax and the decoding process are standardized, but rate-distortion optimization (RDO) techniques were used during the standardization process in order to evaluate the potential coding efficiency improvement provided by a tool proposed for inclusion in the standard.

In this chapter, we introduce the basic concepts of rate-distortion theory and the rate-distortion function, which describe the trade-off between the the amount of data required to encode the video and the obtained quality. Then, we explain the concept of rate-distortion optimization and how RDO techniques are used in video encoders. Finally, we give some details of rate-control module of HEVC which uses RDO techniques.

2.1 Rate-distortion theory

Rate-distortion theory [Ber71] is an important part of Information theory, actively studied for the last 50 years. Starting from the seminal work of Claude Shannon [Sha48, Sha59], R-D theory is strictly related with the concept of source coding or compression, addressing the problem of representing an information source with the fewest number of bits possible for a given reproduction quality [OR98]. In Section 1.2.4 we introduced the concept of lossless coding, where the decoded or decompressed data is an exact copy of the original. In the context of lossy compression, decoded data are not exact copies of the originals, and higher compression ratios are possible at the cost of imperfect source representation. The trade-off between source fidelity and coding rate is the core of R-D theory: a decrease in the bit rate used to encode the source (or the number of bits required for the storage or the transmission of the data) leads to an increase of the output distortion and vice versa, and R-D theory addresses the problem of determining the best compromise between the two.

2.1.1 Rate-distortion models

In Section 1.2.4 the entropy, which measures the amount of information of a random variable X, was defined in eq. (1.14). For two random variables X and Y, the mutual information is defined as:

$$I(X;Y) = H(X) - H(X|Y) \tag{2.1}$$

Considering X as the source signal, Y as the signal received through channel transmission and $d(x,y)$ as a distortion function, the rate-distortion function is defined as:

$$R(D) = \min_{p(y_j|x_j)} I(X;Y) \tag{2.2}$$

where $R(D)$ is the achievable rate at distortion D. For a given source, the rate-distortion region is a closure of achievable rate-distortion pairs (R,D), and a rate-distortion function is defined as the infimum of rates such that, for a given distortion, the couple is in the rate-distortion region of the source.

An analytical solution to this minimization problem is often difficult to obtain, and upper and lower bounds to this functions are used in practical cases; it is known, although, that the rate-distortion function of any source obey some fundamental properties: it is a continuous, monotonically decreasing convex function. A typical example of well known rate-distortion function is given in the following.

We consider a no-memory Gaussian source with zero mean and variance σ_x^2, which is a typical assumption for image data in video coding. Then, the probability density function is:

$$p(x) = \frac{1}{\sqrt{2\pi\sigma_x^2}} e^{-\frac{x^2}{2\sigma_x^2}}. \tag{2.3}$$

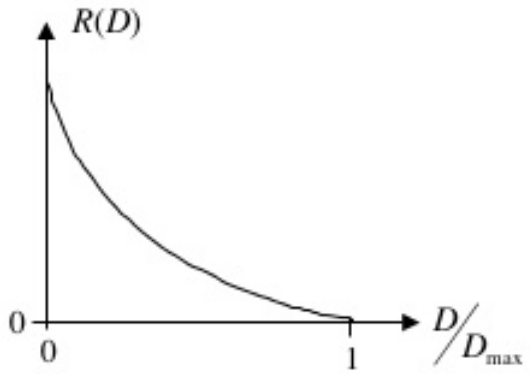

Figure 2.1: R-D function for a Gaussian memory-less source

If the MSE is used as a measure of the distortion, the rate-distortion function is:

$$R(D) = \begin{cases} \frac{1}{2}\log_2(\sigma_x^2/D) & \text{if } 0 \leq D \leq \sigma_x^2 \\ 0 & \text{if } D > \sigma_x^2 \end{cases} \tag{2.4}$$

Figure 2.1 shows this rate-distortion function. According to rate-distortion theory, no compression system exists that performs better than the R-D function: the closer a compression system is to the lower bound, the better it performs. In many practical cases, the rate is constrained by some bit budget. In video coding, since the quantization reduces the bit rate of the compressed signal in exchange of a certain distortion, a typical R-D optimization problem is to find the appropriate quantization step q for each transform coefficient that minimize a distortion measure D between the original and the reconstructed samples, under a constraint on the bit budget:

$$\min_q D(q) \quad \text{subject to} \quad R(q) \leq R_{budget}. \tag{2.5}$$

This problem can be reformulated using the Lagrangian multiplier $\lambda \geq 0$ which transforms the constrained problem into an unconstrained one:

$$\min_q J(q), \quad \text{where} \quad J(q) = D(q) + \lambda R(q) \tag{2.6}$$

where the Lagrangian cost J is minimized for a particular value of λ and each obtained q is an optimal solution [SW98a, WSJ+03]. The Lagrangian optimization will be discussed in Sec. 2.2.1, while the budget-constrained bit allocation will be presented in Sec. 2.2 and analysed in detail in Sec. 2.3 for HEVC video encoder.

In video coding, several works have been done presenting different models that relate the rate to parameters like the quantization parameter (QP) or the quantization step q:

- Linear model
- Quadratic model

- ρ-domain linear model
- Variable frame-rate rate model.

The linear model was introduced in [MSW12] and employed in the final test model of MPEG-2 (TM5). It is defined as:

$$R(q) = \frac{X}{q}, \tag{2.7}$$

where X is a model parameter.

The rate control in VM8 for MPEG-4 reference encoder [YA02] adopted a quadratic rate-quantization model in order to evaluate the quantization step q. It is defined as:

$$R(q) = \frac{a}{q} + \frac{b}{q^2}. \tag{2.8}$$

In order to enhance the accuracy of the RD model, a different version was used in H.264/AVC [LGP+06] and HEVC [NP12]:

$$R(q) = \frac{a \times d}{q} + \frac{b \times d}{q^2}, \tag{2.9}$$

where a and b are model parameters which are updated after encoding each frame and d is the mean absolute difference between the original and the reconstructed frame. Here, q is the quantization step size defined in the standard by a function of the quantization parameter QP. In [SAD12] has been introduced the so-called complexity of the source, using the per pixel gradient value in the R-q model, in order to improve the accuracy of the model.

The ρ-domain linear model proposed in [HM02a], presents a linear relationship between R and the parameter ρ, defined as the percentage of zero coefficients in a frame after quantization. This percentage increases in a monotonic way with the growth of the quantization step, leading to the following R-ρ model:

$$R(q) = \theta(1 - \rho(q)), \tag{2.10}$$

where θ is a constant.

An exponential R-q model for an intra-only rate control scheme defined on the base of extensive testing data, is proposed in [TZS12]:

$$R(q) = \alpha e^{-\beta q}, \tag{2.11}$$

where α and β are the model parameters.

In order to take into account both the impact of frame rate t on the bit rate R under the same quantization step size q, and the impact of q on the rate when the video is coded at a fixed frame rate, an R-D model based on the variation of q and t was presented in

[MXOW12b]:

$$R(q,t) = R_{max}(\frac{q}{q_{min}})^{-a}(\frac{t}{t_{max}})^{b}, \tag{2.12}$$

where q_{min} and t_{max} are chosen based on the underlying application, R_{max} is the actual rate when coding a video at q_{min} and t_{max}, and a and b are the model parameters.

2.1.2 The R-λ model

HEVC uses, in its latest version, a hyperbolic R-λ model for the bit allocation process [LLLZ12]. This model is defined as:

$$\lambda = \alpha \cdot \mathrm{R}^{\beta}, \tag{2.13}$$

where α and β are the model parameters, the rate R is defined in bits per pixel (*bpp*), and λ is the Lagrange parameter used in RDO to decide the coding mode (more details in the next Sections).

Based on previous investigations [LZLX12] which have shown a linear relationship between QP and $\ln(\lambda)$, a second relationship between λ and QP is incorporated into the model:

$$QP = 4.2005 \times \ln(\lambda) + 13.7122. \tag{2.14}$$

In Sec. 2.3 more details will be given about the R-λ model and its implementation in HEVC video encoder.

2.2 Budget-constrained bit allocation

Now we have defined the rate-distortion function and introduced some rate-distortion models used in video coding. In this section we will define the problem of bit allocation under a bit-budget constraint, which is a basic concept in rate-distortion optimization for video encoders. Given a total number of bits available, or budget, R_{budget}, the objective is to distribute the bit budget among the different coding units (macroblocks or frames) minimizing some overall distortion metric. Consider N coding units, each with M different available quantization choices. For each coding unit i encoded with a quantizer Q_i[1], we define its rate $R_i(Q_i)$ and its distortion $D_i(Q_i)$ [OR98]. The budget constrained allocation problem can be stated as find the optimal quantizer $Q(i)$ for each coding unit i such that

$$\sum_{i=1}^{N} R_i(Q_i) \leq R_{budget} \tag{2.15}$$

[1] Q_i indicates a generic quantization choice for coding unit i and, according to the context, can represent a quantization step, a quantization parameter, and so on.

and some metric $f\left(D_1(Q_1), D_2(Q_2), \ldots, D_N(Q_N)\right)$ is minimized.
In video coding different kind of metrics can be used. For example, in a minimum average distortion (MMSE) approach, we have

$$f\left(D_1(Q_1), D_2(Q_2), \ldots, D_N(Q_N)\right) = \sum_{i=1}^{N} D_i(Q_i). \tag{2.16}$$

In minimax (MMAX) problem [SK97b, SK97a], the distortion function reads

$$f\left(D_1(Q_1), D_2(Q_2), \ldots, D_N(Q_N)\right) = \max_{i \in \{1,\ldots,N\}} D_i(Q_i). \tag{2.17}$$

Another example is the lexicographically optimal (MLEX) approach [D.T97], an extension of the minimax solution that compares two solutions by sorting their quantization indices and considering the one represented by the smallest number as the best in the MLEX sense.

2.2.1 Lagrangian optimization

In the case where the rate $R_i(Q_i)$ and the distortion $D_i(Q_i)$ can be measured independently for each coding unit, the classical solution for the budget constrained allocation problem is based on the discrete version of Lagrangian optimization first introduced by Everett [Eve63]. By saying that $R_i(Q_i)$ and $D_i(Q_i)$ are measured independently, we mean that the R-D data for coding unit i can be computed without requiring other coding units to be encoded as well. Lagrangian optimization was first used in source coding application, [SG88, CL89, CLG89] in tree-pruning allocation and entropy constrained allocation [CL89, CLG89] and, since then, by numerous authors [RV93, WG91, ORV94, CL97, KBSC92, LWC93, SB94].

The basic idea of this technique is to transform the constrained problem into an unconstrained one in order to simplify the resolution of it, by defining a Lagrangian cost function $J_i(Q_i) = D_i(Q_i) + \lambda \cdot R_i(Q_i)$, where $\lambda \geq 0$ is the Lagrangian multiplier. Figure 2.2 gives a graphical interpretation of the Lagrangian cost. Choosing a coarser quantizer, the rate decreases and a distortion increases, with a trade-off between the two. The Lagrange multiplier allows to select the specific trade-off point: if $\lambda = 0$, minimizing the Lagrangian cost is equivalent to minimize the distortion (a point closer to the y-axis in Figure 2.2 is selected); if λ is arbitrarily large, minimizing J is equivalent to minimizing the rate (a point closer to the x-axis in Figure 2.2 is selected); intermediate values of λ determine intermediate operating points.

To solve the constrained allocation problem, we need to find an optimal set of Q_i^*, for $i = 1, 2, \ldots, N$, such that minimizing the total distortion within the constraint of total budget R_T:

$$\mathbf{Q}^* = (Q_1^*, Q_2^*, \ldots, Q_N^*) = \arg \min_{(Q_1, Q_2, \ldots, Q_N)} \sum_{i=1}^{N} D_i(Q_i) \tag{2.18}$$

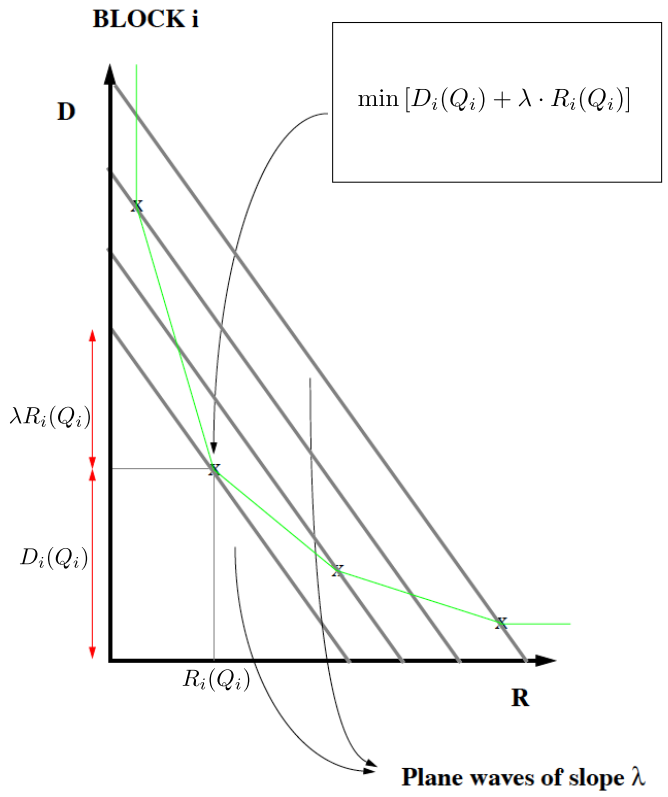

Figure 2.2: For a coding unit i, the minimization of $J_i(Q_i) = D_i(Q_i) + \lambda R_i(Q_i)$ is equivalent to finding the point in the R-D characteristic hit first by a plane wave of slope λ. (Figure from [OR98])

with the constraint that $\sum_{i=1}^{N} R_i(Q_i) \leq R_{budget}$. Using the Lagrangian multiplier, we convert the problem into unconstrained optimization:

$$\mathbf{Q}^* = \arg \min_{(Q_1,Q_2,\ldots,Q_N)} \sum_{i=1}^{N} D_i(Q_i) + \lambda \sum_{i=1}^{N} R_i(Q_i). \tag{2.19}$$

From the independence hypothesis, we can restate eq. 2.19 as:

$$Q_i^* = \arg \min_{Q_i} \left[D_i(Q_i) + \lambda \cdot R_i(Q_i) \right]. \tag{2.20}$$

The point on the R-D curve that minimizes the cost function J is, for each coding unit, the point of tangency of the line of absolute slope λ with the convex hull of the R-D characteristic.

2.2.2 Rate-distortion optimization in video encoders

RDO is widely used in modern video encoders, and the motion estimation, as well as the choice of prediction modes, is performed through Lagrangian optimization [SW98b]. The concepts explained in this section were introduced in H.263 and have been used ever since in the following video encoders H.264/AVC and HEVC.

The motion estimation is performed searching for an MV that minimizes the prediction error prior to residual coding: the criterion for block motion estimation is the minimization of the Lagrangian cost function

$$J_{\text{MOTION}} = D_{\text{MCP}} + \lambda_{\text{MOTION}} R_{\text{MOTION}} \tag{2.21}$$

where the distortion D_{MCP} represents the prediction error measured as the sum of squared differences (SSD)[2], and is weighted against the number of bits R_{MOTION} associated with the MVs using a Lagrange multiplier λ_{MOTION}. A rate-distortion-optimized motion estimation scheme for fixed or variable block sizes was proposed in [SB91, Gir94, CW96a, CW96b, CW98, KLSW97, SK97c]

For the mode choice, in H.263 for each macroblock A of size 16×16 one of the following prediction modes can be chosen: INTRA, SKIP, INTER, INTER+4V (INTER prediction mode with four motion vectors, one for each of the 8×8 blocks in the macroblock). Assuming that bit rate and distortion of the residual coding stage is controlled by the selection of a quantizer step-size Q, the optimal mode decision refers to the minimization of the following Lagrangian functional:

$$J(A,M,Q) = D_{\text{REC}}(A,M,Q) + \lambda_{\text{MODE}} R_{\text{REC}}(A,M,Q) \tag{2.22}$$

[2] $\text{SSD}_A = \sum_{(x,y)\in\mathcal{I}(A)} |F(x,y) - G(x,y)|^2$ where F and G are luminance arrays of the actual and approximated picture, and $\mathcal{I}(A)$ is the set of coordinates where the macroblock A lies.

where $M \in \{\text{INTRA}, \text{SKIP}, \text{INTER}, \text{INTER+4V}\}$ indicates a mode chosen for a particular macroblock, Q is the selected quantizer step size, D_{REC} is the SSD between the original macroblock A and its reconstruction, and R_{REC} is the number of bits associated with choosing M and Q. An algorithm for the minimization of eq. (2.22) given all mode decisions of past macroblocks is presented in [WTO90, WG91].

In order to incorporate macroblock quantization step-size changes, a modification to the rate-constrained mode decision can be adopted. Another prediction mode, INTER+Q, which permits changing Q by a small amount when sending an INTER macroblock, is added to the set of macroblock modes to choose from. For each macroblock, a mode M can be chosen from the set

$$\begin{aligned} M \in \{&\text{INTRA}, \text{SKIP}, \text{INTER}, \text{INTER+4V}, \ldots, \text{INTER+Q(-2)}, \\ &\text{INTER+Q(+2)}, \text{INTER+Q(+4)}\} \end{aligned} \tag{2.23}$$

where, for example, INTER+Q(-2) stands for the INTER mode being coded with quantization step size reduced by two relatively to the previous macroblock. A minimization of the cost function J led to the selection of Q, which becomes dependent to λ_{MODE}. Assuming a typical quantization curve high-rate approximation [JN84, GP68]:

$$R(D) = a \ln\left(\frac{\sigma^2}{D}\right) \tag{2.24}$$

where a is a constant depending on the source probability density function. The minimization of $J = D + \lambda_{\text{MODE}} \cdot R$ for a given value of λ_{MODE} can be accomplished by setting the derivative of J with respect to D equal to zero:

$$\frac{dR(D)}{dD} = -\frac{a}{D} \triangleq -\frac{1}{\lambda_{\text{MODE}}} \tag{2.25}$$

At high bit rates a well-behaved source probability distribution can be approximated as a constant within each quantization interval [GP68], which leads to the high bit-rate approximation $D \cong (2 \cdot \text{QP})^2/12$ (in H.263 QP$\in \{1, 2, \ldots, 31\}$ and $Q = 2{\cdot}\text{QP}$). The approximation then yield $\lambda_{\text{MODE}} \cong c \cdot (\text{QP})^2$, where $c = 4/(12a)$. Although the assumptions may not be completely realistic, it has been proved the proportionality between λ_{MODE} and the square of the quantization parameter, with the constant $c = 0.85$. Experimentally, a relationship between λ_{MOTION} and λ_{MODE} has been found:

$$\lambda_{\text{MOTION}} = \sqrt{\lambda_{\text{MODE}}} \tag{2.26}$$

The three quantities QP, λ_{MODE} and λ_{MOTION} are tied together and each of these quantities can be seen as a dependent variable of the others.

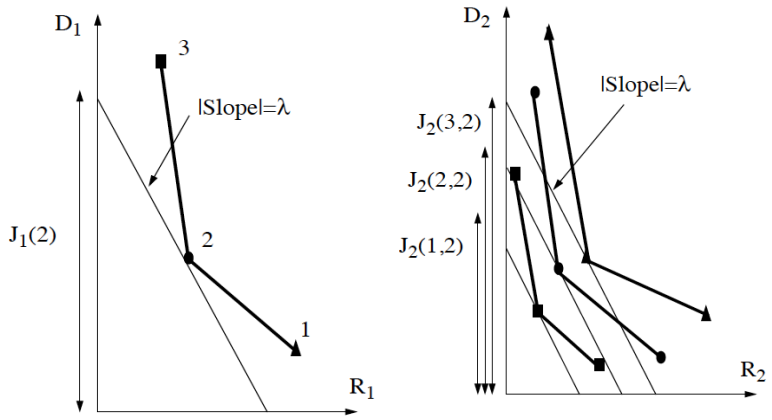

(a) Independent frame's R-D curve (b) Dependent frame's R-D curve

Figure 2.3: Operational R-D characteristics of two frames in a dependent coding framework, where frame 2 depends on frame 1 and each quantizer choice for frame 1 leads to a different $R_2 - D_2$ curve. (Figure from [ROV94])

2.2.3 Dependency problems

So far we considered that the selection of the coding mode is made independently for each coding unit without affecting the other units. However, many practical scenarios involve *dependent* coding frameworks, *i.e.* where the set of available R-D operating points for some coding units depends on the particular choice of R-D point for other coding units, as shown in Figure 2.3. This problem, typical in coding schemes based on prediction [USC93, ROV94], was addressed by Ramchandran *et al.* [ROV94] using an operational R-D framework to search the optimal combination of QPs for the whole GOP. First of all, they consider a two-layer dependency, as shown in Figure 2.3. For a given set of quantization choices, Figure 2.3(a) shows the R-D characteristic for the first independent frame $(R_1(Q_1), D_1(Q_1)$ while Figure 2.3(b) shows dependent frame's R-D curve $(R_2(Q_1, Q_2), D_2(Q_1, Q_2)$. The total distortion is the sum of individual distortions D_1 and D_2 and the problem can be formulated as

$$\min_{Q_1,Q_2} \left[D_1(Q_1) + D_2(Q_1, Q_2)\right] \tag{2.27}$$

$$\text{such that } R_1(Q_1) + R_2(Q_1, Q_2) \leq R_{budget}. \tag{2.28}$$

The independent case seen in Sec. 2.2.1 is a special case of eq. (2.27) and eq. (2.28) where frame 2 does not depend on frame 1, *i.e.* $R_2(Q_1, Q_2) = R_2(Q_2)$ and $D_2(Q_1, Q_2) = D_2(Q_2)$. As in [SG88], it is possible to solve the problem of eq. (2.27) and eq. (2.28) using a Lagrangian multiplier $\lambda \geq 0$ and introducing the Lagrangian cost J:

$$J_1(Q_1) = D_1(Q_1) + \lambda R_1(Q_1) \tag{2.29}$$

$$J_2(Q_1, Q_2) = D_2(Q_1, Q_2) + \lambda R_2(Q_1, Q_2) \tag{2.30}$$

and considering the minimization problem:

$$\min_{Q_1,Q_2} [J_1(Q_1) + J_2(Q_1, Q_2)] \tag{2.31}$$

As a direct extension of Theorem 1 of [SG88] it is possible to state the following:

Fact 2.2.1 *If (Q_1^*, Q_2^*) solves the unconstrained problem of eq. (2.31), then it also solves the constrained problem of eq. (2.27) and eq. (2.28) for the particular case of $R_{budget} = [R_1(Q_1^*) + R_2(Q_1^*, Q_2^*)]$ [ROV94].*

Proof For all Q_1 and Q_2, we have

$$J_1(Q_1^*) + J_2(Q_1^*, Q_2^*) \leq J_1(Q_1) + J_2(Q_1, Q_2) \tag{2.32}$$

i.e.

$$D_1(Q_1^*) + \lambda R_1(Q_1^*) + D_2(Q_1^*, Q_2^*) + \lambda R_2(Q_1^*, Q_2^*) \leq D_1(Q_1) + \lambda R_1(Q_1) + D_2(Q_1, Q_2) + \lambda R_2(Q_1, Q_2) \tag{2.33}$$

or

$$[D_1(Q_1^*) + D_2(Q_1^*, Q_2^*)] - [D_1(Q_1) + D_2(Q_1, Q_2)] \leq \lambda([R_1(Q_1^*) + R_2(Q_1^*, Q_2^*)] - [R_1(Q_1) + R_2(Q_1, Q_2)]). \tag{2.34}$$

Since eq. (2.34) holds for all admissible Q_1, Q_2, it certainly holds for the subset of Q_1, Q_2 for which $[R_1, R_2] \leq R_{budget}$, where $R_{budget} = [R_1(Q_1^*) + R_2(Q_1^*, Q_2^*)]$. Therefore, from eq. (2.34), since $\lambda \geq 0$, we have that

$$[D_1(Q_1^*) + D_2(Q_1^*, Q_2^*)] - [D_1(Q_1) + D_2(Q_1, Q_2)] \leq 0 \tag{2.35}$$

i.e., over all Q_1, Q_2 that meet the rate budget, (Q_1^*, Q_2^*) gives the minimum distortion.

The above result implies that the two-frames problem becomes the search of (Q_1^*, Q_2^*) that solve

$$J_1(Q_1^*) + J_2(Q_1^*, Q_2^*) = \min_{Q_1,Q_2} [J_1(Q_1) + J_2(Q_1, Q_2)] \tag{2.36}$$

$$= \min_{Q_1} [J_1(Q_1) + J_2(Q_1, Q_2^*(Q_1))] \tag{2.37}$$

where $J_2(Q_1, Q_2^*(Q_1)) = \min_{Q_1} [D_2(Q_1, Q_2) + \lambda R_2(Q_1, Q_2)]$ is the minimum Lagrangian cost associated with the dependent frame when the independent frame is quantized with Q_1. For a fixed value of λ, the optimal solution can be found by finding the optimal $Q_2^*(Q_1)$

for all choices of Q_1; further, the convex hull of the composite R-D curve of the dependent allocation problem can be traced by sweeping λ from 0 to inf.

The optimal solution to the general N-frame dependency problem is a simple extension of the previous result: a Lagrangian cost J is introduced

$$J_i(Q_1, Q_2, \ldots, Q_i) = D_i(Q_1, Q_2, \ldots, Q_i) + \lambda R_i(Q_1, Q_2, \ldots, Q_i) \tag{2.38}$$

for $i = 1, 2, \ldots, N$, and the following unconstrained problem

$$\min_{Q_1, Q_2, \ldots, Q_N} [J_1(Q_1) + J_2(Q_1, Q_2) + \cdots + J_N(Q_1, Q_2, \ldots, Q_N)] \tag{2.39}$$

is solved for the λ value which meets the given R_{budget}.
The complexity needed to find the optimal solution, as shown by eq. (2.39), is exponential in the dependency-tree depth N and the computational burden for the *data generation* phase, *i.e.* finding all the $(R_i(Q_1, Q_2, \ldots, Q_i), D_i(Q_1, Q_2, \ldots, Q_i))$ points makes this approach unpractical. In order to obtain a more feasible solution to the complex dependent allocation problem, in [ROV94] the monotonicity property of the R-D curves is used to formulate *pruning conditions* to eliminate sub-optimal operating points. The monotonicity condition implies that a finer quantizer for a past image will lead to a more efficient coding of the residue, in a rate-distortion sense. As in eq. (2.2.1), we assume that the quantizer grades are ordered monotonically from the finest to the coarsest. The quantization choices for the independent and the dependent frame are denoted as i and j, respectively.

Definition A dependent coding system has the monotonicity property if, for any $\lambda \geq 0$:

$$J_2(i, j) \leq J_2(i', j), \qquad \text{for } i \leq i'. \tag{2.40}$$

For $\lambda = 0$, for example, this means that

$$D_2(i, j) \leq D_2(i', j), \qquad \text{for } i \leq i'. \tag{2.41}$$

Monotonicity property has been verified by experimental studies involving MPEG, and is used in order to formulate the following pruning conditions, associated with Figure 2.4.

Lemma 2.2.2 *If*

$$J_1(i) + J_2(i, j) < J_1(i') + J_2(i', j), \qquad \textit{for any } i \leq i', \tag{2.42}$$

then the (i', j) *branch cannot be part of the optimal path, and can be pruned out.*

Proof The lemma is proved by contradiction. Assume that (i', j) for any $i < i'$ is part of the optimal path. Let the optimal quantizer sequence path be $(i', j, k, \ldots, l)$. By

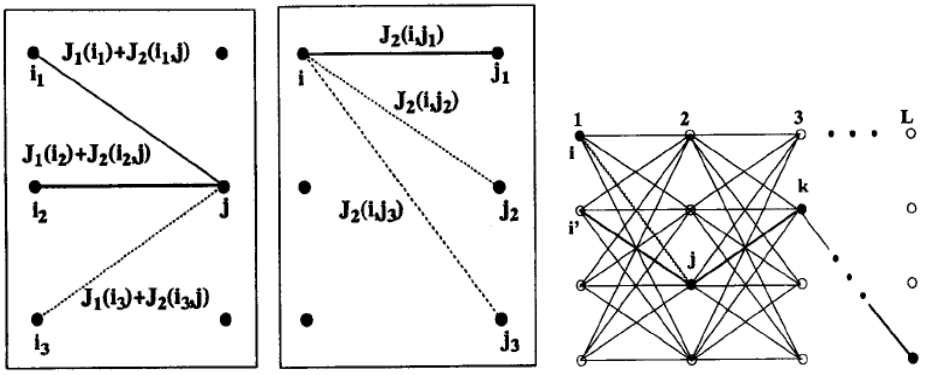

(a) (b) (c)

Figure 2.4: Pruning condition obtained from monotonicity. (a) $J_1(1_2) + J_2(i_2, j)$ is the minimum Lagrangian cost of all branches terminating in node j and, according to Lemma2.2.2, the branch (i_3, j) can be pruned; (b) $J_2(i, j_1)$ is the minimum Lagrangian cost of all branches originating from node i and, according to Lemma2.2.3, the branches (i, j_2) and (i, j_3) can be pruned; (c) diagram used for the proof of 2.2.2. (Figure from [ROV94])

monotonicity, we have

$$J_3(i, j, k) \leq J_3(i', j, k) \tag{2.43}$$

$$\dots$$

$$J_L(i, j, k, \dots, l) \leq J_L(i', j, k, \dots, l) \tag{2.44}$$

Summing up eq. (2.42),(2.43),...,(2.44), the total Lagrangian cost of the path $(i, j, k, \dots, l)$ is smaller than the one of the optimal path $(i', j, k, \dots, l)$, which is a contradiction.

Using a similar proof, it is possible to demonstrate the following

Lemma 2.2.3 *If $J_2(i, j) < J_2(i, j')$ for any $j < j'$, than the (i, j') branch cannot be part of the optimal path, and can be pruned out.*

As a consequence of the above lemma, if $J_!(i) < J_!(i')$ for $i < i'$, the node i' and all the branches from it can be pruned out. Figure 2.5 shows an *I-B-B-P-B-B-P* sequence of MPEG frames, representing a practical case where the pruning condition can be applied. The dependency tree is presented in the compact form of a trellis, where the states represent the quantization choices for the I and P frames. The branches denote the quantizer choices for the two B frames and are populated with the sum of the minimum Lagrangian cost of the B_1 and B_2 frames, *i.e.* $J(B_1) + J(B_2)$, where $J(B_l) = \min_{Q_{B_l}}[D(Q_{B_l}) + \lambda R(Q_{B_l})]$ for $l = 1, 2$. The example in Figure 2.6 shows how the pruning conditions are used to find the optimal path in the dependency tree; in particular, in [ROV94] the Algorithm 2 is presented, where the smallest path obtained, is the optimal solution for a chosen λ. The amount of nodes pruned is dependent on the desired quality slope λ, with better complexity reduction is achieved with higher quality targets. For $\lambda \to 0$ the minimum cost

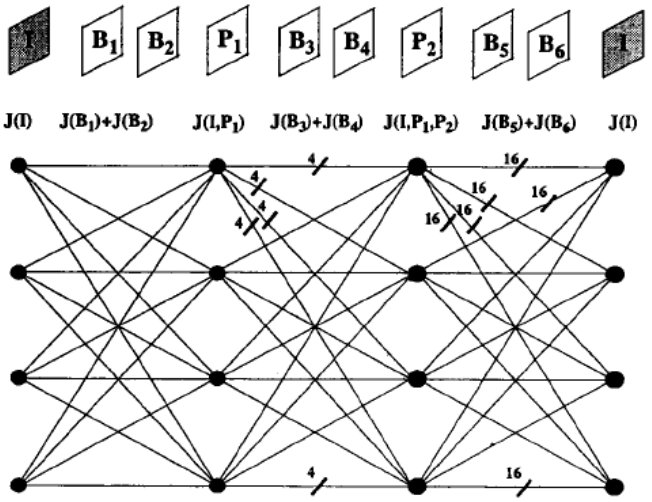

Figure 2.5: MPEG "trellis" diagram. Each stage of the trellis is represented by a multiple branches whose number grows exponentially. (Figure from [ROV94])

path corresponds to the finest quantizer and only a single path has to be grown, while for $\lambda \to \infty$ no gain is provided.

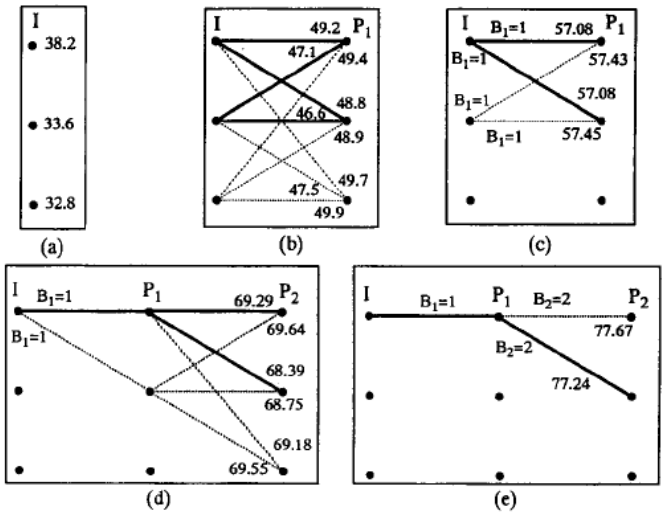

Figure 2.6: Tree pruning using monotonicity property. The numbers are cumulative Lagrangian costs for an example with $\lambda = 10$, where the pruned branches are shown with dashed lines. (Figure from [ROV94])

Algorithm 2 [ROV94]

Step 1: Generate $J(I)$ for all quantizers $q \in Q_I$; see Fig (7a)

Step 2: (*Monotonicity*) Prune out all I-nodes lying below minimum cost node $q^* \in Q_I$ in Step 1

Step 3: Grow $J(I, P_1)$ for all combinations of $q \in Q_{P_1}$ and all remaining $q \in Q_I$ after Step 2. See Fig 7b

Step 4: (*Monotonicity*) Use pruning conditions of Lemmas 2.2.2 and 2.2.3 to eliminate suboptimal I-nodes lying below minimum cost node $q^* \in Q_I$ in Step 1

Step 5: For every surviving $I - P_1$ combination, find the B_1, B_2 quantizer that minimizes $J(B_1) + J(B_2)$, *i.e.*, populate the branch costs of the trellis of Fig (6 ram). See Fig (7c)

Step 6: (*Monotonicity*) Use pruning conditions of Lemmas 2.2.2 and 2.2.3 to eliminate suboptimal $I - B_1 - B_2 - P_1$ combinations; see Fig 7c

Step 7: For all remaining paths, repeat Steps 3 to 6 for the $(P_1 - B_3 - B_4 - P_2)$ and the $(P_2 - B_5 - B_6 - I)$ sets.

2.3 Rate control

In Sec. 2.1 we presented R-D optimization techniques used in video encoders. In the state-of-the-art video encoder HEVC, RDO is used not only as a mode selection scheme, but is adopted in the rate control module. Rate control is a non-normative tool, adopted to adjust the output bit rate and ensure high visual quality of the decoded video in limited network conditions. A crucial task of rate control is to optimally distribute the bit budget within the sequence, because this directly affects the visual distortion of encoded frames originated by the quantization. In this regard, the rate control of H.265/HEVC allocates the bit budget at three different levels: GOP level, frame level, and coding unit (CU) level, as depicted in Figure 2.7.

For the GOP level, the bit allocation (BA) consists in a uniform assignment of the total bit budget for the sequence over the GOPs, with a possible fluctuation related to the number of the remaining frames to encode and the bits still available. The BA at picture-level works in a similar way, with a weighting mechanism to vary the bit assignment for each frame in the current GOP according to their different hierarchical position (non hierarchical allocation, with all weights equal to 1, is available). At frame level and at CTU level, after the bit budget has been allocated, the rate control module compute an optimal QP which will be used in the quantization. Our work, that will be presented in Sec. 3.2, aims to replace the mentioned BA block, which does not take into account sequence

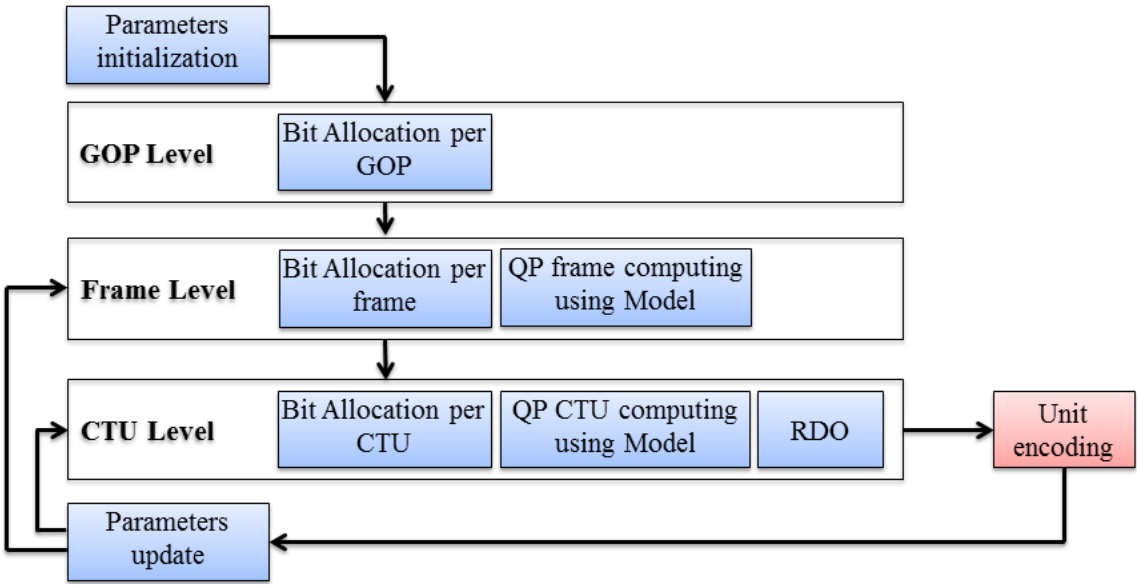

Figure 2.7: Rate control in HEVC.

characteristics such as texture complexity of temporal correlation between the frames for the bit assignment, without modifying the blocks responsible for the QP determination, which is performed with the R-λ model [LLLZ12], nor the overlaying coding tree unit (CTU) level. In the next section some details will be given on the rate control module and how it operates at each level for the BA and the QP evaluation.

2.3.1 Bit Allocation

Suppose that the target bit rate is R_{tar} expressed in bits, the frame rate is f expressed in fps and the number of frames in a GOP is N_{GOP}.

GOP level bit allocation

At GOP level, the target bits in a GOP, as described in [LLLZ12], are determined by

$$T_{\text{GOP}} = N_{\text{GOP}} \cdot \frac{\frac{R_{\text{tar}}}{f} \cdot (N_{\text{coded}} + \text{SW}) - R_{\text{coded}}}{\text{SW}} \tag{2.45}$$

where SW is the size of a smoothing window and is set to 40, N_{coded} is the number of pictures already coded and R_{coded} is the bit cost of these pictures.

Picture level bit allocation

Using the target bits of the current GOP determined by eq. (2.45), the target bit of the current picture is determined by

$$T_{\text{CurrPic}} = \frac{T_{\text{GOP}} - \text{Coded}_{\text{GOP}}}{\sum_{\text{NotCodedPictures}} \omega_i} \cdot \omega_{\text{CurrPic}} \tag{2.46}$$

where $\text{Coded}_{\text{GOP}}$ is the number of coded bits of the current GOP. ω is the bit allocation weight associated to the hierarchical level of the picture in the current GOP, which is the same for all the intra-frames but can be different for the inter-frames according to three possible configurations: equal allocation, hierarchical allocation and adaptive allocation. In the first case, the same weight is assigned to each frame, in the second case a predefined weight is assigned to the P and B frames of the GOP, while in the third case the weight assigned to the frame is updated in relation to the Lagrangian parameter λ defined by eq. (2.13). Tables containing possible values of ω are presented in [LLLZ12]. Furthermore, in HM 13 implementation of HEVC, a refinement method is considered in order to increase the allocated budget of intra-frame:

$$T_{\text{refined}} = a \times \left(\frac{w_I}{T_{\text{CurrPic}}} \right)^b \times T_{\text{CurrPic}} + 0.5, \tag{2.47}$$

where $a = 0.25$, $b = 0.5582$ and w_I is a complexity measure defined in eq. (2.60).

CU level bit allocation

The coding tree unit (CTU), also referred to as largest coding unit (LCU), is the basic processing unit of the High Efficiency Video Coding (HEVC) video standard and conceptually corresponds in structure to macroblock units that were used in several previous video standards [SOHW12a, OSS+12]. When CTU level rate control is enabled, the target number of bits of each CTU is determined by

$$T_{\text{CurrCU}} = \frac{T_{\text{CurrPic}} - \text{Bit}_{\text{header}} - \text{Coded}_{\text{Pic}}}{\sum_{\text{NotCodedCTUs}} \omega_i} \cdot \omega_{\text{CurrCTU}} \tag{2.48}$$

where $\text{Bit}_{\text{header}}$ is the estimated number of bits of all headers, ω_{CurrCTU} and ω_i are, respectively, the weight of the current CTU and of the i^{th} CTU estimated by the coding error, in form of MAD:

$$\text{MAD}_{\text{CTU}} = \frac{1}{N_{\text{pixels}}} \sum_i |rec_i - org_i| \tag{2.49}$$

$$\omega_{\text{CTU}} = \text{MAD}_{\text{CTU}}^2 \tag{2.50}$$

N_{pixels} is the number of pixels of the CTU (the maximum value is 64x64 pixels), rec_i and org_i are the pixel values in reconstructed picture and original picture, respectively.

2.3.2 QP evaluation

After a certain number of bits has been allocated, the controller selects a QP in order to achieve the target number of allocated bits. The most recent method used for HEVC, introduced in HM.11 [LLLZ12] and improved in HM.13 [LLL13], is the R-λ scheme. First of all, a Lagrange multiplier λ is evaluated from a bpp-λ relationship, then the actual QP is evaluated from a λ-QP model, where bpp is defined as the ratio between the number of bits T and the number of pixels in a frame N_f.

Adopting the Hyperbolic model $D = CR^{-K}$ to characterize the relationship between R and D [MF98, DLR04], we can express λ (the slope of the R-D curve) as

$$\lambda = -\frac{\partial D}{\partial R} = CK \cdot R^{-K-1} = a \cdot R^b \tag{2.51}$$

where C and K are model parameters related to the characteristic of the source. Expressing the bit rate in terms of bpp by

$$R = \text{bpp} \cdot f \cdot w \cdot h \tag{2.52}$$

where f is the frame rate, w and h are the width and the height of the picture, we can rewrite eq. (2.51) as

$$\lambda = \alpha \cdot \text{bpp}^{\beta} = \alpha \cdot \frac{T_{\text{CurrPic}}}{N_f} \tag{2.53}$$

where $\alpha = a \cdot (fwh)^b$ and $\beta = b$ are parameters related to video content. The QP value is determined according to eq. (2.14). Furthermore, λ and QP are clipped in a narrow range, in order to guarantee quality consistence:

$$\begin{aligned} &2^{-1}\lambda_l \le \lambda \le 2\lambda_l \\ &2^{\frac{-10}{3}}\lambda_p \le \lambda \le 2^{\frac{10}{3}}\lambda_p \\ &QP_l - 3 \le QP \le QP_l + 3 \\ &QP_p - 10 \le QP \le QP_p + 10 \end{aligned} \tag{2.54}$$

where (λ_l, QP_l) represents the values of λ and QP for the last decoded frame of the same hierarchical level, and (λ_p, QP_p) the values of λ and QP for the last decoded picture. Finally, α and β model parameters are updated using the real encoding bit cost T' and real λ value as follow:

$$\lambda' = \alpha \left(\frac{T'}{N_f}\right)^{\beta} \tag{2.55}$$

$$\alpha' = \alpha[1 + \delta_\alpha(\ln(\lambda) - \ln(\lambda'))] \tag{2.56}$$

$$\beta' = \beta + \delta_\beta(\ln(\lambda) - \ln(\lambda'))\ln\left(\frac{T'}{N_f}\right) \tag{2.57}$$

At CTU level, the allocated budget per CTU is used to compute λ and QP using again eq. (2.53). Again the model parameters are updated according to the Equations (2.55) – (2.57) after encoding each CTU, and again some clipping conditions between λ and QP are defined in order to keep quality smoothness inside a frame:

$$\begin{aligned} &2^{\frac{-1}{3}}\lambda_l \leq \lambda \leq 2^{\frac{1}{3}}\lambda_l \\ &2^{\frac{-2}{3}}\lambda_p \leq \lambda \leq 2^{\frac{2}{3}}\lambda_p \\ &QP_l - 1 \leq QP \leq QP_l + 1 \\ &QP_p - 2 \leq QP \leq QP_p + 2 \end{aligned} \tag{2.58}$$

where (λ_l, QP_l) denote the values of λ and QP for the last decoded CTU, and (λ_p, QP_p) denote the values of λ and QP for the current picture.

A modification to the R-λ model has been implemented for intra-frames:

$$\lambda_u = \alpha \left(\frac{w_I}{\left(\frac{T_{\text{CurrCU}}}{N_{\text{pixels}}}\right)}\right)^\beta \tag{2.59}$$

where the parameters α and β remain constant for the entire frame. The complexity measure w_I is defined as:

$$w_I = \sum_{j=0}^{N_b-1} \text{SATD}(j) \tag{2.60}$$

and is derived from the sum of absolute Hadamard transformed difference (SATD) [KW13]:

$$\text{SATD} = \sum_{k=0}^{7}\sum_{\ell=0}^{7} |h_{k\ell}| \,. \tag{2.61}$$

2.4 Conclusion

In this chapter we introduced some basic concepts of the rate-distortion theory. We started with the definition of the rate-distortion function, then we defined the budget-constrained bit allocation problem, presenting the solution based on the Lagrangian optimization, showing some practical applications in the domain of video coding for the mode selection and the rate control.

In the next chapter, we will present a different approach for the solution of the constrained allocation problem, using convex optimization techniques. We will present a new recursive frame-level rate-distortion model to define the budget allocation as a convex optimization problem, and we will present an efficient algorithm to solve the problem.

Chapter 3

Frame level bit allocation

Contents

Optimization aims at selecting the best element from a set of available alternatives ranked by a give criterion. The problem can be formulated as

$$\underset{x \in D}{\text{minimize}} \quad f(x), \tag{3.1}$$

where D denotes a set of feasible solutions, and $f : D \to \mathbb{R} \cup +\infty$ denotes the objective function.

In the previous chapter, we introduced Lagrangian optimization as a possible solution to the minimization problem, in this chapter we will introduce a different approach to the optimization problem based on *proximal algorithms*; in particular, we will focus on a subclass of proximal algorithm, the *primal-dual methods*. Those methods aim to solve the optimization problem by concurrently solving a primal problem, which corresponds to the original optimization task, as well as a dual formulation of this problem, offering some important computational advantages thanks to their ability to achieve a *full splitting*: each

operator involved in the problem is used separately and no inversion of a linear operator is required. Furthermore, optimization algorithms derived from primal-dual methods can be easily parallelizable.

In this chapter, we will introduce the basic concepts of convex optimization based on proximal algorithms. We will present the proximal operator and introduce the forward-backward splitting, in order to address the problem of optimal frame-level bit allocation for HEVC. We will present our recursive frame-level rate-distortion model, define the bit allocation problem at frame level and present a solution based on the forward-backward splitting. Finally, we will present some results to validate our R-D model and asses the effectiveness of our optimization method.

3.1 Proximal algorithms

Many signal processing problems involve multiple objectives to be optimized, leading to the following generalization of (3.1):

$$\underset{x\in D}{\text{minimize}} \quad \{f_1(x), \ldots, f_R(x)\}, \tag{3.2}$$

where D denotes a set of feasible solutions, and $f_r : D \to \mathbb{R} \cup +\infty$ for every $r \in \{1, \ldots, R\}$ are the objective functions. A major difficulty that arises in solving this multi-objective problem stems from the fact that some of the functions are typically not differentiable, ruling out conventional smooth optimization techniques. In this case, a possible approach consists of resorting to smart approximations in order to smooth the involved non-differentiable functions [Hub64, BTT89, HUL96, BNS13]. Another possibility is, in order to directly address the original non-smooth problem, to apply projection methods [YW82, CCC+12], block-coordinate descent methods [Tse01], or interior-point methods [Wri97], but they often impose restrictive assumptions on the problem to be solved. A new class of efficient convex optimization algorithms, referred to as *proximal algorithms*, has recently emerged to overcome these issues. They are called *proximal* because each non-smooth function in (3.2) is involved via its proximity operator, and their use is spreading rapidly thanks to their ability to solve a large panel of convex optimization problems [CP11c].

3.1.1 Definitions

In the following sections, standard definitions and notations from convex analysis will be used. $\mathbb{R}^N$ is the N-dimensional Euclidean space and $\|\cdot\|$ its norm. For a given function $f : \mathbb{R}^N \to]-\infty, +\infty]$, its domain is $\mathrm{dom} f = \{x \in \mathbb{R}^N \mid f(x) < +\infty\}$. A function with non-empty domain is said to be *proper*. A function f is *convex* if

$$\left(\forall (x, y) \in (\mathbb{R}^N)^2\right) \text{ and } (\forall \lambda \in [0, 1]) \qquad f(\lambda x + (1-\lambda)y) \leq \lambda f(x) + (1-\lambda) f(y). \tag{3.3}$$

A function $f : \mathbb{R}^N \to]-\infty, +\infty]$ whose epigraph $\operatorname{epi} f = \big\{(x, \zeta) \in \operatorname{dom} f \times \mathbb{R} \;\big|\; f(x) \leq \zeta\big\}$ is a closed set, is said to be lower semi-continuous. $\Gamma_0(\mathbb{R}^N)$ is the class of proper lower semi-continuous convex functions from $\mathbb{R}^N$ to $]-\infty, +\infty]$. The conjugate of f, $f^* \in \Gamma_0(\mathbb{R}^N)$ is defined as:

$$f^* : \mathbb{R}^N \to]-\infty, +\infty] : u \to \sup_{x \in \mathbb{R}^N} x^\top u - f(x), \tag{3.4}$$

and, a function $f \in \Gamma_0(\mathbb{R}^N)$ can be expressed in terms of f^* as

$$f = \sup_{u \in \mathbb{R}^N} u^\top(\cdot) - f^*(u). \tag{3.5}$$

The Moreau subdifferential of $f \in \Gamma_0(\mathbb{R}^N)$ at $p \in \mathbb{R}^N$ is defined as

$$\partial f(p) = \big\{t \in \mathbb{R}^N \mid (\forall u \in \mathbb{R}^N) \;\; (u - p)^\top t + f(p) \leq f(u)\big\}. \tag{3.6}$$

Any vector t in $\partial f(p)$ is called *subgradient* of f at p. If f is differentiable at y, then its subdifferential at p reduces to the singleton consisting of its gradient, *i.e.* $\partial f(y) = \{\nabla f(y)\}$. The inf-convolution between f and g in $\Gamma_0(\mathbb{R}^N)$ is defined as

$$f \,\square\, g = \inf_{u \in \mathbb{R}^N} \; f(u) + g(\cdot - u). \tag{3.7}$$

In addition, $(f + g)^* = f^* \,\square\, g^*$, and $u \in \partial f(x) \;\Leftrightarrow\; x \in \partial f^*(u) \Leftrightarrow \; f(x) + f^*(u) = x^\top u$. Finally, considering a non-empty subset $C \subset \mathbb{R}^N$, the indicator function of C is defined as

$$(\forall x \in \mathbb{R}^N) \qquad \iota_C(x) = \begin{cases} 0, & \text{if } x \in C, \\ +\infty, & \text{otherwise,} \end{cases} \tag{3.8}$$

the distance from $x \in \mathbb{R}^N$ to C is $d_C(x) = \inf_{y \in C} \|x - y\|$ and, if C is closed and convex, the projection of $x \in \mathbb{R}^N$ onto C is the unique point $P_C x \in C$ such that $d_C(x) = \|x - P_C x\|$.

3.1.2 Proximity operator

Introduced in the early work by Moreau [Mor65], the *proximity operator* represents a key tool in proximal methods. The proximity operator of a proper lower semi-continuous convex function $f \in \Gamma_0(\mathbb{R}^N)$, is defined as

$$(\forall x \in \mathbb{R}^N) \qquad \operatorname{prox}_f(x) = \operatorname*{arg\,min}_{u \in \mathbb{R}^N} \; \frac{1}{2}\|u - x\|_2^2 + f(u). \tag{3.9}$$

The proximity operator can be interpreted as a sort of implicit subgradient step for the function f, as it is characterized by the inclusion

$$p = \operatorname{prox}_f(x) \quad \Leftrightarrow \quad p \in x - \partial f(p), \tag{3.10}$$

which reduces to

$$p = \operatorname{prox}_f(x) \quad \Leftrightarrow \quad p \in x - \nabla f(p). \tag{3.11}$$

if f is differentiable. Proximity operators have many interesting properties that make them very attractive for iterative minimization algorithms [CCPW07, CP11c, BC11, PB14].

The great advantage of proximal methods is that they provide a unifying framework which allows one to deal with non-smooth functions as well as hard constraints. In the case when f is equal to the indicator function of a non-empty closed convex set $C \subset \mathbb{R}^N$, the proximity operator of f reduces t the projection $\operatorname{prox}_{\iota_C}(x)$ onto this set:

$$(\forall x \in \mathbb{R}^N) \qquad \operatorname{prox}_{\iota_C}(x) = P_C(x) = \underset{u \in C}{\arg\min} \ \|u - x\|_2^2. \tag{3.12}$$

Proximal algorithms can be classified in *primal* [CP11c, PP12, ABDF10] and *primal-dual* [CP11a, CP12, Con13, KP15, Vu13, BnC11] methods. Primal-dual methods, in particular, proceed by solving a primal problem, which is the original optimization task, as well as a dual formulation of the problem. Those methods are able to achieve a *full splitting* (each of the operators involved in the problem is used separately), with the result that no inversion of a linear operator (which is expensive for large-scale problems) is required during the optimization, and are easily parallelizable. A number of primal-dual methods can be derived from the *forward-backward* splitting [CCPVu14].

3.1.3 Forward-backward splitting

Forward-backward approach combine a gradient descend step (forward step) with a computation step involving a proximity operator. Consider a non-smooth function $f \in \Gamma_0(\mathbb{R}^N)$, and a differentiable $g \in \Gamma_0(\mathbb{R}^N)$ with a β-Lipschitz continuous gradient ∇g, *i.e.*,

$$(\forall (x, u) \in \mathbb{R}^N \times \mathbb{R}^N) \qquad \|\nabla g(x) - \nabla g(u)\|_2 \leq \beta \|x - u\|_2 \tag{3.13}$$

where $\beta \in]0, +\infty[$. Suppose that $f(x) + g(x) \to +\infty$ as $\|x\| \to +\infty$. The problem is to

$$\underset{x \in \mathbb{R}^N}{\text{minimize}} \quad f(x) + g(x). \tag{3.14}$$

This method aims at finding a point $\overline{x} \in \mathbb{R}^N$ satisfying the fixed-point condition

$$0 \in \partial f(\overline{x}) + \nabla g(\overline{x}) \quad \Leftrightarrow \quad \overline{x} \in \overline{x} - \nabla g(\overline{x}) - \partial f(\overline{x}) \quad \Leftrightarrow \quad \overline{x} = \operatorname{prox}_f \Big(\overline{x} - \nabla g(\overline{x})\Big). \tag{3.15}$$

It is possible to show [CW05] that, under appropriate technical assumptions, for every $x^{[0]} \in \mathbb{R}^N$, the sequence $(x^{[i]})_{i \in \mathbb{N}}$ generated by

$$x^{[i+1]} = \operatorname{prox}_{\gamma_i f} \Big(x^{[i]} - \gamma_i \nabla g(x^{[i]})\Big) \tag{3.16}$$

converges to a solution to Problem (3.14) for any $\gamma_i \in]0, 2/\beta[$.

The forward-backward splitting generalizes various well-known algorithms, such as the standard gradient descent when $f = 0$, the proximal-point algorithm when $g = 0$, the projected gradient method when f is the indicator function of a closed convex subset of $\mathbb{R}^N$, and the backward-backward splitting when g is the inf-convolution between a function in $\Gamma_0(\mathbb{R}^N)$ and the quadratic function.

If the non-smooth term f denotes a convex function composed with a linear operator, a practical limitation arises from the difficulty of computing the proximity operator of such a function, unless the linear operator satisfies specific properties [BC11, Prop. 23.23], [PCP11, Prop. 3.4]. The *Fenchel-Rockafellar* duality theorem provides a way to circumvent this issue. It can be applied to Problem (3.14) with an additional function $h \in \Gamma_0(\mathbb{R}^M)$ composed with a linear operator $F \in \mathbb{R}^{M \times N}$, and some $w \in \mathbb{R}^N$, namely

$$\underset{x \in \mathbb{R}^N}{\text{minimize}} \quad f(x) + g(x) + h(Fx) - w^\top x. \tag{3.17}$$

(3.17) is usually referred to as the *primal problem*, which is associated with the following *dual problem* involving the conjugate function of $f + g$ and h, yielding [BC11, Definition 15.19]

$$\underset{y \in \mathbb{R}^M}{\text{minimize}} \quad (f^* \,\square\, g^*)(w - F^\top y) + h^*(y). \tag{3.18}$$

The primal and dual problems, under some technical assumptions, are equivalent (in the sense that their objective functions achieve the same optimum value) [BC11, Theorem 15.23]. This fact allows one to deduce that any pair $(\overline{x}, \overline{y})$ of solutions to these problems is such that [BC11, Theorem 19.1]

$$\begin{cases} \overline{x} \in \partial(f^* \,\square\, g^*)(w - F^\top \overline{y}), \\ F\overline{x} \in \partial h^*(\overline{y}). \end{cases} \tag{3.19}$$

In addition it is possible to say that [BC11, Prop. 19.3], if there exists a solution $\overline{y}$ to the dual problem such that $f^* \,\square\, g^*$ is differentiable at $w - F^\top \overline{y}$, then the primal problem admits either no solution or a unique solution such that $\overline{x} = \nabla(f^* \,\square\, g^*)(w - F^\top \overline{y})$.

Primal-dual methods employ the Fenchel-Rockafellar duality in order to decompose the optimization process related to Problem 3.17 into elementary steps: by rewriting h in terms of its conjugate, one obtains

$$\underset{y \in \operatorname{dom} h^*}{\text{maximize}} \quad \underset{x \in \mathbb{R}^N}{\text{minimize}} \quad f(x) + g(x) + y^\top Fx - h^*(y) - w^\top x, \tag{3.20}$$

where $\operatorname{dom} h^* = \big\{ y \in \mathbb{R}^M \;\big|\; h^*(y) < +\infty \big\}$. So doing, one actually aims at solving simul-

taneously both the primal and dual problems in (3.17)-(3.18), leading to

$$\begin{cases} \overline{x} \in \underset{x \in \mathbb{R}^N}{\arg\min}\ f(x) + g(x) - (w - F^\top \overline{y})^\top x, \\ \overline{y} \in \underset{y \in \mathbb{R}^M}{\arg\min}\ h^*(y) - y^\top F \overline{x}. \end{cases} \tag{3.21}$$

The goal of primal-dual methods is to find a pair $(\overline{x}, \overline{y}) \in \mathbb{R}^N \times \mathbb{R}^M$ such that

$$\begin{cases} 0 \in \partial f(\overline{x}) + \nabla g(\overline{x}) - w + F^\top \overline{y} \\ 0 \in \partial h^*(\overline{y}) - F\overline{x}, \end{cases} \quad \Leftrightarrow \quad \begin{cases} \overline{x} = \mathrm{prox}_f \left(\overline{x} - \nabla g(\bar{x}) + w - F^\top \overline{y}\right) \\ \overline{y} = \mathrm{prox}_{h^*} \Big(\overline{y} + F\overline{x}\Big). \end{cases} \tag{3.22}$$

The above condition guarantees, under technical assumptions, that $\overline{x}$ is a solution to (3.17), $\overline{y}$ is a solution to (3.18), and $(\overline{x}, \overline{y})$ is a solution to (3.20) [BC11, Theorem 19.1, Proposition 19.18]. Thanks to (3.22), the Problem (3.17) can be solved through the separate evaluation of operators prox_f, ∇g, and prox_h, which naturally leads to algorithms easier to implement. Furthermore, the Lipschitz-differentiable function is activated through its gradient, which is easier to compute than its proximity operator. As pointed out in [Chi14], Problem (3.17) can actually include an arbitrary number of non-smooth functions by setting

$$F = [F_1^\top \dots\ F_R^\top]^\top, \qquad y = [y_1^\top \dots\ y_R^\top]^\top, \qquad h(y) = h_1(y_1) + \cdots + h_R(y_R),$$

with $F_r \in \mathbb{R}^{M_r \times N}$, $y_r \in \mathbb{R}^{M_r}$, and $h_r \in \Gamma_0(\mathbb{R}^{M_r})$ for every $r \in \{1, \dots, R\}$.

Some primal-dual methods can be derived from a more general version of the forward-backward splitting [CCPVu14], such as the one illustrated in Algorithm 3, as well as some primal-dual methods are based on other approaches, like the one in Algorithm 4. A survey on primal-dual methods can be found in [KP15].

Algorithm 3 FBPD method [Con13, Vu13]

Initialization

$$\left\lfloor \begin{array}{l} \text{choose } \left(x^{[0]}, y^{[0]}\right) \in \mathbb{R}^N \times \mathbb{R}^M \\ \text{set } \tau > 0 \text{ and } \sigma > 0 \text{ such that} \\ \qquad \tau\left(\beta/2 + \sigma\|F\|^2\right) < 1 \end{array} \right.$$

For $i = 0, 1, \ldots$

$$\left\lfloor \begin{array}{l} \widehat{x}^{[i]} = \nabla g(x^{[i]}) - w + F^\top y^{[i]} \\ x^{[i+1]} = \mathrm{prox}_{\tau f}\left(x^{[i]} - \tau\, \widehat{x}^{[i]}\right) \\ \widehat{y}^{[i]} = F\big(2x^{[i+1]} - x^{[i]}\big) \\ y^{[i+1]} = \mathrm{prox}_{\sigma h^*}\left(y^{[i]} + \sigma\, \widehat{y}^{[i]}\right) \end{array} \right.$$

Algorithm 4 M+LFBF method [CP12]

Initialization

$$\left\lfloor \begin{array}{l} \text{choose } \left(x^{[0]}, y^{[0]}\right) \in \mathbb{R}^N \times \mathbb{R}^M \\ \text{set } \gamma \in \left]0, (\beta + \|F\|)^{-1}\right[\end{array} \right.$$

For $i = 0, 1, \ldots$

$$\left\lfloor \begin{array}{l} \widehat{x}^{[i]} = \nabla g(x^{[i]}) - w + F^\top y^{[i]} \\ p^{[i]} = \mathrm{prox}_{\gamma f}\left(x^{[i]} - \gamma\, \widehat{x}^{[i]}\right) \\ v^{[i]} = \mathrm{prox}_{\gamma h^*}\left(y^{[i]} + \gamma\, F x^{[i]}\right) \\ y^{[i+1]} = v^{[i]} + \gamma F\left(p^{[i]} - x^{[i]}\right) \\ \widetilde{x}^{[i]} = \nabla g(p^{[i]}) - w + F^\top v^{[i]} \\ x^{[i+1]} = p^{[i]} - \gamma\left(\widetilde{x}^{[i]} - \widehat{x}^{[i]}\right) \end{array} \right.$$

3.2 Rate allocation based on R-D modelling

Accurate Rate-Distortion (R-D) modelling plays a fundamental role in optimal bit allocation. Due to the different characteristics of frames, as well as the sophisticated compression techniques employed in coding algorithms, analytic R-D modelling is still an open problem.

The first contribution of this thesis is the proposition of a suitable R-D model for the frames of a GOP able to describe dependencies between the distortions of the frames; we used the same theoretical foundations as in [USC93], but we extend the R-D model by letting the exponential decay vary at each frame, allowing us to better represent the intrinsic non-stationarities in a group of frames (in [USC93], it is explicitly required that the exponential decay needs to be the same for all the frames).

First of all we exploited the dependencies between distortions inside a GOP. We consider I-P-P-P as GOP structure, where I denotes intra-predicted frames, and P denotes inter-predicted frames. To enter into detail of the concepts previously expressed, we refer to the coding scheme of Figure 3.1.

The first input frame I_n is encoded in intra mode, independently from the others. The spatial coding operates in three stages, as explained in Sec. 1.2: block-wise Discrete Cosine Transform (DCT), scalar quantization of the transformed coefficients (Q) and lossless coding of quantization indices (VLC). The resulting output $\widehat{Q}_{I_n}$ is sent to the decoder. Furthermore, the quantization indices of I_n are sent to the feedback loop, where they are used to reconstruct a decoded version $\widetilde{I}_n$ of the input frame. This quantity is kept in a buffer and will contribute to the temporal prediction of the next frames.

The following frames in the same GOP are encoded in inter mode: the prediction P_n of

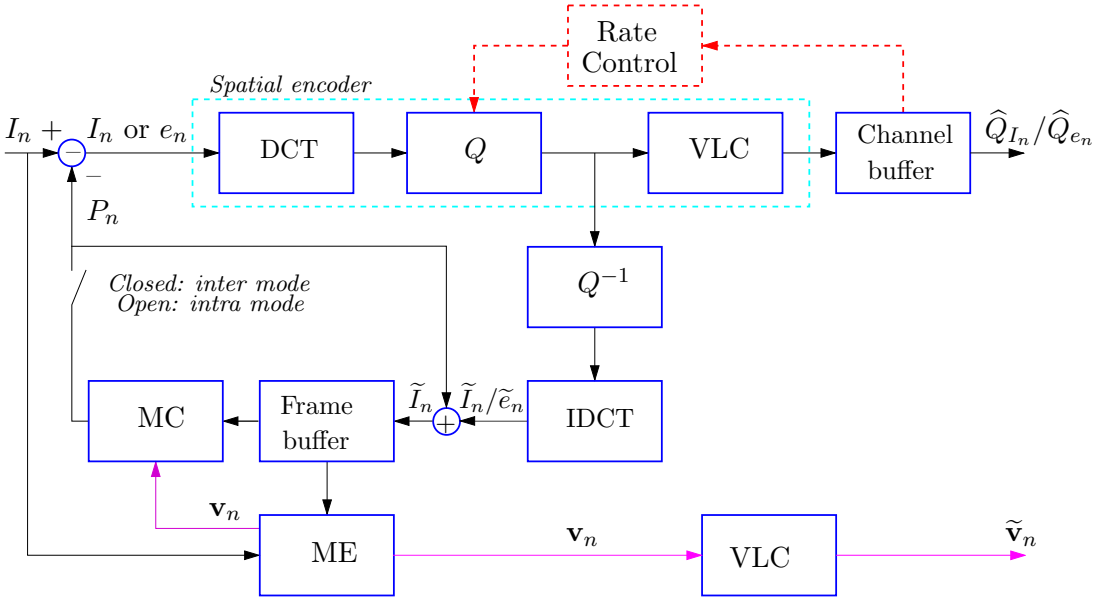

Figure 3.1: Hybrid video compression system. In H.264/AVC and HEVC spatial prediction is performed on intra-frame

the input frame I_n generated by the feedback loop. The spatial encoder is fed with the prediction error $e_n = I_n - P_n$ and the output $\widehat{Q}_{e_n}$ is sent to the decoder. Moreover, the quantization indices of e_n are sent to the feedback loop, where they are used to reconstruct the decoded version $\widetilde{e}_n$ of the prediction error. This quantity is then used to compute $\widetilde{I}_n = P_n + \widetilde{e}_n$ (the decoded version of the frame I_n), which is stored in the buffer and will contribute to the temporal prediction of the next frames.

The temporal prediction consists of two stages: motion estimation (ME) and motion compensation (MC). The ME unit estimates the motion occurred between the input frame I_n and the previously decoded frame $\widetilde{I}_{n-1}$. The result is a field $\mathbf{v}_n$ that contains the motion vector of each block from I_n to $\widetilde{I}_{n-1}$. The motion vector field $\mathbf{v}_n$ is fed into the MC unit, which generates the prediction P_n from $\widetilde{I}_{n-1}$ and $\mathbf{v}_n$ through a uniquely defined operation f such that $P_n = f(\widetilde{I}_{n-1}, \mathbf{v}_n)$. The vector field $\mathbf{v}_n$ is then losslessly coded (VLC) and sent to the decoder.

3.2.1 Recursive frame-level rate-distortion model

Our goal is to have a global frame based distortion model, using the model in [SW98a], in order to formulate the bit-allocation as a convex optimization problem. First, we show that the distortion of a P-frame, when compressed at high-resolution, can be modelled as

$$D_n = \alpha_n \left(M_n + D_{n-1}\right) 2^{-2\,r_n}, \tag{3.23}$$

where r_n is the rate allocated to the frame, $M_n \triangleq \mathbb{E}\{[I_n - f(I_{n-1}, \mathbf{v}_n)]^2\}$ is the error in the motion compensation, and D_{n-1} is the distortion of the previous frame. Second, we

eliminate the recursion in D_n by expressing it in function of rates $(r_0, \ldots, r_n)$. Finally, we formulate the optimization problem deriving from this formulation.

Consider a GOP $I = (I_0, \ldots, I_{N-1})$ of size $N > 0$. For every $n \in \{0, \ldots, N-1\}$, we assume that the frame I_n is a realization of a wide-sense stationary discrete-time random process. We also assume that I_0 is an I-frame and, for every $n \in \{1, \ldots, N-1\}$, I_n is a P-frame and $\mathbb{E}\{e_n\} = 0$.

For every $n \in \{0, \ldots, N-1\}$, the distortion D_n is measured as the MSE between I_n and $\widetilde{I}_n$

$$D_n = \mathbb{E}\{[I_n - \widetilde{I}_n]^2\}. \tag{3.24}$$

The distortion D_0 affecting the I-frame $\widetilde{I}_0$ is directly connected to the amount of bits $r_0 \in \mathbb{N}$ used in the coding stage

$$D_0 = \alpha_0 \, \sigma_0^2 \, 2^{-2\,r_0}, \tag{3.25}$$

where $\alpha_0 \in \mathbb{R}$ and $\sigma_0^2 \in \mathbb{R}$ are, respectively, the pdf shape factor and the variance of the residual DCT coefficients.

The distortion of the P-frame I_n is equal to the distortion of the prediction error e_n:

$$D_n = \mathbb{E}\{[I_n - \widetilde{I}_n]^2\} = \mathbb{E}\{[e_n + P_n - (\widetilde{e}_n + P_n)]^2\} = \mathbb{E}\{[e_n - \widetilde{e}_n]^2\}. \tag{3.26}$$

It follows that D_n can be approximated by $D_n = \alpha_n \, \sigma_n^2 \, 2^{-2\,r_n}$, where α_n is the shape factor of the pdf that models the prediction error, $\sigma_n^2 = \mathbb{E}\{e_n^2\}$ and r_n is the amount of bits used to code $\widetilde{e}_n$. Now, let us turn to σ_n^2. Firstly, we note that

$$\begin{aligned} e_n &= I_n - P_n \\ &= I_n - f(I_{n-1}, \mathbf{v}_n) + f(I_{n-1}, \mathbf{v}_n) - P_n \\ &= I_n - f(I_{n-1}, \mathbf{v}_n) + f(I_{n-1}, \mathbf{v}_n) - f(\widetilde{I}_{n-1}, \mathbf{v}_n) \end{aligned} \tag{3.27}$$

The term $M_n \triangleq \mathbb{E}\{[I_n - f(I_{n-1}, \mathbf{v}_n)]^2\}$ is the error in the motion compensation, while $\mathbb{E}\{[f(I_{n-1}, \mathbf{v}_n) - f(\widetilde{I}_{n-1}, \mathbf{v}_n)]^2\}$ is the distortion of the prediction P_n. By the hypothesis of wide-sense stationarity, the latter term is equal to the distortion of I_{n-1}

$$\mathbb{E}\{[f(I_{n-1}, \mathbf{v}_n) - f(\widetilde{I}_{n-1}, \mathbf{v}_n)]^2\} = \mathbb{E}\{[I_{n-1} - \widetilde{I}_{n-1}]^2\} = D_{n-1}.$$

Therefore, it is reasonable to assume that $I_n - f(I_{n-1}, \mathbf{v}_n)$ and $f(I_{n-1}, \mathbf{v}_n) - f(\widetilde{I}_{n-1}, \mathbf{v}_n)$ are uncorrelated, and it has been experimentally shown that this hypothesis is verified in real codecs [Mau10]. This leads to $\sigma_n^2 = \mathbb{E}\{[I_n - f(I_{n-1}, \mathbf{v}_n)]^2\} + \mathbb{E}\{[f(I_{n-1}, \mathbf{v}_n) - f(\widetilde{I}_{n-1}, \mathbf{v}_n)]^2\} = M_n + D_{n-1}$.

Using induction we can demonstrate that the distortion of the frame I_n reads

$$(\forall n \in \{1, \dots, N-1\}) \qquad D_n = \sum_{\ell=0}^{n} \alpha^{(\ell,n)} M_\ell \, 2^{\sum_{j=\ell}^{n} -2\, r_j}, \tag{3.28}$$

where $\alpha^{(\ell,n)} = \prod_{j=\ell}^{n} \alpha_j$ and $M_0 = \sigma_0^2$. When $n = 0$, eq. (3.28) reduces to (3.29)

$$D_0 = \alpha_0 M_0 2^{-2\, r_0} = \alpha_0 \sigma_0^2 \, 2^{-2\, r_0}. \tag{3.29}$$

Now, let us assume that eq. (3.28) holds for D_{n-1}, with $n > 0$. By plugging D_{n-1} into (3.23), we get

$$\begin{aligned} D_n &= \alpha_n (M_n + D_{n-1}) 2^{-2\, r_n} \\ &= \alpha_n (M_n + \sum_{\ell=0}^{n-1} \alpha^{(\ell,n-1)} M_\ell \, 2^{-2 \sum_{j=\ell}^{n-1} r_j}) 2^{-2\, r_n} \\ &= \alpha_n M_n 2^{-2\, r_n} + \sum_{\ell=0}^{n-1} \alpha^{(\ell,n)} M_\ell \, 2^{-2 \sum_{j=\ell}^{n} r_j} \\ &= \sum_{\ell=0}^{n} \alpha^{(\ell,n)} M_\ell \, 2^{-2 \sum_{j=\ell}^{n} r_j}. \end{aligned} \tag{3.30}$$

This proves that eq. (3.28) holds for every $n \in \{0, 1, \dots, N-1\}$.

3.2.2 R-D model for I and P frames

In our optimal allocation technique a crucial factor is the choice of an appropriate R-D model. For a given distortion metric, there exist in the literature several functions that describe the R-D relationship, and it is fundamental to choose one that is able to describe this relationship in an accurate way but at the same time that it is simple enough to be inserted in an convex optimization algorithm.

In the previous calculations we used the typical R-D curve in high-rate approximation, which is, for its simpleness, the best way to formalize our convex optimization problem. The distortion of a frame, when compressed at high-resolution, can be expressed as

$$D = \alpha \sigma^2 2^{-2R}. \tag{3.31}$$

A different model we focused on was proposed in [PADZ11] and in [PAZD11] and is based on a modification of the classical R-D model, introducing some sequence dependent parameters in the argument of the power function that make it more elastic. For intra-coded frame:

$$R(D) = G \cdot \left(\frac{a_0}{D + b_0} + c_0 \right) \tag{3.32}$$

where a_0, b_0 and c_0 are model parameters. G is the average gradient of a frame defined as

$$G = \frac{1}{W \cdot H} \sum_{j=2}^{H} \sum_{i=2}^{W} (|p_{i,j} - p_{i,j-1}| + |p_{i,j} - p_{i-1,j}|) \tag{3.33}$$

where $p_{i,j}$ is the luminance value at the location (i, j) in the current frame, W and H are the width and height of the current frame. For inter-coded frames, since the DCT coefficients are assumed to be of zero-meaned Laplacian distribution, the following rate-distortion function is employed

$$R(D) = a_1 log\left(\frac{\sigma^2}{D}\right) + b_1 \tag{3.34}$$

where a_1 and b_1 are model parameters and σ^2 is the variance of the DCT coefficients. Since we are interested in the expression of D as a function of R, we inverted the relationships obtaining:

$$D(R) = \frac{a_0 \cdot G}{R - c_0 \cdot G} - b_0 \tag{3.35}$$

for I-frames, and

$$D(R) = \sigma^2 \, 2^{-\frac{R-b_1}{a_1}} \tag{3.36}$$

for P-frames.

After testing the validity of this model we have proposed a R-D relationship based on a modification of the classical model with the addition of a new parameter β to make it more flexible. We used the same theoretical foundation as in [USC93] but we extended the R-D model by letting the exponential decay factor to vary at each frame, allowing us to better represent the intrinsic non-stationarities in a group of frames. The distortion of the $n - th$ frame is expressed as:

$$D_n = a_n \cdot 2^{-\beta_n r_n} \tag{3.37}$$

where a_n and β_n are sequence dependent parameters. In particular we can express a_n for a I-frame as:

$$a_n = \alpha_0 \cdot \sigma_0^2 \tag{3.38}$$

and for a P-frame

$$a_n = \alpha_n (M_n + D_{n-1}) \tag{3.39}$$

where α_0, α_n, σ_0^2, M_n and D_{n-1} have the same meaning of the previous section. With this new R-D model we can easily modify our mathematical recursive model (3.30):

$$D_n = \sum_{\ell=0}^{n} \alpha^{(\ell,n)} \, M_\ell \, 2^{-\sum_{j=\ell}^{n} \beta_j r_j}. \tag{3.40}$$

Sequence	R^2 *with* (3.37)	R^2 *with* (3.31)	R^2 *with* [PAZ$^+$13]
hall	0.997	0.975	0.455
foreman	0.995	0.908	0.912
football	0.985	0.762	0.849
container	0.985	0.824	0.774
coastguard	0.984	0.395	0.596
akiyo	0.980	0.974	0.745
mother daughter	0.979	0.979	0.597
eric	0.972	0.791	0.948

Table 3.1: Distortion estimation accuracy for different sequences

3.2.3 Model validation

The first experiments were performed using H.264/AVC [SWL03] video encoder on several sequences. The estimation of model parameters (α_n, β_n, M_n) was performed by encoding each sequence with different QPs. For each frame, we recorded the values of D and R produced at the encoder output and, after a logarithmic transformation of D, we estimated the model parameters through a linear regression. The motion-estimation parameters M_n are obtained by encoding each sequence with a modified version of the encoder that computes M_n for each frame, using a $QP = 1$ so that the quantization does not affect the motion estimation and compensation functions of the encoder.

First of all we compared the R-D model proposed in eq. (3.37) to the classical R-D model of eq. (3.31), and to the model proposed in [PAZ$^+$13]. The validation was performed on the basis of the R^2 metric [DF99], which was designed to quantitatively measure the degree of deviation from a given model. It is defined as

$$R^2 = 1 - \frac{\sum_i (X_i - \widehat{X_i})^2}{\sum_i (X_i - \overline{X})^2}, \tag{3.41}$$

where X_i and $\widehat{X_i}$ are the real and the estimated values of one data point, and $\overline{X}$ is the mean of all data points; the closer the value of R^2 is to 1, the more accurate the model.

Table 3.1 shows the R^2 values associated to the R-D function of given in Equations (3.31) – (3.35). For all the sequences, the proposed model (3.37) shows superior fitting performance, giving R^2 values very close to 1 and higher than (3.31) and (3.35). As observed from the table, for all the test sequences, the proposed model gives higher R^2 values, which indicates higher accuracy. Figure 3.2 shows a visual comparison of the fitting performance of the three R-D models and how well each of them can approximate the distortion values of H.264/AVC.

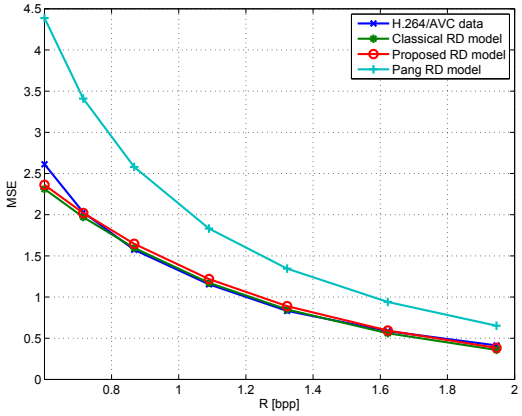

(a) Sequence *akiyo*.

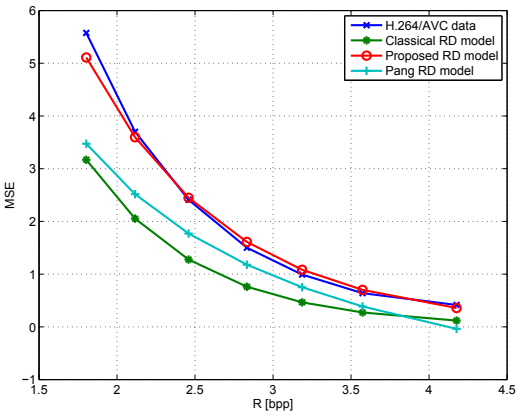

(b) Sequence *coastguard*.

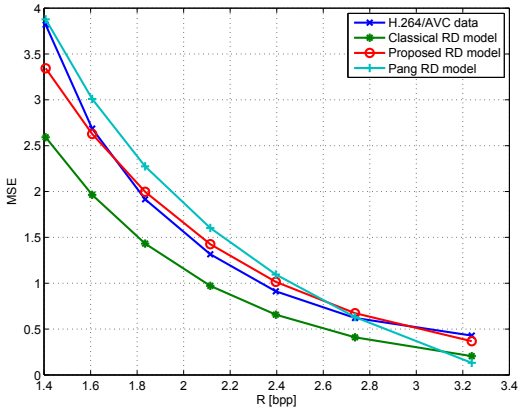

(c) Sequence *eric*.

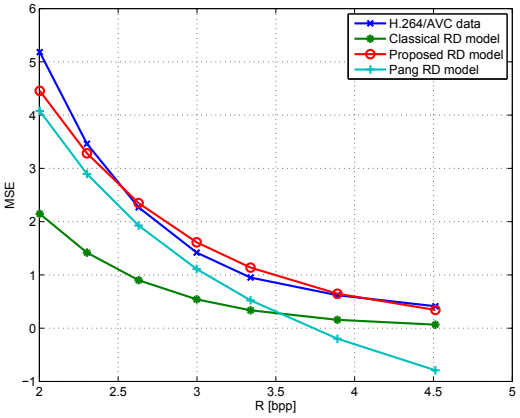

(d) Sequence *football*.

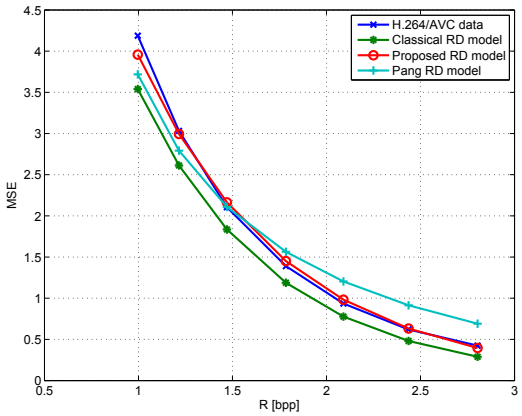

(e) Sequence *foreman*.

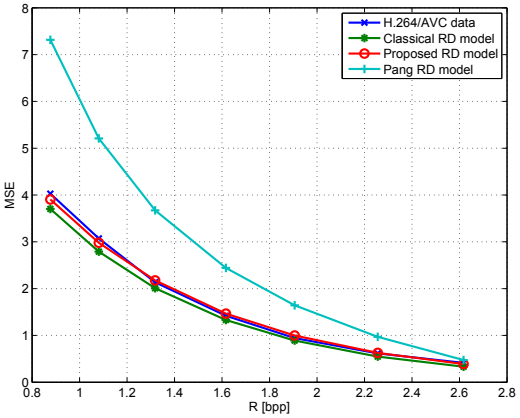

(f) Sequence *hall*.

Figure 3.2: Fitting performance of the three presented models.

3.2.4 Frame-level bit-rate allocation: problem formulation

Optimal rate allocation consists of finding the rate vector $r = (r_0, \dots, r_{N-1})$ that minimizes the global distortion while keeping the total rate under a given budget $\eta > 0$, that is

$$\underset{r \in [0,+\infty[^N}{\text{minimize}} \quad \sum_{n=0}^{N-1} D_n(r_0, \dots, r_n) \qquad \text{s. t.} \qquad \sum_{n=0}^{N-1} r_n \leq \eta. \tag{3.42}$$

By using the distortion function proposed in eq. (3.40), the above formulation boils down to a convex optimization problem that can be *efficiently* and *exactly* solved by the primal-dual proximal algorithms introduced in Sec. 3.1.

To gain some insight into the solution of Problem (3.42), we can introduce a vector $u = (u_{n\ell})_{0 \leq n \leq N-1, 0 \leq \ell \leq n}$ defined as

$$u_{n\ell} = -\sum_{j=\ell}^{n} \beta_j r_j, \tag{3.43}$$

which allows us to express the global distortion as a separable sum of exponentials

$$\varphi(u) = \sum_{n=0}^{N-1} \sum_{\ell=0}^{n} \alpha^{(n,\ell)} M_\ell \, e^{u_{n\ell}}. \tag{3.44}$$

Therefore, Problem (3.42) can be reformulated as follows

$$\underset{r \in \mathbb{R}^N}{\text{minimize}} \quad \varphi(\mathsf{L} r) + \iota_C, \tag{3.45}$$

where $\mathsf{L} \colon \mathbb{R}^N \mapsto \mathbb{R}^{\frac{N(N+1)}{2}}$ is the linear operator that maps the vector $r \in \mathbb{R}^N$ into the vector $u \in \mathbb{R}^{\frac{N(N+1)}{2}}$ defined in (3.43), $C \subset \mathbb{R}^N$ is the non-empty closed convex set defined as

$$C = \big\{ r \in [0, +\infty[^N \;\big|\; \sum_{n=0}^{N-1} r_n \leq \eta \big\}, \tag{3.46}$$

and ι_C denotes the indicator function of C, equal to 0 if $r \in C$ and $+\infty$ otherwise, so as to enforce the bit budget constraint.

For the resolution of Problem (3.45), we employ the Forward-Backward Primal-Dual algorithm [Con13] introduced in Section 3.1.3, which consists of iterating the following steps for a given initialization $(r^{[0]}, u^{[0]})$:

$$(\forall i \in \mathbb{N}) \quad \left| \begin{array}{l} r^{[i+1]} = \operatorname{prox}_{\tau \iota_C} \Big(r^{[i]} - \tau \mathsf{L}^\top u^{[i]} \Big) \\ u^{[i+1]} = \operatorname{prox}_{\gamma \varphi^*} \Big(u^{[i]} + \gamma \, \mathsf{L} \big(2 r^{[i+1]} - r^{[i]} \big) \Big) \end{array} \right. \tag{3.47}$$

where $\tau > 0$ and $\gamma > 0$ are two algorithmic parameters, whereas φ^* denotes the convex

Algorithm 5 FBPD [Con13] for solving Problem (3.45)

Inputs : $\eta, (\alpha_n, \beta_n, M_n)_{0 \leq n \leq N-1}$
Output : r
Initialization
  select $r^{[0]} \in \mathbb{R}^N$ and $u^{[0]} \in \mathbb{R}^{\frac{N(N+1)}{2}}$
  set $\tau > 0$ and $\gamma > 0$ such that $\tau\gamma\|\mathsf{L}\|^2 \leq 1$
For $i = 0, 1, \ldots$
  $r^{[i+1]} = P_C\big(r^{[i]} - \tau\, \mathsf{L}^\top u^{[i]}\big)$
  $u^{[i+1]} = \mathrm{prox}_{\gamma\varphi^*}\Big(u^{[i]} + \gamma\, \mathsf{L}\big(2r^{[i+1]} - r^{[i]}\big)\Big)$

conjugate of the function φ.

The main advantage of proximity operators is that the functions to be optimized do not need to be differentiable. This allows us to enforce the constraint C defined in eq. (3.46) through its indicator function, as the proximity operator of ι_C coincides to the *orthogonal projection* onto C, yielding (3.12). Consequently, the iterations in (3.47) lead to Algorithm 5, which is guaranteed to converge to a solution to Problem (3.45) for a suitable choice of τ and γ [Con13], and can be efficiently implemented on both multi core and GPGPU architectures [GCPP12].

Algorithm 5 has the ability to decompose the optimization process into elementary steps, such as P_C, $\mathrm{prox}_{\varphi^*}$, L and $\mathsf{L}^\top$. For what concerns the linear operator L defined in (4.5), its adjoint $\mathsf{L}^\top u$ yields a vector $r \in \mathbb{R}^N$ such that

$$r_n = -\beta_n \sum_{j=n}^{N-1} \sum_{\ell=0}^{n} u_{j\ell}. \tag{3.48}$$

In order to set the parameters τ and γ in Algorithm 5, one needs to compute the spectral norm of L, which is equal to the largest eigenvalue of the positive-semi-definite matrix $\mathsf{L}^\top\mathsf{L}$. This quantity can be estimated with Gelfand's Formula [Lax].

Moreover, the projection onto the set C can be efficiently computed with the linear-time algorithm proposed in [Con14], while the proximity operator of φ^* reads

$$\mathrm{prox}_{\gamma\varphi^*}(u) = \left[\gamma W\left(\frac{\alpha^{(n,\ell)}\, M_\ell\, e^{u_{n\ell}/\gamma}}{\gamma}\right)\right]_{0 \leq n \leq N-1, 0 \leq \ell \leq n} \tag{3.49}$$

where W denotes the Lambert W function.

3.2.5 Comparison with H.264/AVC

In order to evaluate the performance of the proposed algorithm, we implemented a MATLAB toolbox for:

Sequence	1.31 bpp	1.15 bpp	0.76 bpp
akiyo	3.38	6.78	3.23
football	2.28	0.95	2.26
coastguard	0.99	0.55	1.11
eric	0.10	0.12	0.19
foreman	0.080	0.026	0.015

Table 3.2: PSNR increase for several bitrates [dB]

- Parameter estimation.
- Bit allocation using the convex optimization algorithm.

In our experiments, we selected five video sequences composed of 84 frames at CIF resolution 352×288. We encoded all the sequences with a GOP structure IPP...P of size $N = 12$, a frame rate of 30 pictures per second and CABAC as entropy coder. For the motion estimation, we set the maximum search range to ±16. Moreover, we estimated the model parameters $(\alpha_n, \beta_n, M_n)_{0 \le n \le N-1}$ by encoding the sequences in H.264/AVC with the rate control disabled, in order to manually fix seven different quantization parameters: $10, 12, 14, \ldots, 22$. For each frame, we recorded the values of D and R produced at the encoder output and, after a logarithmic transformation of D, we estimated the model parameters by resorting to a linear regression. We then encoded all the sequences with the rate control of H.264/AVC enabled, setting seven different target bit-rates ranging from 2.2 to 4.0 Mb/s and reported the results in the following. The input of the convex optimization algorithm is a matrix obtained by the combination of the estimated parameters, and the output is a vector of the estimated rate for each frame, from which we estimated the distortion of each frame by applying the R-D model in eq. (3.25) and eq. (3.23).

In order to assess the validity of our rate allocation method, we compared it with the standard rate control algorithm of H.264/AVC [SWL03]. For the sequences *akiyo, coastguard, eric, football, foreman* and *hall*, Figures 3.3 to 3.8 report on the left the rates allocated by the proposed method (solid red line) and by H.264/AVC (dashed blue line), as a function of the frame number, while on the right display the corresponding distortions; in particular, for H.264/AVC it is shown the distortion produced encoding the sequences with the rate control activated, while for our method the distortion is simply evaluated from our R-D model using the allocated rates. As we can see from the figures, the rate allocation of the proposed method is quite different from the reference, especially for I-frames. Furthermore, our distribution of rates is more uniform within the GOP. This is an important result, because often the H.264/AVC encoder shows a sub-optimal greedy behaviour: it allocates the largest part of the bit budget to the first frames of the GOP and hence it rapidly runs out of bits for the remaining GOP frames, causing an increase of the global distortion. Moreover, we collected in Figure 3.9 the average distortion as a function of the average rate, and in Tab. 3.2 the corresponding PSNR increments. These

results show that the distortion achieved with the proposed method is always lower than the one obtained by the standard rate-control algorithm.

These results have been published in a conference paper at ICASSP 2014 [FCCPP14].

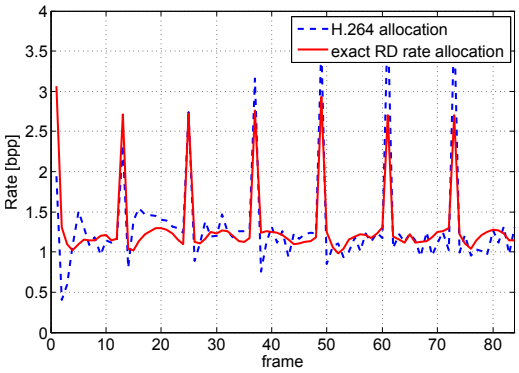

(a) Rates vs frame numbers

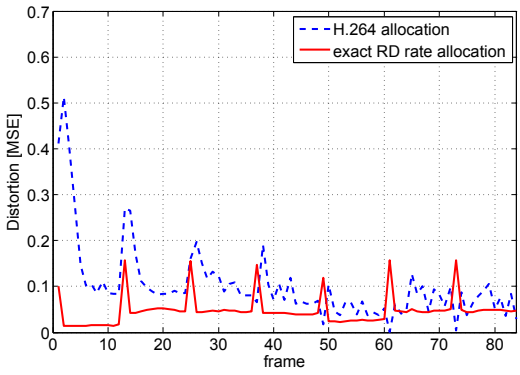

(b) Distortion vs frame numbers

Figure 3.3: Sequence *akiyo*

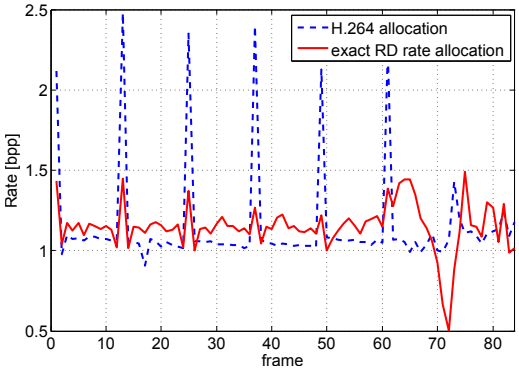

(a) Rates vs frame numbers

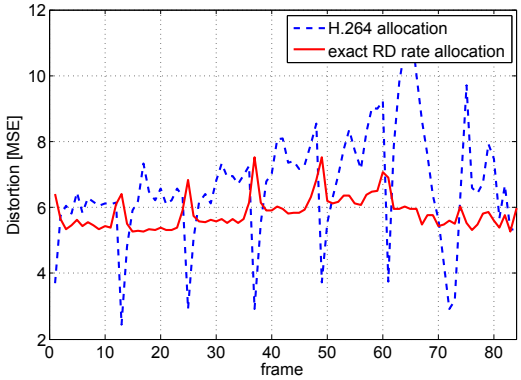

(b) Distortion vs frame numbers

Figure 3.4: Sequence *coastguard*

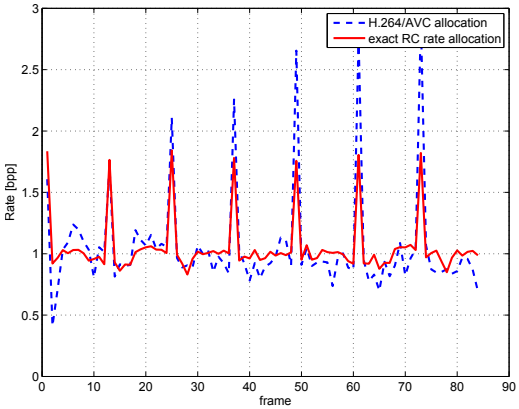

(a) Rates vs frame numbers

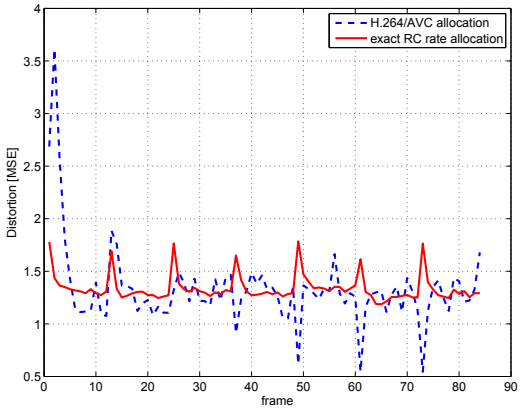

(b) Distortion vs frame numbers

Figure 3.5: Sequence *eric*

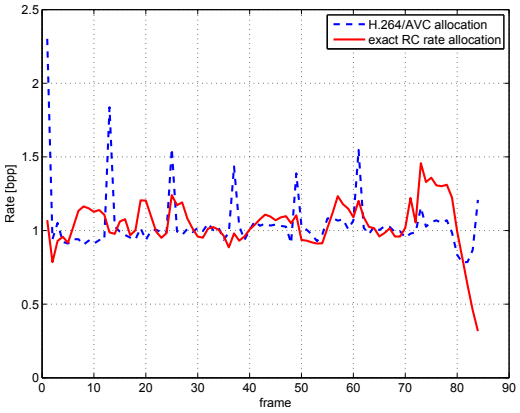

(a) Rates vs frame numbers

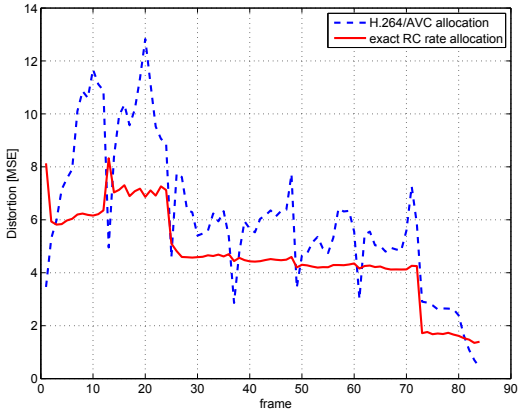

(b) Distortion vs frame numbers

Figure 3.6: Sequence *football*

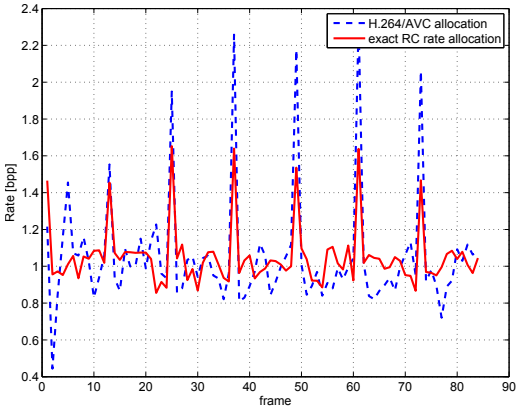

(a) Rates vs frame numbers

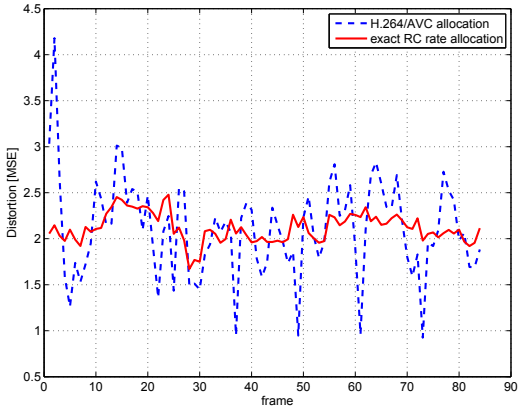

(b) Distortion vs frame numbers

Figure 3.7: Sequence *foreman*

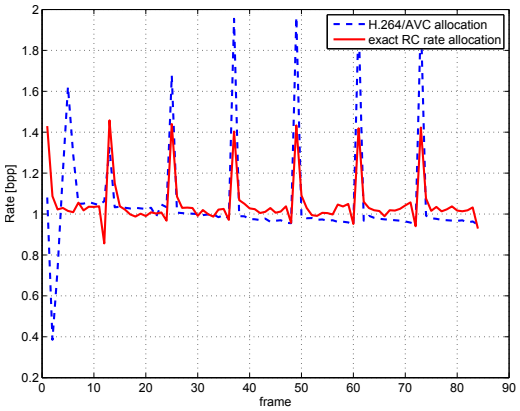

(a) Rates vs frame numbers

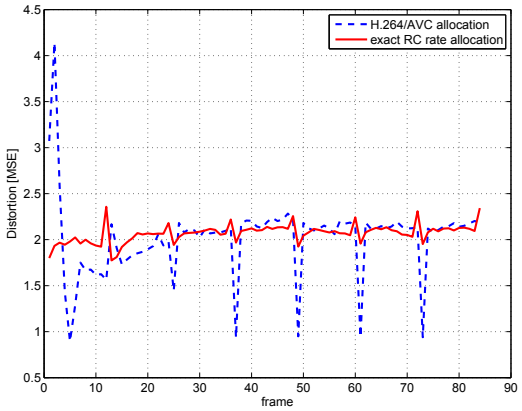

(b) Distortion vs frame numbers

Figure 3.8: Sequence *hall*

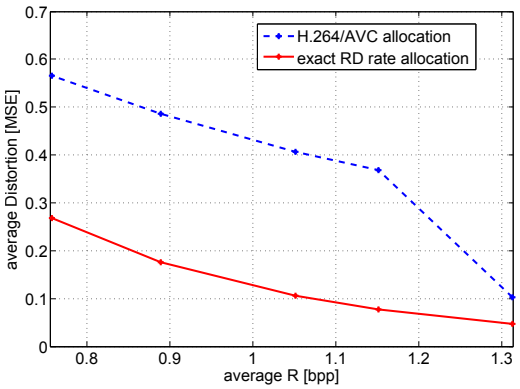

(a) Sequence *akiyo*.

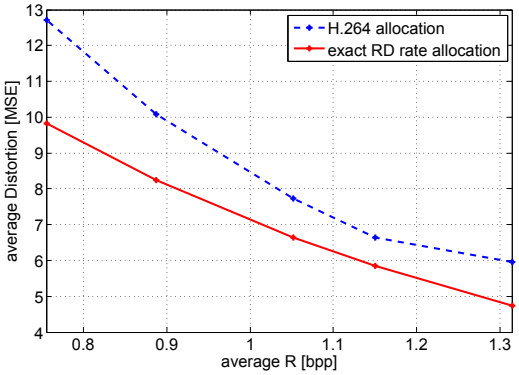

(b) Sequence *coastguard*.

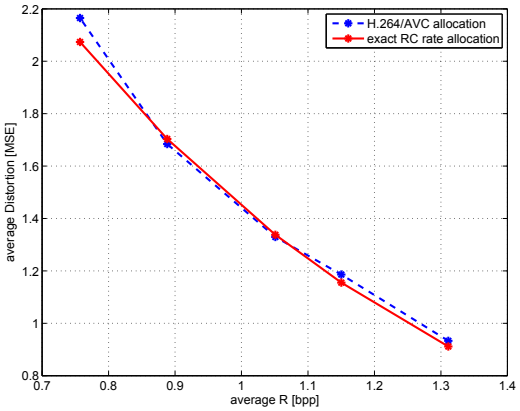

(c) Sequence *eric*.

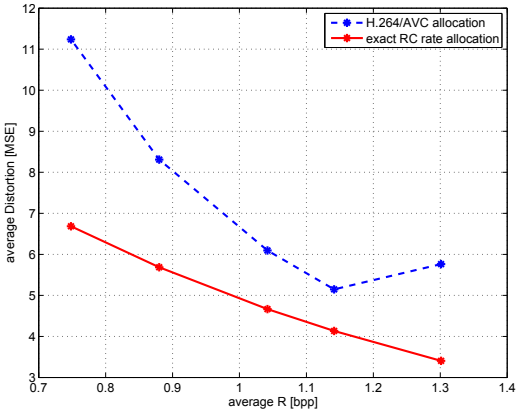

(d) Sequence *football*.

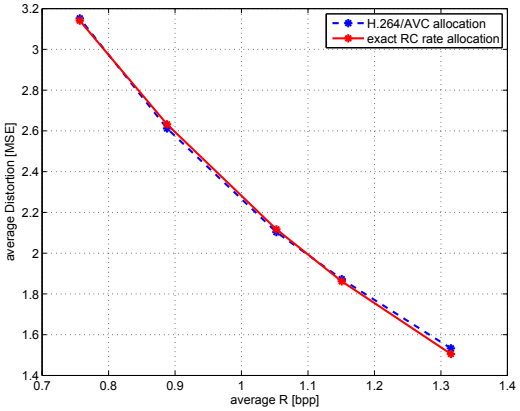

(e) Sequence *foreman*.

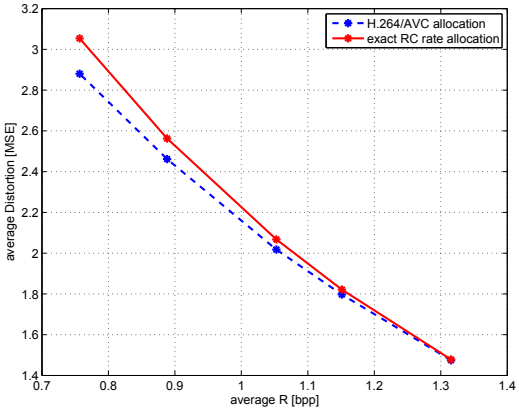

(f) Sequence *hall*.

Figure 3.9: Comparison between actual and estimated distortion.

3.3 Conclusions

In this chapter we presented a different approach for the rate allocation, based on convex optimization approach. Firstly, we have introduced the proximity operator and the primal dual methods used for constrained minimization problems. Secondly, we illustrated our recursive frame-level R-D model, we formulated the bit allocation as a convex optimization problem and we proposed an efficient algorithm to solve it. Finally, we showed the accuracy of the proposed R-D model and the potential gain that can be obtained using optimal rates in the rate control module of H.264/AVC, even though our method was not integrated in the encoder.

In the next chapter, we will focus on the state-of-the-art HEVC video encoder. In particular, we will evaluate the accuracy of our R-D model for typical HEVC video sequences, we will integrate our method into the HEVC encoder, and provide a large number comparisons with the encoder rate control module and a bit allocation method based on an exhaustive research. We will also apply our method on multi-view video coding.

Chapter 4

Experimental results

Contents

As discussed in the previous chapters, the optimal rate allocation is a non-trivial problem, because of the frame-level dependency induced by motion compensation. The methods proposed in the literature to deal with the frame-level rate allocation are either theoretical in nature [USC93], computationally demanding [ROV94], approximated [PAZ+13], or based on the MINMAX criterion.

Our proposition is an efficient solution to exactly solve the frame-level rate allocation problem formulated with the MINAVE criterion. Our approach is based on a recursive R-D model presented in Section 3.2 in which the error variance of a residual frame is decoupled in two terms: the distortion of the frame used to build the prediction, and the inaccuracy of motion estimation. In this chapter we present some experimental results that show the effectiveness of the proposed method: we integrated our method in the H.265/HEVC encoder and compared the R-D performance of our approach with the rate-control module of H.265/HEVC and the Ramchandran method [ROV94]. Finally, we adapted our method to the multi-view scenario integrating our rate allocation algorithm to MV-HEVC.

4.1 Optimal frame-level bit-allocation for HEVC video encoder

In this section, experimental results are presented to validate our convex optimization algorithm for frame-level bit-allocation presented in Section 3.2 on the HEVC codec. We embedded our method into the reference implementation of the HEVC encoder (*HM.13 RExt-6.0*),[1] which is able to encode only the Luma component of a video sequence, in order to precisely asses the validity of our R-D model and easily evaluate the overall performances.

In our experiments, we used several sequences of class A, B, C, D, and E from HEVC common test conditions [Bos13], presenting significantly different characteristics in terms of smooth and complex scenes, and slow and fast motion. Class A sequences are 150 frames long, the other 200 frames long. The configuration of the encoder is set as follows: GOP structure of I-P-P-P with a single reference frame (each P frame in a GOP only depends on the previous one), in order to have the best correspondence with the proposed R-D model; the maximum search range for motion estimation is set to 64. Four different target bit rates are selected for each sequence, in order to cover a PSNR range from 35 dB to 42 dB, as reported in Table 4.1.

First of all, we verified the accuracy of the R-D model proposed in (3.37) on the new set of sequences on the basis of the R^2 metric [DF99] and, again, we compared our model to the classical R-D model (3.31), and to the model proposed in [PAZ+13]. The results of this comparison are presented in Table 4.2, which shows how the proposed model offers superior fitting performance as in the case of H.264/AVC sequences. The optimization problem, defined as in (3.42), where the distortion is defined as in (3.40), is solved using Algorithm 5, presented in Section 3.2.4.

4.1.1 Implementation

The experimental framework is composed of three steps, as shown in Figure 4.1 and explained in the following.

- **Parameter estimation (S)**. A standard version of HEVC reference software HM.13 RExt-6.0 is used to encode the sequences at different QPs: 10, 12, 14, 16, 18, 20, 22, 24, 26, 28, 30, 32, 34, 36, 38, 40. The parameters M_n are obtained by encoding the sequences with a modified version of HM.13 RExt-6.0 that computes M_n for each frame, using a $QP = 1$ (as explained in Section 3.2.3).
- **Bit allocation (BA)**. The estimated parameters are used in Algorithm 5 to optimally allocate the rates under a bit budget constraint. The different target bit rates used for each sequence are reported in Table 4.1. For a fixed target bit rate, the algorithm allocates the bits to each frame of a GOP by minimizing the global distortion.

[1] Source code available at *https://hevc.hhi.fraunhofer.de/svn/* under the branch *svn_HEVCSoftware/tags/HM-13.0+RExt-6.0/*

Class	*Sequence*	*Resolution*	*Frame Rate* [fps]	*Target Bit Rates* [Mbps]
A	SteamLocomotive (10 bit)	2560 x 1600	60	10 25 70 140
	NebutaFestival (10 bit)		60	100 200 250 300
	PeopleOnStreet		30	15 25 45 80
	Traffic		30	15 30 40 50
B	BasketballDrive	1920 x 1080	50	30 35 40 45
	BQTerrace		60	30 35 40 45
	Cactus		50	10 15 20 30
	Kimono1		24	10 15 20 25
	ParkScene		24	10 15 20 25
C	BasketballDrill	832 x 480	50	2 3 4 5
	BQMall		60	2 3 4 5
	PartyScene		50	2 3 4 5
	RaceHorses		30	1 2 3 4
D	BasketballPass	416 x 240	50	1 1.5 2 2.5
	BlowingBubbles		50	1 1.5 2 2.5
	BQSquare		60	1 1.5 2 2.5
	RaceHorses		30	0.5 1 1.5 2
E	FourPeople	1280 x 720	60	2 3 4 5
	KristenAndSara		60	2 3 4 5
	vidyo1		60	2 3 4 5
	vidyo3		60	2 3 4 5
	vidyo4		60	2 3 4 5

Table 4.1: Sequences used in our tests. Values of target bit rare are set according to the resolution, frame rate and movement characteristics of each sequence in order to cover a PSNR range from 35 dB to 42 dB

Sequence	R^2 *with* (3.37)	R^2 *with* (3.31)	R^2 *with* [PAZ$^+$13]
BasketballDrive	0.992	0.986	0.937
BQTerrace	0.998	0.921	0.727
Cactus	0.999	0.922	0.913
Kimono1	0.999	0.941	0.972
ParkScene	0.999	0.947	0.963
BasketballDrill	0.974	0.940	0.970
BQMall	0.999	0.916	0.975
RaceHorses (832x480)	0.998	0.952	0.934
BlowingBubbles	0.999	0.937	0.916
BQSquare	0.997	0.903	0.925
RaceHorses(416x240)	0.991	0.963	0.893

Table 4.2: Distortion estimation accuracy for different HEVC sequences

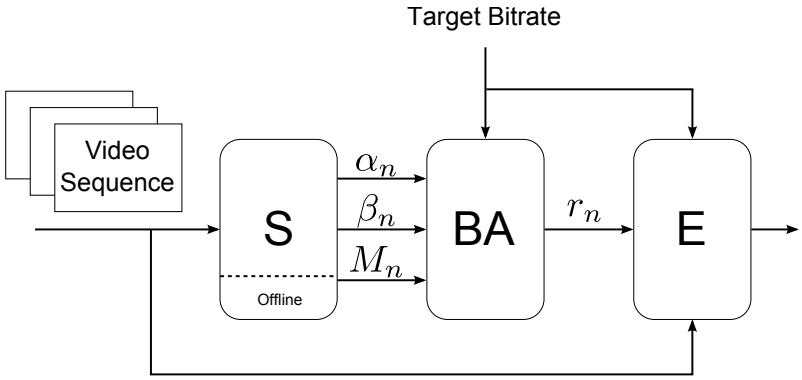

Figure 4.1: Flowchart of the proposed method: parameter estimation (block **S**), bit allocation (block **BA**), and video encoding (block **E**).

- **Encoding (E)**. The encoder is a modified version of *HM.13 RExt-6.0*, where the rate control module accepts the rates computed in the previous step.

4.1.2 Comparison with R-λ rate control

In order to assess the validity of our bit rate allocation method, we compared it to the R-λ rate control scheme implemented in the reference software of HEVC. Bjontegaard Δ bitrate (BDBR) and Bjontegaard Δ PSNR (BDPSNR)[Bjo01] are deployed to measure the average performance over the four target bitrates for each sequence. For BDPSNR, a positive number indicates a PSNR gain achieved by our method at the same bit rate; for BDBR, a negative number in the table indicates a rate reduction achieved at the same PSNR quality. Figure 4.2 shows the average PSNR as a function of the average rate for our method compared to HM R-λ for six sequences. Table 4.3 presents the rate-distortion performance of HM R-λ and our scheme for each sequence, and the average results for each class. As shown in the table, our method outperforms the conventional encoder in terms of average PSNR for all video sequences at different bitrate; in particular, we have a consistent gain for all the Class B sequences with a maximum of 1.32 dB in terms of Δ PSNR and a bit rate reduction of 30.73 %.

Table 4.4 reports the execution times of the compared methods. For our method, the table shows the times relative to the parameter estimation (block **S** in Figure 4.1), the convex optimization algorithm (block **BA** in Figure 4.1), and the video encoding (block **E** in Figure 4.1). From the table, it is clear how the parameter estimation takes 90% of the total time, but it is important to note how this phase was not optimized and the number of encoding operation performed to estimate the parameters is larger than strictly necessary, even though we did not perform an intensive analysis on this specific topic.

Another advantage of the proposed method over HM R-λ is a better stability in terms of bit rate. As shown in Figures 4.3 to 4.7, HM R-λ produces strong fluctuations around the target bit rate over the GOPs, while our method is much more stable, reaching the target bit rate for every GOP. Those fluctuations have a strong impact on the *subjective*

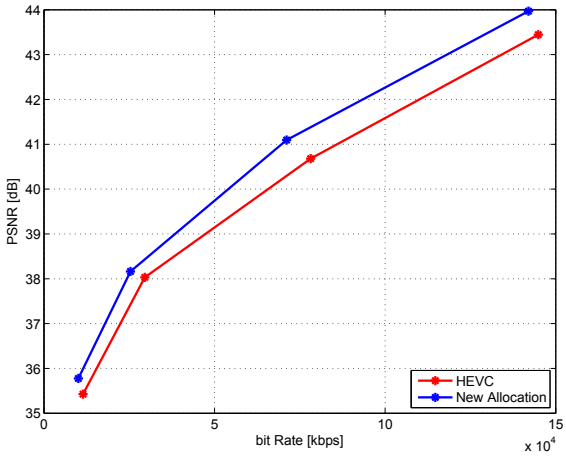

(a) Sequence *SteamLocomotive*.

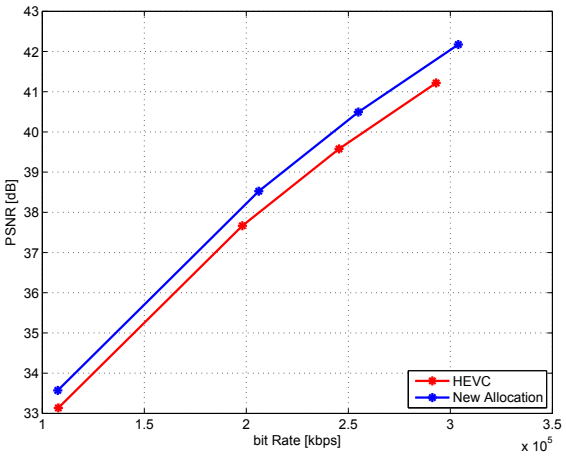

(b) Sequence *NebutaFestival*.

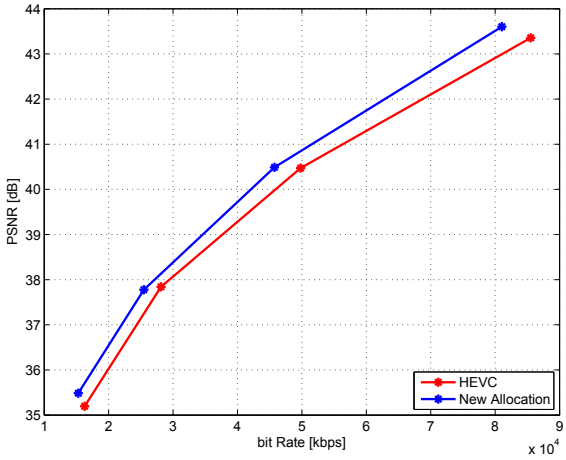

(c) Sequence *PeopleOnStreet*.

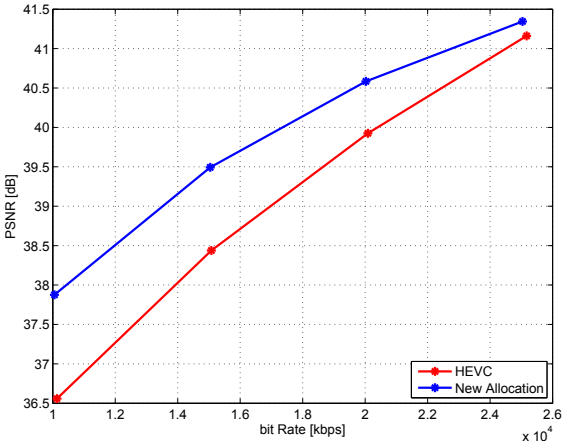

(d) Sequence *ParkScene*.

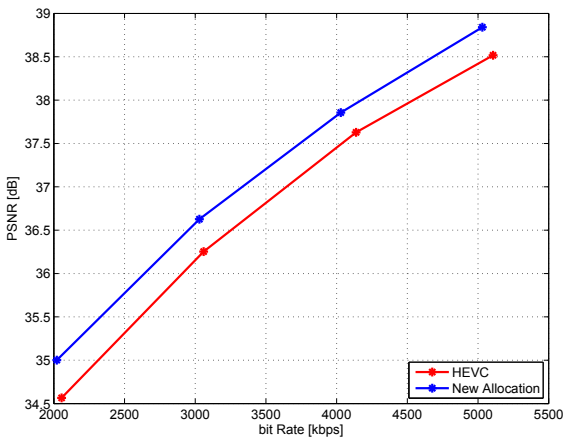

(e) Sequence *BasketballDrill*.

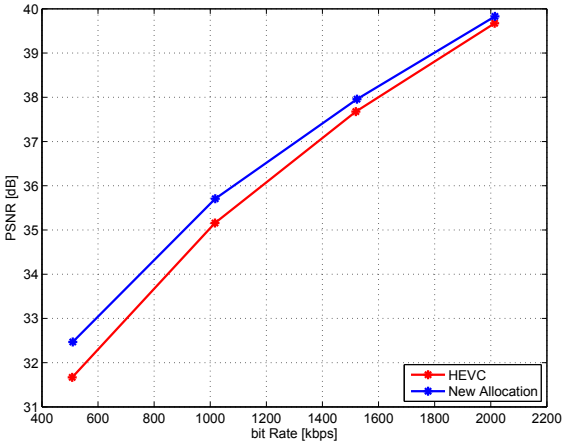

(f) Sequence *RaceHorses* (416x240).

Figure 4.2: R-D performance of HM R-λ and the proposed method.

Sequence	BDPSNR (dB)	BDBR (%)	av. BDPSNR (dB)	av. BDBR (%)
SteamLocomotiveTrain	0.62	-18.62	0.41	-8.68
NebutaFestival	0.50	-5.97		
PeopleOnStreet	0.45	-8.74		
Traffic	0.10	-1.41		
BasketballDrive	1.02	-28.00	0.93	-24.85
BQTerrace	1.01	-26.47		
Cactus	0.89	-30.73		
Kimono1	0.82	-21.21		
ParkScene	0.93	-17.84		
BasketballDrill	0.41	-9.06	0.49	-10.77
BQMall	0.59	-12.06		
PartyScene	0.43	-9.54		
RaceHorses (832x480)	0.55	-12.41		
BasketballPass	0.12	-1.89	0.74	-11.32
BlowingBubbles	0.99	-15.25		
BQSquare	1.32	-19.80		
RaceHorses (416x240)	0.52	-8.35		
FourPeople	0.43	-6.87	0.23	-5.86
KristenAndSara	0.22	-6.79		
vidyo1	0.17	-6.34		
vidyo3	0.23	-4.83		
vidyo4	0.12	-4.48		

Table 4.3: Bjontegaard metric of the proposed technique with respect to the reference the HM R-λ over various sequences.

Sequence	*Proposed*			HM R-λ
	S	BA	E	
SteamLocomotiveTrain	288470	0.03	15652	21494
NebutaFestival	480322	0.03	35806	55445
PeopleOnStreet	333428	0.03	23474	19575
Traffic	249457	0.05	17155	14536
BasketballDrive	312915	0.05	18192	13197
BQTerrace	344397	0.03	18323	10135
Cactus	332231	0.03	20409	12355
Kimono1	261911	0.04	17601	13892
ParkScene	309619	0.03	19889	12300
BasketballDrill	55801	0.04	2187	1548
BQMall	60668	0.04	1864	1357
PartyScene	78543	0.04	1963	1435
RaceHorses (832x480)	26410	0.03	2759	1908
BasketballPass	11466	0.03	649	468
BlowingBubbles	17305	0.03	756	455
BQSquare	17673	0.03	701	385
RaceHorses (416x240)	16571	0.03	932	646
FourPeople	93957	0.03	3224	2279
KristenAndSara	89341	0.03	3409	2286
vidyo1	87383	0.04	3411	2344
vidyo3	73906	0.03	3320	2242
vidyo4	82536	0.04	3383	2334

Table 4.4: Time comparison (in seconds) with the HM R-λ. For our method, the time values concern the parameter estimation (S), the convex optimization algorithm (BA), and the video encoding (E); each value is an average of the times obtained with four fixed target bit rates.

quality of the video sequences, which dramatically decrease for the last GOPs, as shown in the right plots of Figures 4.3 to 4.7. Moreover, Figures 4.8 to 4.17 illustrate some subjective quality results of the proposed method and the rate control of HEVC. For each sequence, the top pictures correspond to our method, whereas the bottom ones correspond to HM R-λ. Those figures present the frame No. 90 and the frame No. 198 for the sequences *BasketballDrive, Kimono, BQTerrace, Cactus* and *ParkScene* for both methods, and they give a visual example of the quality fluctuations pointed out in Figures 4.3 to 4.7, showing a constant visual quality for our method over the whole sequence, while the quality loss of HM results in severe blocking artefacts.

4.1.3 Comparison with an exhaustive search method

In order to evaluate the performance of our method, we decided to compare it with the bit allocation technique proposed by Ramchandran *et al.* [ROV94] and introduced in Section 2.2.3; the optimality of this method is guaranteed by the fact that it chooses the quantizers combination with the minimum Lagrangian cost among all the possible combinations. In [ROV94], two *pruning condition* (2.2.2, 2.2.3) implied by the monotonicity property of the R-D curves (2.40), which are proven to not affect the optimality of the solution, are introduced in order to ease the computational burden, and *suboptimal heuristics* are proposed to obtain an additional reduction of the complexity in exchange to performance lost. We compared our method to this suboptimal, but feasible, solution in terms of R-D performance and execution time.

The first step to implement [ROV94] was the *data generation* phase: in order to generate the R-D, we encoded each sequence with all the possible QP combinations along the frames. The complexity of this phase is clearly exponential with the number of frames, and it is possible to calculate the number of encoding operations per sequence as $\sum_{n=1}^{N} q^n = \frac{q^{N+1}-1}{q-1}$, where N is the number of encoded frames, and q is the number of used QP. In order to have a reasonable encoding time, we choose $N = 4$ and $q = 9$, using the QPs 20, 22, 25, 27, 30, 32, 35, 37, 40; again, we used as encoder HM.13 RExt-6.0 with the rate control disabled, and an I-P-P-P configuration. We implemented in Matlab:

- a tree where the nodes of level n contain the R-D data of the n-th encoded frame for each quantization choice,
- the Lagrangian cost functions for a fixed value λ,
- the tree pruning conditions implied by the monotonicity of R-D curves [ROV94] to eliminate suboptimal points.

For each sequence, we defined a set of λ values, and for each of them we selected the optimal path, that is the combination of QPs, with the minimum Lagrangian cost; among all the optimal R-D points, we selected four with a PSNR inside the range of 35 dB $\sim$

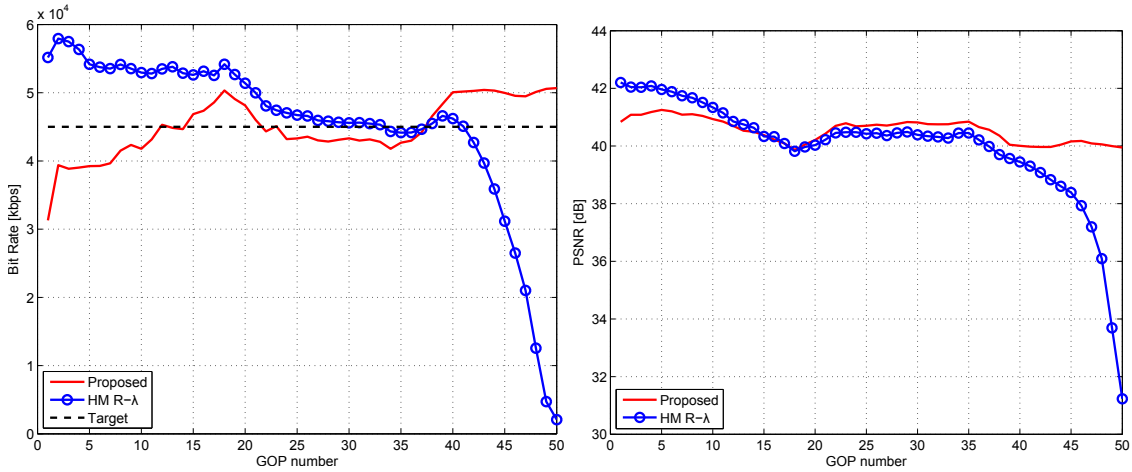

Figure 4.3: Bit rate vs. GOP number (left) and PSNR vs. GOP number (right) for the sequence *BasketballDrive*.

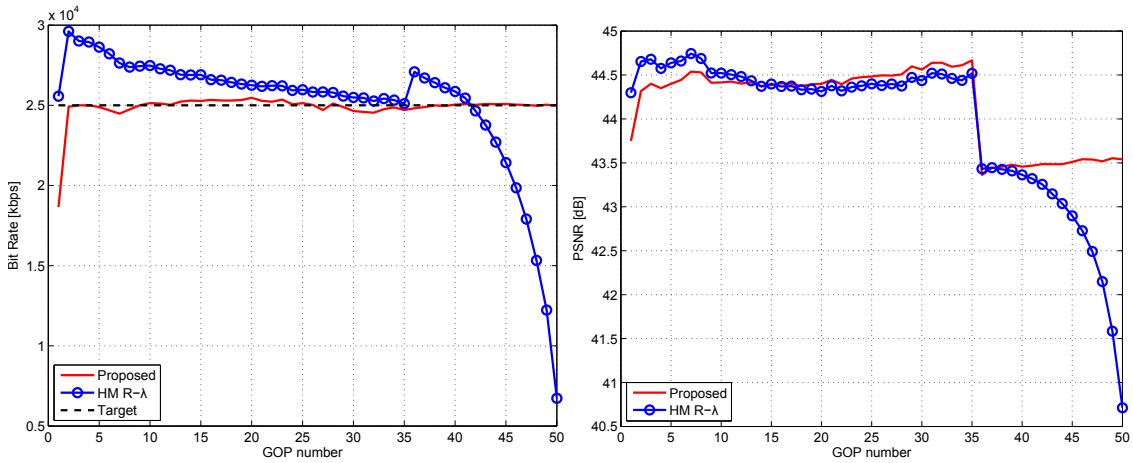

Figure 4.4: Bit rate vs. GOP number (left) and PSNR vs. GOP number (right) for the sequence *Kimono1*.

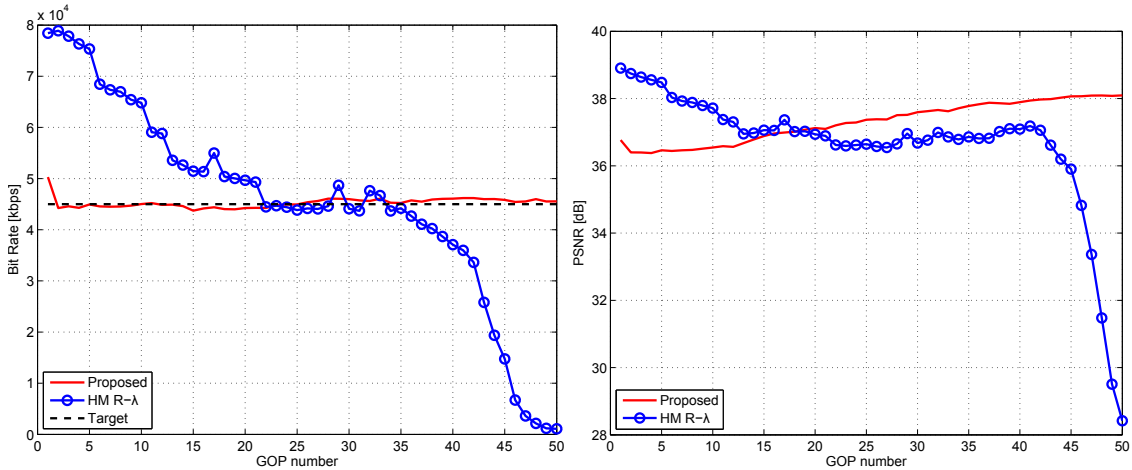

Figure 4.5: Bit rate vs. GOP number (left) and PSNR vs. GOP number (right) for the sequence *BQTerrace*.

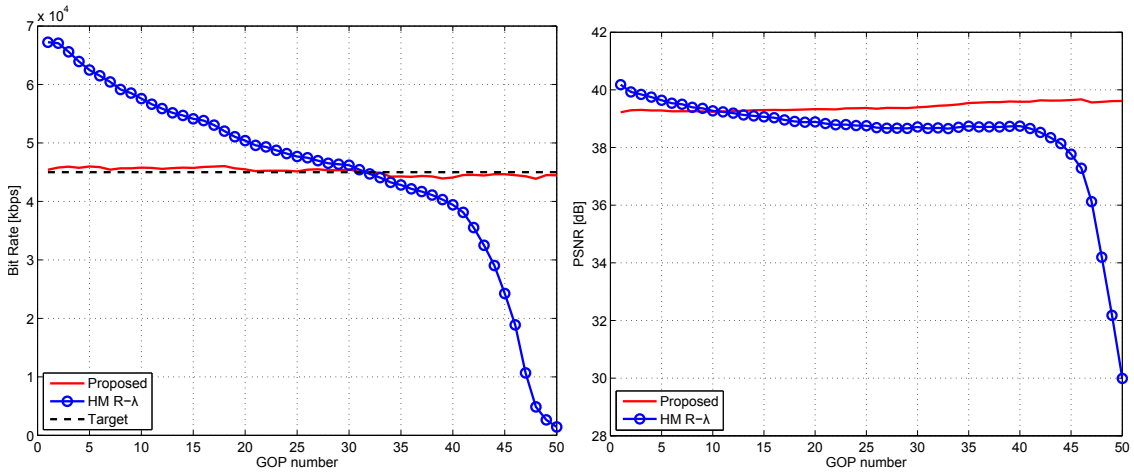

Figure 4.6: Bit rate vs. GOP number (left) and PSNR vs. GOP number (right) for the sequence *Cactus*.

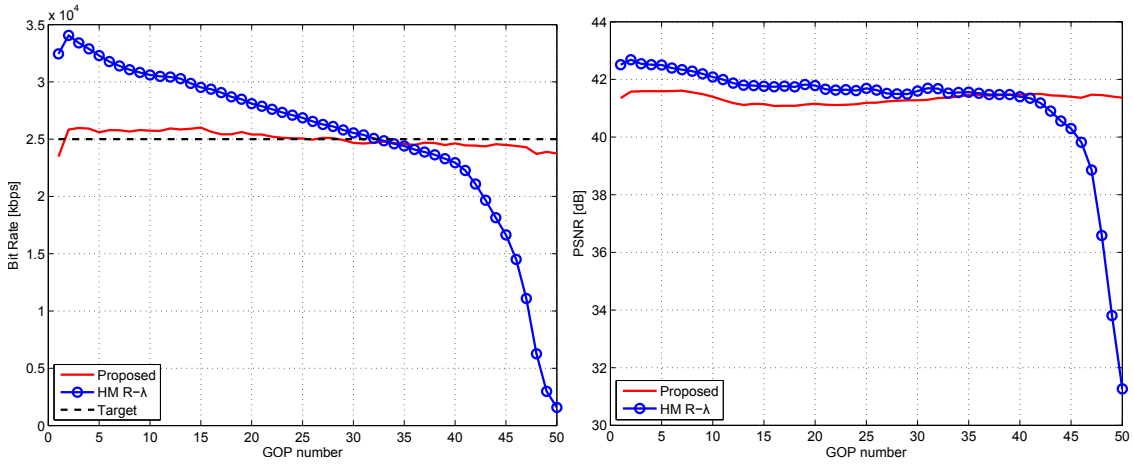

Figure 4.7: Bit rate vs. GOP number (left) and PSNR vs. GOP number (right) for the sequence *ParkScene*.

(a) Proposed method.

(b) HM R-λ.

Figure 4.8: Subjective quality of sequence *BasketballDrive* at 30 Mbps for frame No. 90.

(a) Proposed method.

(b) HM R-λ.

Figure 4.9: Subjective quality of sequence *BasketballDrive* at 30 Mbps for frame No. 198.

(a) Proposed method.

(b) HM R-λ.

Figure 4.10: Subjective quality of sequence *Kimono* at 10 Mbps for frame No. 90.

(a) Proposed method.

(b) HM R-λ.

Figure 4.11: Subjective quality of sequence *Kimono* at 10 Mbps for frame No. 198.

(a) Proposed method.

(b) HM R-λ.

Figure 4.12: Subjective quality of sequence *BQTerrace* at 30 Mbps for frame No. 90.

(a) Proposed method.

(b) HM R-λ.

Figure 4.13: Subjective quality of sequence *BQTerrace* at 30 Mbps for frame No. 198.

(a) Proposed method.

(b) HM R-λ.

Figure 4.14: Subjective quality of sequence *Cactus* at 10 Mbps for frame No. 90.

(a) Proposed method.

(b) HM R-λ.

Figure 4.15: Subjective quality of sequence *Cactus* at 10 Mbps for frame No. 198.

(a) Proposed method.

(b) HM R-λ.

Figure 4.16: Subjective quality of sequence *ParkScene* at 10 Mbps for frame No. 90.

(a) Proposed method.

(b) HM R-λ.

Figure 4.17: Subjective quality of sequence *ParkScene* at 10 Mbps for frame No. 198.

42 dB, and used the relative bit rate values as *target bit rates* for our method. Table 4.5 shows, fro the sequence *BlowingBubbles*, the values of λ used in our experiments and, for each λ, the optimal encoding path selected according to the pruning conditions presenting the used QPs for each of the 4 frames of the sequence as well as the distortion and the bit rate associated, and the number of encoding operation to fill the tree.

An example of full constellation of R-D points without applying the pruning conditions is presented in Figure 4.18 for the sequence *Cactus*; the four optimal points associated to the selected λ values and situated on the convex hull of the constellation are presented in red. By applying the pruning conditions, the number of points in the constellation are cut in a percentage dependent to λ, with higher quality target (smaller λ) achieving a better reduction. Table 4.6 presents the R-D performance of the suboptimal heuristics of [ROV94] and our method in terms of BDBR and BDPSNR, showing that our method performs slightly worse than [ROV94], with a difference in terms of bit rate smaller than 7% for several sequences, and an average difference of 9%. The only exception, represented by sequence *NebutaFestival*, is explained by the fact that our method exploit all the possible bit-rate allocations, while for [ROV94] we choose a subset of possible QPs, which is large enough for all the others experiments, except for this case. Fig 4.19 shows the R-D performance of the proposed method and [ROV94] applying the pruning conditions and the suboptimal heuristics, and it is possible to note how the use of the *greedy pruning* affect the performance of [ROV94] in a negligible way.

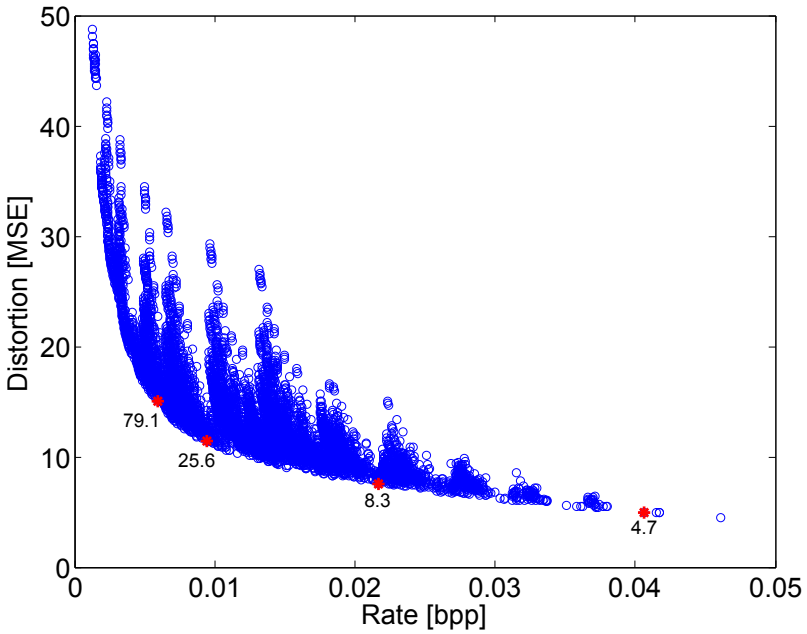

Figure 4.18: R-D operating points for sequence *Cactus*. Each point represents a QP combination. The points used in the comparisons are marked in red.

Moreover, we compared the execution times of these methods. Table 4.7 shows the setup time of [ROV94], that is the total encoding time to fully populate the dependency

Lambda	QP1	QP2	QP3	QP4	# of Encoding Operations	# of Nodes	Bitrate [Mbps]	Distortion [MSE]
10	22	22	22	22	126	16	3778.60	6.60
12.7	22	22	22	22	135	17	3778.60	6.60
16.24	22	25	25	25	144	18	2907	8.94
20.7	22	25	25	25	253	20	2907	8.94
26.4	25	27	27	25	153	20	2263.40	12.57
33.6	25	27	27	27	162	21	2064.40	13.49
42.8	25	27	27	27	171	23	2064.40	13.49
54.6	27	30	30	30	171	23	1534.80	19.37
69.5	27	30	30	30	180	24	1534.80	19.37
88.6	30	30	30	30	189	26	1175	25.82
112.9	30	30	30	32	189	26	1124.60	26.71
143.8	30	32	32	32	207	28	1082	28.34
183.3	32	32	32	32	207	29	882.90	35.14
233.6	32	32	32	32	225	31	882.90	35.14
297.6	35	35	35	35	225	32	579.40	53.16
379.3	35	35	35	35	234	33	579.40	53.16
483.3	35	35	35	37	243	34	563.90	54.30
615.8	37	37	37	37	243	35	434.10	69.60
784.8	37	37	37	37	252	36	434.10	69.60
1000	40	40	40	40	252	37	273.40	100.53

Table 4.5: λ values used for sequence *BlowingBubbles*. In green the four values selected for further comparison.

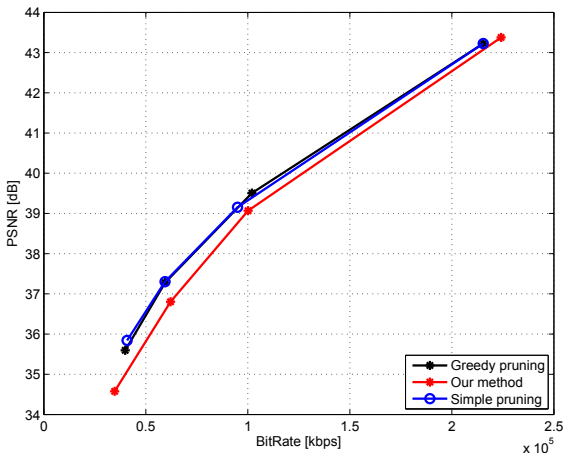

(a) Sequence *SteamLocomotive*.

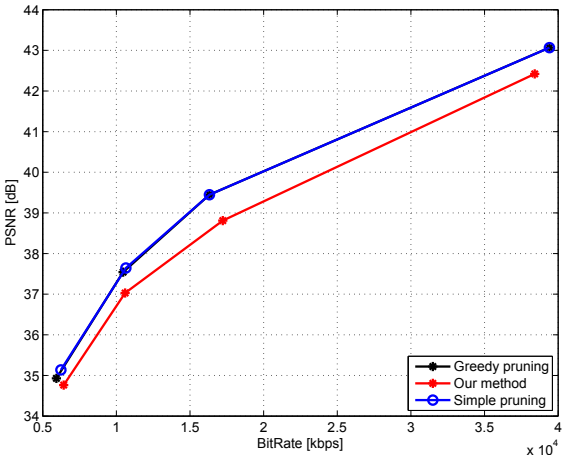

(b) Sequence *Traffic*.

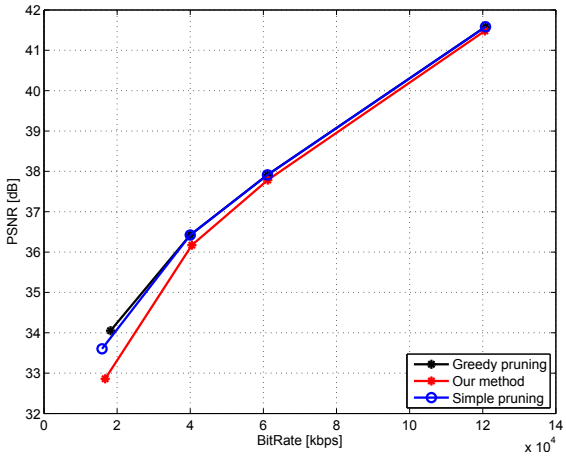

(c) Sequence *BQTerrace*.

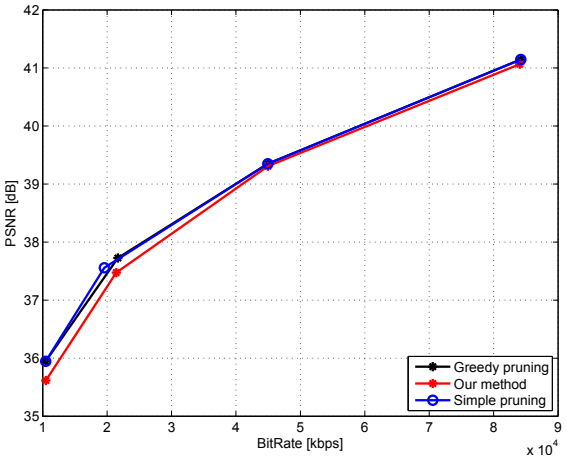

(d) Sequence *Cactus*.

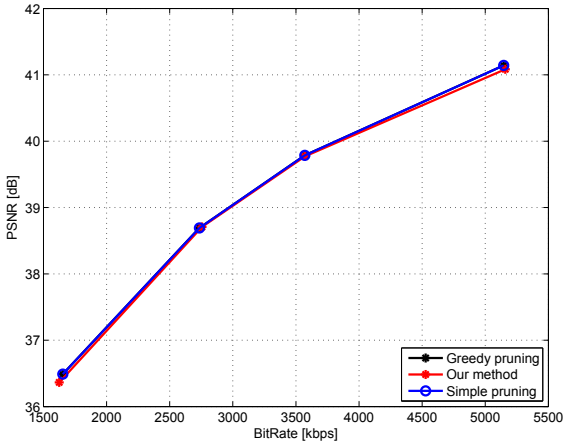

(e) Sequence *Kimono*.

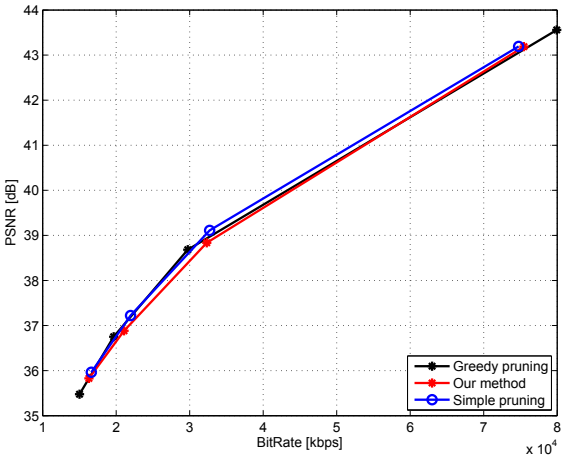

(f) Sequence *PeopleOnStreet*.

Figure 4.19: R-D performance of the proposed method and [ROV94] applying the pruning conditions and the suboptimal heuristics (here defined as *greedy pruning*).

tree, obtained by summing the encoding time of the 7380 encoding operations. The cost of encoding just 4 frames using 9 QPs is measured in hundreds of hours for most of the sequences, and makes [ROV94] impossible to use in practical applications. More reasonable times are obtained when [ROV94] uses a tree pruning strategy, as it leads to a smaller number of encoding operations.

Table 4.8 presents a comparison of execution times between our method and the one in [ROV94]. The global time of our method is given by the sum of three contributions: the parameter estimation (90% of the global time), the convex optimization algorithm (a small fraction of the global time), and the video encoding (about the 10% of the global time). The global time of [ROV94] is given by the sum of two contributions: the dataset generation (99% of the total time), and the search for the best R-D point. These times depend on the chosen λ value: a smaller λ implies the pruning of a higher number of R-D points (less encoding operations to perform), resulting in a smaller time. Table 4.8 shows that the method in [ROV94] requires at least four times the time required by our method, with a difference of two magnitude orders in the worst case and an average ratio of 91.

Sequence	BDPSNR (dB)	BDBR (%)	av. BDPSNR (dB)	av. BDBR (%)
SteamLocomotiveTrain	-0.38	7.49	-0.19	6.10
NebutaFestival	0.51	-5.41		
PeopleOnStreet	-0.17	3.35		
Traffic	-0.72	18.96		
BasketballDrive	-0.01	0.16	-0.18	5.01
BQTerrace	-0.30	6.44		
Cactus	-0.16	6.01		
Kimono1	-0.03	0.77		
ParkScene	-0.40	12.00		
BasketballDrill	-0.79	18.96	-0.55	12.86
BQMall	-0.74	17.75		
RaceHorses (832x480)	-0.10	1.88		
BasketballPass	-0.68	12.36	-0.66	11.13
BlowingBubbles	-0.61	11.54		
BQSquare	-0.97	14.81		
RaceHorses (416x240)	-0.40	5.79		

Table 4.6: Comparison in performance of [ROV94] and the proposed method method using the Bjontegaard metrics.

Class	*Sequence*	*Setup Time (h)*
A	SteamLocomotiveTrain	955
	NebutaFestival	1577
	PeopleOnStreet	798
	Traffic	615
B	BasketballDrive	412
	BQTerrace	474
	Cactus	402
	Kimono1	293
	ParkScene	353
C	BasketballDrill	71
	BQMall	78
	RaceHorses (832x480)	100
E	BasketballPass	17
	BlowingBubbles	31
	BQSquare	26
	RaceHorses (416x240)	28

Table 4.7: Total encoding time for a full population of the dependency tree.

Sequence	*Setup Time (s)*			*Execution Time (s)*				*Global Time (s)*		
	Proposed	Method in [ROV94]		*Proposed*		Method in [ROV94]		*Proposed*	Method in [ROV94]	
	S	*Max*	*Min*	BA	+ E	*Max*	*Min*	S+BA+E	*Max*	*Min*
SteamLocomotiveTrain	9579	1470060	37355	0.03	193.518	61.631	1.511	9773	1470122	37356
NebutaFestival	14359	2051171	52867	0.04	1198.331	63.194	1.628	15557	2051234	52869
PeopleOnStreet	8643	1462725	27515	0.03	387.052	106.361	1.566	9030	1462831	27516
Traffic	6897	1225989	22674	0.04	289.185	110.398	1.939	7186	1226099	22676
BasketballDrive	4424	968370	12904	0.12	286.642	150.672	3.921	4711	968521	12908
BQTerrace	4830	941150	18827	0.05	350.262	125.125	1.408	5180	941275	18828
Cactus	4759	932963	17079	0.05	358.504	158.755	1.359	5118	933122	17080
Kimono1	3652	600207	10151	0.03	359.219	132.866	1.183	4011	600340	10152
ParkScene	4318	822478	14018	0.05	462.142	170.827	1.430	4780	822649	14019
BasketballDrill	785	103651	2276	0.04	48.079	86.823	1.516	833	103738	2278
BQMall	886	178867	2893	0.05	54.164	220.521	1.525	940	179088	2895
RaceHorses (832x480)	1008	149803	1858	0.04	91.317	105.121	1.530	1099	149908	1860
BasketballPass	149	38520	578	0.04	15.412	191.807	1.597	164	38712	580
BlowingBubbles	248	69695	994	0.04	24.602	180.332	1.676	273	69875	996
BQSquare	251	55029	962	0.05	22.731	169.733	1.718	274	55199	964
RaceHorses (416x240)	241	58712	972	0.05	28.290	161.830	1.780	269	58874	974

Table 4.8: Comparison of global times. For our method, the time values concern the parameter estimation (S), the convex optimization algorithm (BA), and the video encoding (E). For the method in [ROV94], the times concern a large λ (Max) and a small λ (Min).

In summary, our method presents a strong gain over the standard HM R-λ rate control scheme with a better stability in terms of bit rate, whereas the small loss w.r.t. the method in [ROV94] is largely compensated by a much faster execution time. These results have been presented in a journal paper submitted to IEEE Transaction on image processing and currently under review.

4.2 Optimal frame-level bit-allocation for multi-view video encoder

The results presented for H.264/AVC and HEVC clearly show the effectiveness and versatility of our recursive R-D model used in combination with the proposed optimization method. The last part of this thesis work was the application of the proposed method in the context of multi-view video coding. Optimal rate allocation is a challenging tasks to perform in multi-view video coding, because together with the dependency between frames induced by motion compensation, the dependency between different views has to be considered.

Firstly, we generalize our approach to the scenario in which the dependency between frames is represented by a bi-dimensional graph (instead of a linear chain), in order to accommodate the more intricate prediction schemes used in MV coding. Secondly, we integrate the proposed algorithm in the MV-HEVC encoder, so as to compare the R-D performance of our approach with the standard MV-HEVC rate control.

4.2.1 Rate-Distortion model for MV videos

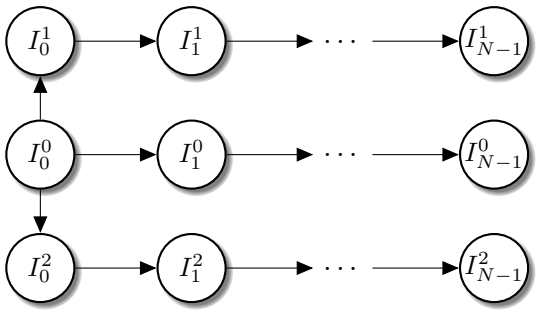

Figure 4.20: Dependency graph used in the paper.

In order to adapt our recursive R-D to the MV case, we consider the scenario where the dependency between frames can be represented as the graph depicted in Figure 4.20, where I_n^k denotes the n-th frame of the k-th view, with $k = 0$ being the central view and $k \geq 1$ being the side views. Using the R-D model in (3.37), we can demonstrate by the induction principle that the distortion D_n^k actually depends on all the frames involved in the chain of predictions leading to I_n^k. In the central view, the distortion D_n^0 is thus a

function of the rates $r_0^0, \ldots, r_n^0$ allocated in the central view, yielding

$$D_n^0 = \sum_{\ell=0}^{n} \alpha_{\ell,n}^0 \, M_\ell^0 \, \exp\Big\{ - \sum_{j=\ell}^{n} \beta_j^0 \, r_j^0 \Big\}, \tag{4.1}$$

where $\alpha_{\ell,n}^0 = \prod_{j=\ell}^{n} \alpha_j^0$. In the k-th side view (with $k \geq 1$), the distortion D_n^k depends not only from the rate $r_0^k, \ldots, r_n^k$ allocated in the same view, but also from the rate r_0^0 allocated to the first frame I_0^0 of the central view, leading to

$$D_n^k = \sum_{\ell=0}^{n} \alpha_{\ell,n}^k \, M_\ell^k \, \exp\Big\{ - \beta_0^0 \, r_0^0 - \sum_{j=\ell}^{n} \beta_j^k \, r_j^k \Big\}. \tag{4.2}$$

where $\alpha_{\ell,n}^k = \prod_{j=\ell}^{n} \alpha_0^0 \, \alpha_j^k$.

Optimal rate allocation consists in finding the vector of rates that minimizes the global distortion while keeping the total rate under a given budget $\eta > 0$, leading to

$$\underset{r \in [0,+\infty[^{KN}}{\text{minimize}} \quad \sum_{k=0}^{K-1} \sum_{n=0}^{N-1} D_n^k(r) \qquad \text{s.t.} \qquad \sum_{k=0}^{K-1} \sum_{n=0}^{N-1} r_n^k \leq \eta, \tag{4.3}$$

where r is the vector of rates defined as

$$r = \Big[r_0^0, \ldots, r_{N-1}^0, \ldots, r_{N-1}^{K-1} \Big]^\top, \tag{4.4}$$

and D_n^k is defined in (4.1)-(4.2). To gain some insight into the solution of Problem (4.3), we introduce a vector $u = (u_{n,\ell}^k)_{0 \leq k \leq K-1, \, 0 \leq n \leq N-1, \, 0 \leq \ell \leq n}$ defined as

$$u_{n,\ell}^k = \begin{cases} \displaystyle\sum_{j=\ell}^{n} \beta_j^k \, r_j^k, & \text{if } k = 0, \\ \beta_0^0 \, r_0^0 + \displaystyle\sum_{j=\ell}^{n} \beta_j^k \, r_j^k, & \text{if } k \geq 1, \end{cases} \tag{4.5}$$

which allows us to express the global distortion as a separable sum of exponentials

$$F(u) = \sum_{k=0}^{K-1} \sum_{n=0}^{N-1} \sum_{\ell=0}^{n} \alpha_{n,\ell}^k \, M_\ell^k \, \exp\{-u_{n,\ell}^k\}. \tag{4.6}$$

Therefore, Problem (4.3) can be reformulated as follows

$$\underset{r \in \mathbb{R}^{KN}}{\text{minimize}} \quad F(Lr) \qquad \text{s.t.} \qquad r \in C, \tag{4.7}$$

where $L \colon \mathbb{R}^N \mapsto \mathbb{R}^{\frac{KN(N+1)}{2}}$ is the linear operator that maps the vector $r \in \mathbb{R}^N$ into the vector $u \in \mathbb{R}^{\frac{KN(N+1)}{2}}$ defined in (4.5), and, again, C is the non-empty closed convex set

defined as

$$C = \Big\{ r \in [0, +\infty[^{KN} \mid \sum_{k=0}^{K-1} \sum_{n=0}^{N-1} r_n \leq \eta \Big\}. \tag{4.8}$$

Among the approaches proposed in the literature to solve this class of problems, we resort again to proximal algorithms [CP11d, CPPPP14, KP15], which can handle a wide class of convex optimization problems involving smooth and non-smooth penalizations, as well as hard constraints. In particular, we employ the M+LFBF algorithm proposed in [CP11b], which guarantees the convergence in a reasonable time even for large-scale problems, offers robustness to numerical errors, and its structure makes it suitable for parallel implementations.

4.2.2 Implementation

To evaluate the performance of the proposed algorithm, simulations were conducted using the reference software and experimental evaluation methodology has been developed. The experimental framework shares the same structure of the one developed for HEVC video encoder and presented in Section 4.1.1; it is composed of three steps, that are parameter estimation, bit allocation, and encoding, as explained in the following.

- **Parameter estimation** A standard version of the reference software HM 16.0 is used to encode the sequences at different QPs: 10, 12, 14, 16, 18, 20, 22, 24, 26, 28, 30, 32, 34, 36, 38, 40. The parameter $(M_n)_{0 \leq n \leq N-1}$, which represents the inter-view residual/motion prediction, is obtained by encoding the sequences with a modified version of HM 16.0 that computes M_n for each frame, using a $QP = 1$.

- **Bit allocation** The algorithm takes the estimated parameters of the sequence as input, providing as output the number of bits for each frame that minimizes the total distortion over each GOP, under the constraint of a defined target bit rate. Table 4.9 reports the target bit rates used for each sequence.

- **Encoding** The encoder used in the final step of our experiments is a modified version of HM 16.0 where the rate control module is able to accept an external file containing the result of the previous step and set the number of bits allocated for each GOP and for each frame on these values. The base view is coded as the center view and the two dependent views are encoded as left and right view, with a configuration that reproduces the dependency graph of Figure 4.20. The average luma PSNR values and bit rates for all three views are reported in Table 4.10 as total results.

4.2.3 Rate-Distortion performance comparison

To assess the validity of our bit rate allocation method, we compared it with the standard rate control algorithm of MV-HEVC. The R-D curves of the proposed method and

Sequence	Resolution	Frame Rate [fps]	Target Bit Rate [Mbps]
Balloons	1024x768	30	1.5 2.7 3.6 4.5
Kendo			2.1 2.4 3.0 4.5
Newspaper_CC			9 12 15 21
Undo_Dancer	1920x1088	25	10.2 25.2 40.2 60
GT_Fly			4.5 10.5 15 21
Poznan_Hall2			0.6 1.8 2.4 4.2
Poznan_Street			10.2 21 30 51

Table 4.9: Sequence characteristic and used target bit rates

MV-HEVC are shown in Figures 4.21 and 4.22 for two sequences "*Poznan_Hall2*" and "*Newspaper_CC*" for the three view used. From that, we can see that our method can achieve a larger PSNR value at each target bit rate.

Table 4.10 shows the rate-distortion performance of our method compared to straightforward MV-HEVC evaluated with the Bjontegaard metrics [Bjo01]. For each sequence an average value over the three views of the gain in terms of Bjontegaard bitrate (BDBR) and Bjontegaard PSNR (BDPSNR) is presented. The results indicate that our method provides an average bit rate savings of 20% relative to standard MV-HEVC with an average gain of 0.70 dB in terms of PSNR. In terms of allocation accuracy, the difference between the target bit rate and the achieved bit rate is for each sequence lower than 10%, with an average value among all sequence of 7.5%.

Sequence	BDPSNR (dB)	BDBR (%)
Balloons	1.20	-21.52
Kendo	0.35	-7.86
Newspaper_CC	0.65	-23.35
Undo_Dancer	0.49	-12.88
GT_Fly	0.83	-20.34
Poznan_Hall2	0.59	-34.72
Poznan_Street	0.82	-23.61
Average	0.70	-20.61

Table 4.10: Average PSNR gain and bit rate savings compared to straightforward HEVC multi-view extension (MV-HEVC).

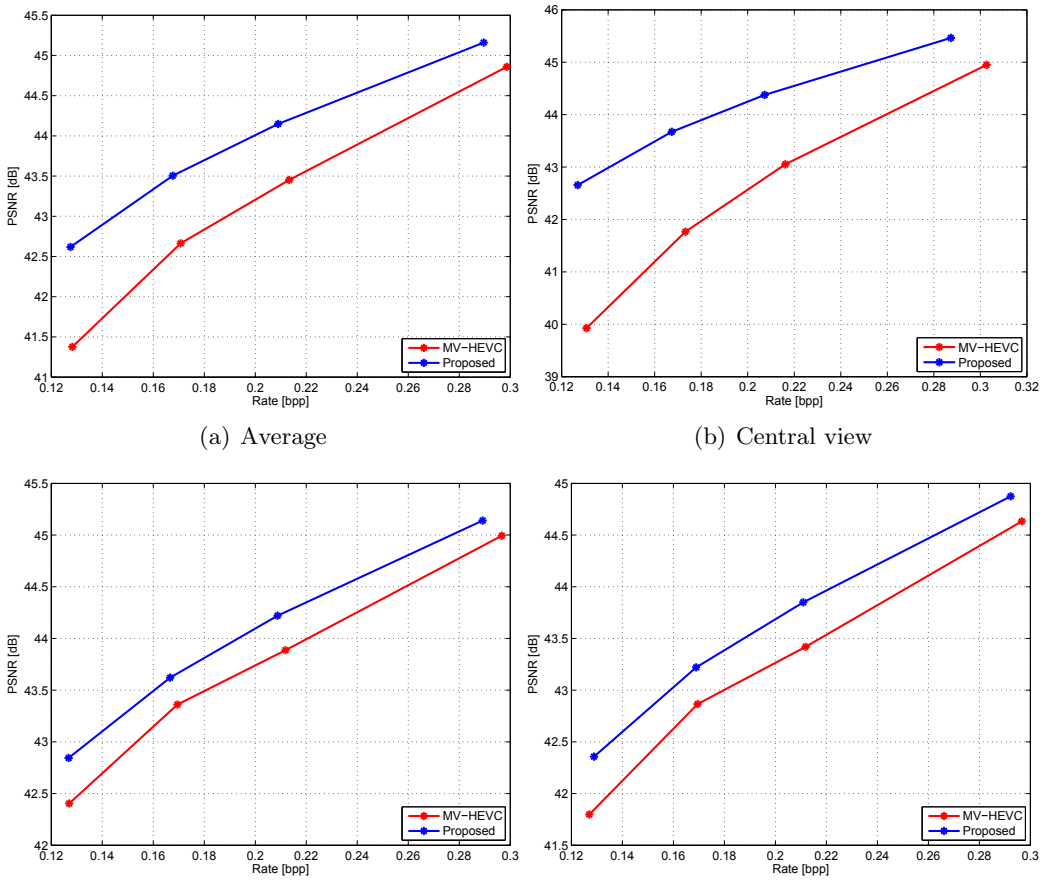

(a) Average (b) Central view

(c) Left view (d) Right view

Figure 4.21: The rate distortion curves of the proposed method as well as the rate control in the reference software for sequence *Newspaper_CC*.

In conclusion, the obtained results demonstrate that our analytical R-D model allows us to accurately describe the temporal and inter-view dependencies in a group of frames. Furthermore, our experiments indicate that the optimal rate allocation, when supported by an accurate R-D model, attains better results (in the R-D sense) than the standard rate control in MV-HEVC. The higher performance of our approach is related to its ability to take into account the characteristics of the video sequence and the temporal and inter-view correlation between the frames. The results of our experiments, conducted on different standard test sequences, demonstrate the effectiveness of our proposition. These results have been accepted for publication in a conference paper at ICIP 2016 [FCCPP16].

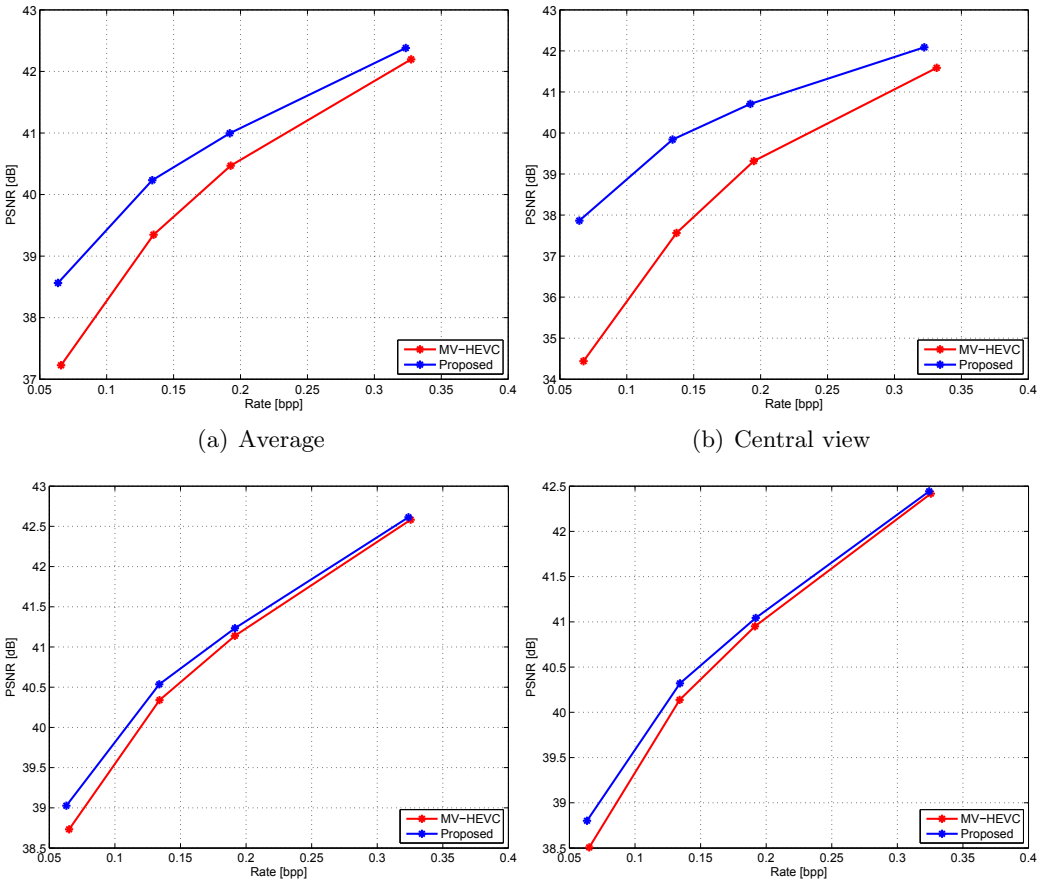

(a) Average (b) Central view

(c) Left view (d) Right view

Figure 4.22: The rate distortion curves of the proposed method as well as the rate control in the reference software for sequence *Poznan_Street*.

4.3 Conclusion

In this chapter we presented experimental results to validate our convex optimization algorithm for frame level bit allocation. First of all, we verified the accuracy of the proposed R-D model to the typical HEVC sequences. We integrated our method in the HEVC encoder and compare the results to the HM R-λ rate control scheme in terms of R-D performance; we also compared our method to the exhaustive research method presented in Section 2.2.3. The experimental results presented indicate that our optimal rate allocation attains better results (in terms of Δ PSNR and % bit rate) than the standard rate control in HEVC and the comparison with the exhaustive search method in [ROV94] showed an average loss of 9% in terms of bit rate, which is widely compensated by an execution time that is two hundred times faster.

Finally, we implemented our method in the MV-HEVC video encoder: we adapted our R-D to the multi-view scenario by taking into account the inter-view dependencies and changed the minimization algorithm consequently. The results of our experiments

presented in the end of the chapter and conducted on different standard test sequences demonstrate the effectiveness of our proposition.

Conclusions and future works

Objectives of the thesis

The purpose of this thesis was to develop an optimal frame-level bit-allocation method. Existing methods implemented in modern video codecs such as H.264/AVC and H.265/HEVC, are based on simple heuristic formulas which take into account parameters such as the number of frames in a GOP, the bits still available and the occupancy of the buffer. Those methods do not take into account the characteristics of the sequences and the dependency between consecutive frames, resulting, as shown in the previous chapter, in strong fluctuations of the bit rate around the assigned target bit rate that have a huge impact on the visual quality of the encoded sequence, which dramatically decrease for the last encoded GOPs.

Our method is based on an accurate R-D model for the frames of a GOP able to describe dependencies between the distortions of the frames. This R-D model allowed us to formulate the bit allocation problem as a convex optimization problem which was solved, in an accurate and efficient way, using convex optimization techniques. The method was successfully integrated into an HEVC video encoder and adapted to the multi-view scenario in order to be used in MV-HEVC.

Summary

Recursive frame-level rate-distortion model

A recursive R-D model for the frames of a GOP has been proposed. We extended the classical R-D model proposed in [USC93] by letting the exponential decay vary at each frame. The distortion of each frame inside a GOP is expressed as a function of the rate used to encode the frame, and we are able to take into account the dependencies between the frames using the motion estimation error, and the texture characteristics of the sequence using the variance of the frame and two model parameters α and β which change the exponential decay of the original model.

The accuracy of the proposed model has been verified on the basis of the R^2 metric, which was designed to quantitatively measure the degree of deviation from a given model,

showing high fitting performance, superior to other R-D models taken into consideration.

Frame-level bit-rate allocation

An efficient algorithm based on modern convex optimization has been proposed. The proposed R-D model allowed us to formulate the frame-level allocation problem as a convex optimization problem and, among the possible minimization solutions, a Forward-Backward Primal-Dual algorithm has been developed in collaboration with Dr. Giovanni Chierchia. The complexity of the algorithm is not affected by the total number of frames in a video sequence, thanks to the fact that it is implemented so that the optimization process works in parallel over the GOPs.

A first set of experiments performed on H.264/AVC video encoder showed how the rate allocation of the proposed method is quite different from the reference, especially for I-frames, and more uniform within the GOP, avoiding the sub-optimal greedy behaviour of H.264/AVC which allocates the largest part of the bit budget to the first frames of the GOP and hence it rapidly runs out of bits for the remaining GOP frames, causing an increase of the global distortion.

Integration in HEVC

The proposed method has been applied to the state of the art video encoder HEVC. The rate control module of *HM.13 RExt-6.0* has been modified in order to integrate the convex optimization-based bit allocation algorithm and the results were compared to the standard R-λ rate control scheme of HEVC in terms of Bjontegaard bitrate and Bjontegaard PSNR. Experiments have proved that our method outperform the conventional encoder for all video sequences at different bit rates with a maximum gain of 1.32 dB in terms of Δ PSNR and a maximum bit rate reduction of 30.7%, providing a better stability in terms of bit rate, reaching the target bit rate for every GOP and providing a constant visual quality over the whole sequence, while the fluctuations around the target bit rate over the GOPs presented by HM resulted in a severe quality loss for the last GOPs of each sequence.

We also compared our method with the bit allocation technique proposed in [ROV94] and based on an exhaustive search among all the possible quantizer combinations for the solution with the minimum Lagrangian cost. As expected, the exhaustive search outperformed our solution in terms of Δ PSNR, but the contained lost is counterbalanced by a much lower complexity, with an execution time between four times and a hundred times shorter.

Finally, our method has been adapted to the multi-view scenario and implemented in MV-HEVC. The obtained results demonstrated that our analytical R-D model allows to accurately describe the temporal and inter-view dependencies in a group of frames, attaining better results in the R-D sense than the standard rate control in MV-HEVC.

Perspectives for future work

At the time of concluding this manuscript, some interesting perspectives can be proposed to further continue the work done in this thesis. The proposed method has been proven to attain better results than standard rate control, but has been developed for a very specific coding structure, *i.e.* I-P-P-P with one reference frame. We are aware of the importance of considering a number of reference frames equal to $K > 1$, as well as the inclusion of B-frames in the predictive structure, and we are currently working on this topic to have a more general rate-allocation method.

Number of reference frame greater than one

Our idea is to generalize the prediction error introducing a weight $\omega_{n,n-1}$ which takes into consideration the percentage of blocks of frame n predicted from frame $n-i$, letting us to express M_n of eq.(3.27) as:

$$\omega_{n,n-1} \cdot \mathbb{E}\left\{[I_n - f(I_{n-1}, \mathbf{v}_{n,n-1})]^2\right\} + \omega_{n,n-2} \cdot \mathbb{E}\left\{[I_n - f(I_{n-2}, \mathbf{v}_{n,n-2})]^2\right\} + \ldots + \omega_{n,n-K} \cdot \mathbb{E}\left\{[I_n - f(I_{n-K}, \mathbf{v}_{n,n-K})]^2\right\} = \sum_{i=1}^{K} \omega_{n,n-i} \cdot M_{n,n-i}$$

and the distortion D_n as:

$$D_n = \alpha_n \cdot [(\omega_{n,n-1} \cdot M_{n,n-1} + \omega_{n,n-2} \cdot M_{n,n-2} + \ldots + \omega_{n,n-K} \cdot M_{n,n-K}) + (\omega_{n,n-1} \cdot D_{n,n-1} + \omega_{n,n-2} \cdot D_{n,n-2} + \ldots + \omega_{n,n-K} \cdot D_{n,n-K})] \cdot 2^{-2r_n}.$$

Using the induction principle, the distortion of the generic frame n reads as:

$$\sum_{l=0}^{n} \prod_{j=1}^{n} \alpha_j \left(\sum_{k=0}^{j-1} \omega_{j,k} \cdot M_{j,k} \right) \cdot 2^{-2\sum_{j=l}^{n} r_j} + \phi$$

where the function contains a combination of $\alpha_u \omega_{u,v}$ and $\alpha_i \omega_{i,h}$ of non-consecutive frames. The formalization of the function ϕ and the estimation of weights $\omega_{n,n-1}$ is a non-trivial problem, which requires more research work.

Inclusion of B-frames

The problem of a different prediction structure including bi-predictive frames is currently under investigation. Considering an I-B-P-B-P structure with an alternation of B-frames, in even positions inside a GOP, which depend from the previous and the following frame, and P-frames, in odd positions, which only depend from the previous P (or I) frame. The distortion of a generic P-frame is the same as in eq. (3.30), while the distortion for a

generic B-frame becomes:

$$D_n = \omega_{n,n-1}\alpha_n(M_{n,n-1} + D_{n-1}) \cdot 2^{-2r_n} + \omega_{n,n+1}\alpha_n(M_{n,n+1} + D_{n+1}) \cdot 2^{-2r_n}$$

where, again, the weight $\omega_{n,n-i}$ takes into consideration the percentage of blocks in frame n predicted from frame $n-i$. We can derivate a recursive expression for the distortion of a generic frame, different for even or odd values of k:

$$D_k = \begin{cases} \displaystyle\sum_{l=0}^{k/2} \left(\prod_{j=l}^{k/2} \alpha_{2j} \right) M_{2l} \cdot 2^{-2\sum_{j=l}^{k/2} r_{2j}}, & \text{for } k = 2n \\ \omega_{k,k-1}\alpha_k \left[M_{k,k-1} + \displaystyle\sum_{l=0}^{(k-1)/2} \left(\prod_{j=l}^{(k-1)/2} \alpha_{2j} \right) M_{2l} \cdot 2^{-2\sum_{j=l}^{(k-1)/2} r_{2j}} \right] + & \\ + \omega_{k,k+1}\alpha_k \left[M_{k,k+1} + \displaystyle\sum_{l=0}^{(k+1)/2} \left(\prod_{j=l}^{(k+1)/2} \alpha_{2j} \right) M_{2l} \cdot 2^{-2\sum_{j=l}^{(k+1)/2} r_{2j}} \right], & \text{for } k = 2n+1 \end{cases}$$

As mentioned before, the estimation of weights $\omega_{n,n-1}$ is a non-trivial problem, which requires more research work, even though it represents an important point to develop in a more general allocation method.

Compression of multi-spectral satellite images

In recent years many satellite earth observation programs have been lunched with the purpose of change detection, systematic crop monitoring, fast situation awareness, activity monitoring, atomized map updates and so on. In the context of multi-spectral image acquisition a huge amount of data has to be stored, and HEVC, with its excellent rate-distortion performance, could represents a very efficient compression tool even though it has been conceived for a totally different kind of data.

Since satellites have typically a few days **revisit time** (time elapsed between observations of the same point on earth by a single satellite), it is reasonable to expect a strong temporal correlation between consecutive images of the same scene, similar to natural video signals, in addition to the inter-band correlation. Our idea is to describe those temporal and inter-band dependencies using our recursive frame level R-D model in order to improve the compression achievable with HEVC applied to this different types of signals, which can be assimilated to multi-view video sequences.

Publications

Journal articles

1. Aniello Fiengo, Giovanni Chierchia, Marco Cagnazzo, and Beatrice Pesquet-Popescu, "Rate allocation in predictive video coding using a convex optimization framework", *IEEE Transactions on Image Processing*, Accepted for publication.

Conference papers

1. Aniello Fiengo, Giovanni Chierchia, Marco Cagnazzo, and Beatrice Pesquet-Popescu, "A convex-optimization framework for frame-level optimal rate allocation in predictive video coding", *Proceedings of ICASSP 2014*, Florence, Italy, May 2014.

2. Aniello Fiengo, Giovanni Chierchia, Marco Cagnazzo, and Beatrice Pesquet-Popescu, "Convex optimization for frame-level rate allocation in MV-HEVC", *Proceedings of ICIP 2016*, Phoenix, Arizona, USA, September 2016.

Bibliography

[ABDF10] M. V. Afonso, J. M. Bioucas-Dias, and M. A. T. Figueiredo, "Fast image recovery using variable splitting and constrained optimization". vol. 19 (9), pp. 2345–2356, 2010. *Cited in Sec.* (document), 3.1.2

[ACAB07] T. André, M. Cagnazzo, M. Antonini, and M. Barlaud, "A JPEG2000-compatible full scalable video coder". *EURASIP Journal of Image and Video Processing*, vol. 2007, p. 11, 2007. *Cited in Sec.* (document)

[ANR74] N. Ahmed, T. Natarajan, and K. Rao, "Discrete cosine transform". *IEEE Transactions on Computers*, pp. 90–93, January 1974. *Cited in Sec.* 1.2.3

[BC11] H. H. Bauschke and P. L. Combettes, *Convex Analysis and Monotone Operator Theory in Hilbert Spaces*, Springer, Jan. 2011. *Cited in Sec.* (document), 3.1.2, 3.1.3

[Ber71] T. Berger, *Rate-Distortion Theory. A mathematical theory for data compression*, Prentice-Hall, 1971. *Cited in Sec.* (document), 2.1

[Bjo01] G. Bjontegaard, "Calculation of average PSNR differences between RD-curves", in *VCEG Meeting*, 2001. *Cited in Sec.* (document), 4.1.2, 4.2.3

[BnC11] L. M. Briceño-Arias and P. L. Combettes, "A monotone + skew splitting model for composite monotone inclusions in duality". vol. 21 (4), pp. 1230–1250, Oct. 2011. *Cited in Sec.* (document), 3.1.2

[BNS13] F. Baus, M. Nikolova, and G. Steidl, "Fully smoothed l1-tv models: Bounds for the minimizers and parameter choice". vol. 48 (2), pp. 295–307, Feb. 2013. *Cited in Sec.* (document), 3.1

[Bos13] F. Bossen, "Common test conditions and software reference configurations", in *Joint Collaborative Team on Video Coding of ITU-T SG*, Geneva, Switzerland, 2013. *Cited in Sec.* (document), 4.1

[Bov00] A. Bovik, *Handbook of Image & Video Processing*, Elsevier Academic Press, 2000. *Cited in Sec.* 1.1, 1.2, 1.2.2

[BTT89] A. Ben-Tal and M. Teboulle, "A smoothing technique for nondifferentiable optimization problems". *Lecture Notes in Mathematics*, vol. 1405, pp. 1–11, 1989. *Cited in Sec.* (document), 3.1

[CAAB04] M. Cagnazzo, T. André, M. Antonini, and M. Barlaud, "A model-based motion compensated video coder with JPEG2000 compatibility", in *Proceedings of IEEE International Conference on Image Processing*, vol. 4, pp. 2255–2258, Singapore, Oct. 2004. *Cited in Sec.* (document)

[CBL72] D. Connor, R. Brainard, and J. Limb, "Interframe coding for picture transmission", in *Proceedings of The IEEE*, vol. 60, pp. 779–790, July 1972. *Cited in Sec.* 1.1.2

[CCC+12] Y. Censor, W. Chen, P. L. Combettes, R. Davidi, and G. T. Herman, "On the effectiveness of projection methods for convex feasibility problems with linear inequality constraints". vol. 51 (3), pp. 1065–1088, 2012. *Cited in Sec.* (document), 3.1

[CCPVu14] P. L. Combettes, L. Condat, J.-C. Pesquet, and B. C. Vũ, "A forward-backward view of some primal-dual optimization methods in image recovery", Paris, France, Oct. 2014. *Cited in Sec.* (document), 3.1.2, 3.1.3

[CCPW07] C. Chaux, P. L. Combettes, J.-C. Pesquet, and V. R. Wajs, "A variational formulation for frame-based inverse problems". vol. 23 (4), pp. 1495–1518, Jun. 2007. *Cited in Sec.* (document), 3.1.2

[CEGK98] G. Cote, B. Erol, M. Gallant, and F. Kossentini, "H. 263+: Video coding at low bit rates". *IEEE Transactions on Circuits and Systems For Video Technology*, vol. 8 (7), pp. 849–866, 1998. *Cited in Sec.* 1.3

[Chi14] G. Chierchia, *Éclatement épigraphique de contraintes convexes. Application à la restauration d'images, la classification supervisée, et la détection d'images falsifiées*, Ph.D. thesis, Telecom ParisTech, 2014. *Cited in Sec.* 3.1.3

[CL89] P. A. Chou and T. Lookabaugh, "Entropy-constrained vector quantization". *IEEE Transactions on Acoustics, Speech, and Signal Processing*, vol. 37, pp. 31–42, January 1989. *Cited in Sec.* (document), 2.2.1

[CL97] J.-J. Chen and D. W. Lin, "Optimal bit allocation for coding of video signals over atm networks". *IEEE J. on Sel. Areas in Comm*, vol. 15, pp. 1002–1015, 1997. *Cited in Sec.* (document), 2.2.1

[CLG89] P. A. Chou, T. Lookabaugh, and R. Grey, "Optimal pruning with applications to tree-structured source coding and modeling". *IEEE Transactions on Information Theory*, vol. 35, pp. 299–315, 1989. *Cited in Sec.* (document), 2.2.1

[Con13] L. Condat, "A primal-dual splitting method for convex optimization involving Lipschitzian, proximable and linear composite terms". vol. 158 (2), pp. 460–479, 2013. *Cited in Sec.* (document), 1, 3.1.2, 3, 3.2.4, 5

[Con14] ———, "Fast projection onto the simplex and the l1 ball". 2014, http://hal.archives-ouvertes.fr/hal-01056171. *Cited in Sec.* 3.2.4

[CP11a] A. Chambolle and T. Pock, "A first-order primal-dual algorithm for convex problems with applications to imaging". vol. 40 (1), pp. 120–145, May 2011. *Cited in Sec.* (document), 3.1.2

[CP11b] P. L. Combettes and J.-C. Pesquet, "Primal-dual splitting algorithm for solving inclusions with mixtures of composite, Lipschitzian, and parallel-sum type monotone operators". 2011. *Cited in Sec.* 4.2.1

[CP11c] ———, "Proximal splitting methods in signal processing", in H. H. Bauschke, R. S. Burachik, P. L. Combettes, V. Elser, D. R. Luke, and H. Wolkowicz, eds., *Fixed-Point Algorithms for Inverse Problems in Science and Engineering*, pp. 185–212, Springer-Verlag, New York, 2011. *Cited in Sec.* (document), 3.1, 3.1.2

[CP11d] ———, "Proximal splitting methods in signal processing", in *Fixed-Point Algorithms for Inverse Problems in Science and Engineering*, pp. 185–212, Springer-Verlag, New York, 2011. *Cited in Sec.* 4.2.1

[CP12] ———, "Primal-dual splitting algorithm for solving inclusions with mixtures of composite, Lipschitzian, and parallel-sum type monotone operators". vol. 20 (2), pp. 307–330, Jun. 2012. *Cited in Sec.* (document), 3.1.2, 4

[CPD13] M. Cagnazzo, B. Pesquet-Popescu, and F. Dufaux, *Emerging technologies for 3D video: content creation, coding, transmission and rendering*, Chap. 3D Video Representation and Formats, Wiley, 2013. *Cited in Sec.* 1.5.5

[CPPPP14] G. Chierchia, N. Pustelnik, J.-C. Pesquet, and B. Pesquet-Popescu, "Epigraphical projection and proximal tools for solving constrained convex optimization problems". *Signal, Image and Video Processing*, Jul. 2014. *Cited in Sec.* (document), 4.2.1

[CSR+07] N. Cherniavsky, G. Shavit, M. F. Ringenburg, R. E. Ladner, and E. A. Riskin, "Multistage: A MINMAX bit allocation algorithm for video coders". vol. 17 (1), pp. 59–67, 2007. *Cited in Sec.* (document)

[CT65] J. Cooley and J. Tukey, "An algorithm for the machine calculation of complex fourier series". *Mathematics of Computation*, vol. 19, pp. 297–301, 1965. *Cited in Sec.* 1.2.3

[CT91] T. Cover and J. Thomas, *Elements of Information Theory*, Wiley, New York, 1991. *Cited in Sec.* (document)

[CW96a] M. Chen and A. Wilkon, "Rate-distortion optimal motion estimation for video coding", in *IEEE International Conference on Acoustics, Speech, and Signal Processing*, 1996. *Cited in Sec.* 2.2.2

[CW96b] M. Chen and A. Willson, "Design and optimization of a differentially coded variable block size motion compensation system", in *IEEE International Conference on Image Processing*, 1996. *Cited in Sec.* 2.2.2

[CW98] ———, "Rate-distortion optimal motion estimation algorithms for motion-compensated transform video coding". *IEEE Transactions on Circuits and Systems for Video Technology*, vol. 8 (2), pp. 147–158, April 1998. *Cited in Sec.* 2.2.2

[CW05] P. L. Combettes and V. R. Wajs, "Signal recovery by proximal forward-backward splitting". vol. 4 (4), pp. 1168–1200, Nov. 2005. *Cited in Sec.* 3.1.3

[DF99] J. L. Devore and N. R. Farnum, *Applied Statistic for Engineers and Scientists*, Duxbury, 1999. *Cited in Sec.* (document), 3.2.3, 4.1

[DLR04] M. Dai, D. Loguinov, and H. Radha, "Rate-distortion modeling of scalable video coders", in *Proceedings of IEEE International Conference on Image Processing*, Singapore, 2004. *Cited in Sec.* 2.3.2

[D.T97] H. D.T., *Fast and efficient algorithms for text and video compression*, Ph.D. thesis, Brown University, 1997. *Cited in Sec.* (document), 2.2

[Eve63] H. Everett, "Generalized lagrange multiplier method for solving problems of optimum allocation of resources". *Operations Research*, vol. 11, pp. 399–417, 1963. *Cited in Sec.* (document), 2.2.1

[FCCPP14] A. Fiengo, G. Chierchia, M. Cagnazzo, and B. Pesquet-Popescu, "A convex-optimization framework for frame-level optimal rate allocation in predictive video coding", in *Proceedings of IEEE International Conference on Acoustics, Speech and Signal Processing*, Florence, Italy, 2014. *Cited in Sec.* 3.2.5

[FCCPP16] ———, "Convex optimization for frame-level rate allocation in mv-hevc", in *Proceedings of IEEE International Conference on Image Processing*, Phoenix, Arizona, 2016. *Cited in Sec.* 4.2.3

[FG03] M. Flierl and B. Girod, "Generalized b pictures and the draft h. 264/avc video-compression standard". *IEEE Transactions on Circuits and Systems For Video Technology*, vol. 13 (7), pp. 587–597, 2003. *Cited in Sec.* 1.4.3

[GCPP12] R. Gaetano, G. Chierchia, and B. Pesquet-Popescu, "Parallel implementations of a disparity estimation algorithm based on a proximal splitting method", San Diego, USA, 2012. *Cited in Sec.* (document), 3.2.4

[GG92] A. Gersho and R. Gray, "Scalar quantization i: Structure and performance", in *Vector Quantization and Signal Compression*, vol. 159 of *The Springer International Series in Engineering and Computer Science*, pp. 133–172, Springer US, 1992. *Cited in Sec.* 1.2.1

[Gir94] B. Girod, "Rate-constrained motion estimation", in *SPIE Visual Communications and Image Processing Conference*, pp. 1026–1034, September 1994. *Cited in Sec.* 2.2.2

[GP68] H. Gish and J. N. Pierce, "Asymptotically efficient quantizing". *IEEE Tranansactions on Information Theory*, vol. 14, pp. 676–683, 1968. *Cited in Sec.* 2.2.2

[H2615] "H.265 : High efficiency video coding", April 2015. *Cited in Sec.* (document), 1.5.5

[Had93] J. Hadamard, "Resolution d'une question relative aux determinants". *Bulletin des Sciences Mathematiques Series 2*, vol. 17, pp. 240–246, 1893. *Cited in Sec.* 1.2.3

[Has97] B. G. Haskell, *Digital video: an introduction to MPEG-2*, Springer, 1997. *Cited in Sec.* 1.3

[HJH99] J. M. Henderson, P. A. W. Jr., and A. Hollingworth, "The effects of semantic consistency on eye movements during complex scene viewing". *J. Exp. Psychol. Hum. Percept. Perform.*, vol. 25 (1), pp. 210–228, Feb. 1999. *Cited in Sec.* (document)

[HKZK11] S. Hu, S. Kwong, T. Zhao, and C. C. J. Kuo, "Rate control optimization for temporal-layer scalable video coding". vol. 21 (8), pp. 1152–1162, Aug. 2011. *Cited in Sec.* (document)

[HM02a] Z. He and S. Mitra, "Optimum bit allocation and accurate rate control for video coding via ρ-domain source modeling". *IEEE Transactions on Circuits and Systems for Video Technology*, vol. 12 (10), pp. 840–849, 2002. *Cited in Sec.* 2.1.1

[HM02b] Z. He and S. K. Mitra, "A linear source model and a unified rate control algorithm for dct video coding". vol. 12 (11), pp. 970–982, 2002. *Cited in Sec.* (document)

[HMK+10] W.-J. Han, J. Min, I.-K. Kim, E. Alshina, A. Alshin, T. Lee, J. Chen, V. Seregin, S. Lee, Y. M. Hong, M.-S. Cheon, N. Shlyakhov, K. McCann, T. Davies, and J.-H. Park, "Improved video compression efficiency through flexible unit representation and corresponding extension of coding tools". *IEEE Transactions on Circuits and Systems for Video Technology*, vol. 20 (12), pp. 1709 –1720, December 2010. *Cited in Sec.* (document), 1.5.1

[HOB+12] P. Helle, S. Oudin, B. Bross, D. Marpe, M. Bici, K. Ugur, J. Jung, G. Clare, and T. Wiegand, "Block merging for quadtree-based partitioning in HEVC". *IEEE Transactions on Circuits and Systems for Video Technology*, (99), 2012. *Cited in Sec.* (document), 1.5.3

[Hub64] P. J. Huber, "Robust estimation of a location parameter". vol. 35 (1), pp. 73–101, 1964. *Cited in Sec.* (document), 3.1

[Huf52] D. Huffman, "A method for the construction of minimum-redundancy codes". vol. 40 (9), pp. 1098–1101, Sep. 1952. *Cited in Sec.* 1.2.4

[HUL96] J.-B. Hiriart-Urruty and C. Lemaréchal, *Convex Analysis and Minimization Algorithms, Part I: Fundamentals*, vol. 305, Springer-Verlag, 1996. *Cited in Sec.* (document), 3.1

[HV92] P. G. Howard and J. S. Vitter, "Practical implementations of arithmetic coding", Tech. Rep., Brown University, 1992. *Cited in Sec.* 1.2.4

[Int90] International Telecommunication Union - Telecommunication Standardization Sector, *Video codec for audiovisual services at $p \times 64$ kbits/s*, Aug. 1990, ITU-T Recommendation H.261. *Cited in Sec.* 1.4.1

[ISO] "Mpeg1: Video compression standard". *Cited in Sec.* 1.3

[JN84] N. S. Jayant and P. Noll, *Digital Coding of Wavefoms*, Prentice Hall, 1984. *Cited in Sec.* 2.2.2

[Joi09] Joint Video Team of ISO/IEC MPEG & ITU-T VCEG, *H.264/MPEG-4 AVC Reference Software Manual*, Jul. 2009. *Cited in Sec.* 1.4, 1.4.4

[Kar47] H. Karhunen, "Über lineare methoden in der wahrscheinlich-keitsrechnung". *Ann. Acad. Sci. Fennicae, Ser. A. I.*, vol. 37, pp. 1–79, 1947. *Cited in Sec.* 1.2.3

[KBSC92] S.-Z. Kiang, R. L. Baker, G. J. Sullivan, and C.-Y. Chiu, "Recursive optimal pruning with applications to tree structured vector quantizers". *IEEE Transactions on Image Processing*, vol. 1, pp. 162–169, 1992. *Cited in Sec.* (document), 2.2.1

[KLSW97] F. Kossentini, Y. Lee, M. Smith, and R. Ward, "Predictive rd optimized motion estimation for very low bit rate video coding". *IEEE Journal on Selected Areas in Communications*, vol. 15 (9), pp. 1752–1763, December 1997. *Cited in Sec.* 2.2.2

[KP15] N. Komodakis and J.-C. Pesquet, "Playing with duality: An overview of recent primal-dual approaches for solving large-scale optimization problems". 2015, to appear. *Cited in Sec.* (document), 3.1.2, 3.1.3, 4.2.1

[KW13] M. Karczewicz and X. Wang, "Intra Frame Rate Control Based SATD", in *JCT-VC M0257, 13th meeting of Joint Collaborative Team on Video Coding of ITU-T SG 16 WP 3 and ISO/IEC JTC 1/SC 29/WG 11*, Incheon, KR, 2013. *Cited in Sec.* 2.3.2

[Lax] P. B. Lax, *Functional Analysis*, Wiley-Interscience. *Cited in Sec.* 3.2.4

[LBH+12] J. Lainema, F. Bossen, W.-J. Han, J. Min, and K. Ugur, "Intra coding of the hevc standard". *IEEE Transactions on Circuits and Systems For Video Technology*, vol. 22 (12), pp. 1792–1801, December 2012. *Cited in Sec.* (document), 1.5.2

[LCGK10] J. Liu, Y. Cho, Z. Guo, and C. C. J. Kuo, "Bit allocation for spatial scalability coding of H.264/SVC with dependent rate-distortion analysis". vol. 20 (7), pp. 967–981, Jul. 2010. *Cited in Sec.* (document)

[LF80] G. Legge and J. Foley, "Contrast masking in human vision". *Journal of Optical Society of America*, vol. 70 (12), pp. 1458–1471, December 1980. *Cited in Sec.* 1.1.2

[LGP+06] Z. Li, W. Gao, F. Pan, S. Ma, K. Lim, G. Feng, X. Lin, S. Rahardja, H. Lu, and Y. Lu, "Adaptive rate control for h.264". *Elsevier Journal of Visual Communication and Image Representation*, vol. 17 (2), pp. 376–406, Apr. 2006. *Cited in Sec.* 2.1.1

[Lim90] J. Lim, *Two-Dimensional Signal and Image Processing,*, Prentice-Hall, 1990. *Cited in Sec.* 1.1.2

[Lio91] M. Liou, "Overview of the px64 kbit/s video coding standard". *Communications of the ACM*, vol. 34 (4), pp. 59–63, 1991. *Cited in Sec.* 1.3

[LJ03] J. Lee and B. Jeon, "Fast mode decision for h.264/avc with variable motion block sizes", in S. Verlag, ed., *Computer and Information Sciences - ISCIS*, pp. 723–730, 2003. *Cited in Sec.* 1.4.1

[LJL+03] P. List, A. Joch, J. Lainema, G. Bjontegaard, and M. Karczewicz, "Adaptive deblocking filter". *IEEE Transactions on Circuits and Systems For Video Technology*, vol. 13, pp. 614–619, July 2003. *Cited in Sec.* 1.4.4

[LJPP08] G. Laroche, J. Jung, and B. Pesquet-Popescu, "R-D optimized coding for motion vectors predictor selection". *IEEE Transactions on Circuits and Systems for Video Technology*, vol. 18 (12), pp. 1681–1691, Dec. 2008. *Cited in Sec.* (document), 1.5.3

[LJS+12] H. Liu, J. Jung, J. Sung, J. Jia, and S. Yea, "3D-CE2.h: Results of illumination compensation for inter-view prediction", ITU-T SG16 WP3 and ISO/IEC JTC1/SC29/WG11 JCT3V-B0045, October 2012. *Cited in Sec.* 1.5.5

[LLL13] B. Li, H. Li, and L. Li, "Adaptive bit allocation for R-lambda model rate control in HM", in *JCT-VC M0036, 13th meeting of Joint Collaborative Team on Video Coding of ITU-T SG 16 WP 3 and ISO/IEC JTC 1/SC 29/WG 11*, Incheon, KR, 18-26 Apr. 2013. *Cited in Sec.* 2.3.2

[LLLZ12] B. Li, H. Li, L. Li, and J. Zhang, "Rate control by R-lambda model for HEVC", in *JCT-VC K0103, 11th meeting of Joint Collaborative Team on Video Coding of ITU-T SG 16 WP 3 and ISO/IEC JTC 1/SC 29/WG 11*, Shanghai, CN, 10-19 Oct. 2012. *Cited in Sec.* (document), 2.1.2, 2.3, 2.3.1, 2.3.2

[Llo82] S. Lloyd, "Least squares quantization in PCM". *IEEE Transactions on Information Theory*, vol. 28 (2), pp. 129–137, Mar. 1982. *Cited in Sec.* 1.2.1

[Loé48] M. Loéve, *Fonctions aleatoires de seconde ordre, in P. Levy, Processus Stochastiques et Mouvement Brownien*, Gauthier-Villars, Paris, France, 1948. *Cited in Sec.* 1.2.3

[LO98] L.-J. Lin and A. Ortega, "Bit-rate control using piecewise approximated rate-distortion charateristics". vol. 8 (4), pp. 446–459, Aug. 1998. *Cited in Sec.* (document)

[LWC93] D. W. Lin, M.-H. Wang, and J.-J. Chen, "Optimal delayed-coding of video sequences subject to a buffer-size constraint", in *SPIE Visual Communications and Image Processing*, 1993. *Cited in Sec.* (document), 2.2.1

[LZLX12] B. Li, D. Zhang, H. Li, and J. Xu, "QP determination by lambda value", in *JCT-VC I0426, 9th meeting of Joint Collaborative Team on Video Coding of ITU-T SG 16 WP 3 and ISO/IEC JTC 1/SC 29/WG 11*, Geneva, CH, 2012. *Cited in Sec.* 2.1.2

[Mau10] T. Maugey, *Distributed video coding of multiview sequences*, Ph.D. thesis, Telecom ParisTech, 2010. *Cited in Sec.* 3.2.1

[MF98] S. Mallat and F. Falzon, "Analysis of low bit rate image transform coding". *IEEE Transactions on Signal Processing*, vol. 46 (4), pp. 1027–1042, Apr. 1998. *Cited in Sec.* 2.3.2

[MGL05] S. Ma, W. Gao, and Y. Lu, "Rate-Distortion Analysis for H . 264 / AVC Video Coding and its Application to Rate Control". *IEEE Transactions on Circuits and Systems for Video Technology*, vol. 15 (12), pp. 1533–1544, 2005. *Cited in Sec.* (document)

[Mit96] J. Mitchell, *MPEG Video: Compression Standard*, Chapman and Hall, ITP, New York, 1996. *Cited in Sec.* 1.1.2

[Mor65] J. J. Moreau, "Proximité et dualité dans un espace hilbertien". *Bull. Soc. Math. France*, vol. 93, pp. 273–299, 1965. *Cited in Sec.* (document), 3.1.2

[MPP08] T. Maugey and B. Pesquet-Popescu, "Side information estimation and new schemes for multiview distributed video coding". vol. 19 (8), pp. 589–599, Dec. 2008. *Cited in Sec.* (document)

[MSW03] D. Marpe, H. Schwarz, and T. Wiegand, "Context-based adaptive binary arithmetic coding in the H.264/AVC video compression standard". *IEEE Transactions on Circuits and Systems for Video Technology*, vol. 13 (7), pp. 620–636, Jul. 2003. *Cited in Sec.* 1.4.4

[MSW12] S. Ma, J. Si, and S. Wang, "A study on the rate distortion modeling for High Efficiency Video Coding", in *Proceedings of IEEE International Conference on Image Processing*, pp. 181–184, Sep. 2012. *Cited in Sec.* 2.1.1

[Mul85] T. Mullen, "The contrast sensitivity of human color vision to red-green and blueyellow chromatic gratings". *Journal of Physiology*, vol. 395, pp. 381–400, 1985. *Cited in Sec.* 1.1.2

[MXOW12a] Z. Ma, M. Xu, Y. Ou, and Y. Wang, "Modeling of rate and perceptual quality of compressed video as functions of frame rate and quantization stepsize and its applications". *IEEE Transactions on Circuits and Systems for Video Technology*, vol. 22 (5), pp. 671–682, 2012. *Cited in Sec.* (document)

[MXOW12b] ———, "Modeling of rate and perceptual quality of compressed video as functions of frame rate and quantization stepsize and its applications". *IEEE Transactions on Circuits and Systems for Video Technology*, vol. 22 (5), pp. 671–682, 2012. *Cited in Sec.* 2.1.1

[NP77] A. Netravali and B. Prasada, "Adaptive quantization of picture signals using spatial masking", in *Proceedings of the IEEE*, vol. 65, pp. 536–548, April 1977. *Cited in Sec.* 1.1.2

[NP12] M. Naccari and F. Pereira, "Quadratic modeling rate control in the emerging HEVC standard", in *Proceedings of Picture Coding Symposium*, pp. 401–404, 2012. *Cited in Sec.* 2.1.1

[OR98] A. Ortega and K. Ramchandran, "Rate-distortion techniques in image and video compression". vol. 15 (6), pp. 23–50, 1998. *Cited in Sec.* (document), 2.1, 2.2

[ORV94] A. Ortega, K. Ramchandran, and M. Vetterli, "Optimal trellis-based buffered compression and fast approximations". *IEEE Transactions on Image Processing*, vol. 3 (3), pp. 26–40, 1994. *Cited in Sec.* (document), 2.2.1

[OSS+12] J.-R. Ohm, G. J. Sullivan, H. Schwarz, T. K. Tan, and T. Wiegand, "Comparison of the coding efficiency of video coding standards - including high efficiency video coding (HEVC)". *IEEE Transactions on Circuits and Systems for Video Technology*, vol. 22 (12), pp. 1669–1684, 2012. *Cited in Sec.* 1.5, 2.3.1

[PADZ11] C. Pang, O. Au, J. Dai, and F. Zou, "Frame complexity guided Lagrange multiplier selection for H. 264 intra-frame coding". *Signal Processing Letters, IEEE*, 2011. *Cited in Sec.* 3.2.2

[PAZ+13] C. Pang, O. Au, F. Zou, J. Dai, X. Zhang, and W. Dai, "An analytic framework for frame-level dependent bit allocation in hybrid video coding". *IEEE Tranansactions on Circuits and Systems*, vol. 23 (6), pp. 990–1002, Jun. 2013. *Cited in Sec.* (document), **??**, **??**, 3.2.3, 4, 4.1, **??**

[PAZD11] C. Pang, O. C. Au, F. Zou, and J. Dai, "An Analytic Framework for Frame-Level Dependent Bit Allocation in Hybrid Video Coding". *2011 IEEE 13th International Workshop on Multimedia Signal Processing*, 2011. *Cited in Sec.* 3.2.2

[PB14] N. Parikh and S. Boyd, "Proximal algorithms". vol. 1 (3), pp. 123–231, 2014. *Cited in Sec.* (document), 3.1.2

[PCP11] N. Pustelnik, C. Chaux, and J.-C. Pesquet, "Parallel ProXimal Algorithm for image restoration using hybrid regularization". vol. 20 (9), pp. 2450–2462, Sep. 2011. *Cited in Sec.* 3.1.3

[PP12] J.-C. Pesquet and N. Pustelnik, "A parallel inertial proximal optimization method". vol. 8 (2), pp. 273–305, Apr. 2012. *Cited in Sec.* (document), 3.1.2

[PPCD14] B. Pesquet-Popescu, M. Cagnazzo, and F. Dufaux, eds., *Motion Estimation Techniques*, Elsevier E-Reference Signal Processing, 2014. *Cited in Sec.* 1.2.2

[Ric04] I. Richardson, *H.264 and MPEG-4 Video Compression: Video Coding for Next-generation Multimedia*, Wiley, 2004. *Cited in Sec.* 1.3

[RM00] P. Read and M. Meyer, *Restoration of Motion Picture Film*, Butterworth-Heinemann, 2000. *Cited in Sec.* 1.1

[ROV94] K. Ramchandran, A. Ortega, and M. Vetterli, "Bit allocation for dependent quantization with applications to multiresolution and mpeg video coders". vol. 3 (5), pp. 533–545, 1994. *Cited in Sec.* (document), 3, 4, 2.3, 2.2.3, 2.2.1, 2.4, 2.5, 2.6, 2, 4.1.3, 4.19, 4.6, 4.8, 4.3

[RS01] S. Rane and G. Sapiro, "Evaluation of JPEG-LS, the new lossless and controlled-lossy still image compression standard, for compression of high-resolution elevation data". *IEEE Transactions on Geoscience and Remote sensing*, vol. 39, pp. 2298–2306, Oct. 2001. *Cited in Sec.* 1.2

[RV93] K. Ramchandran and M. Vetterli, "Best wavelet packet bases in a rate-distortion sense". *IEEE Transactions on Image Processing*, vol. 2 (2), pp. 160–175, Apr. 1993. *Cited in Sec.* (document), 2.2.1

[SAD12] L. Sun, O. Au, and W. Dai, "An adaptive frame complexity based rate quantization model for intra-frame rate control of high efficiency video coding (hevc)". *APSIPA ASC*, pp. 1–6, 2012. *Cited in Sec.* 2.1.1

[Sal07] D. Salomon, *Data Compression: The Complete Reference, Fourth Edition*, 2007. *Cited in Sec.* 1.2

[SB91] G. Sullivan and R. Baker, "Rate-distortion optimized motion compensation for video compression using fixed or variable size blocks", in *Global Telecommunication Conference*, pp. 85–90, December 1991. *Cited in Sec.* 2.2.2

[SB94] G. Sullivan and L. Baker, "Effcient quadtree coding of images and video". *IEEE Transactions on on Image Processing*, vol. 3, pp. 327–331, 1994. *Cited in Sec.* (document), 2.2.1

[SG88] Y. Shoham and A. Gersho, "Efficient bit allocation for an arbitrary set of quantizers". *IEEE Transactions on Acoustics, Speech, and Signal Processing*, vol. 36, pp. 1445–1453, Sep. 1988. *Cited in Sec.* (document), 2.2.1, 2.2.3

[Sha48] C. E. Shannon, "A mathematical theory of communication". *The Bell System Technical Journal*, vol. 27, pp. 379–423,623–656, Oct. 1948. *Cited in Sec.* (document), 2.1

[Sha59] C. Shannon, "Coding theorems for a discrete source with a fidelity criterion". *IRE National Convention Record*, pp. 142–163, 1959. *Cited in Sec.* (document), 2.1

[SK97a] G. Schuster and A. Katsaggelos, "The min-max approach in video coding", in *ICASSP*, pp. 3105–3108, April 1997. *Cited in Sec.* (document), 2.2

[SK97b] ———, "The minimum-average and minimum-maximum criteria in lossy compression". *Vistas in Astronomy*, vol. 41 (3), pp. 427–437, 1997. *Cited in Sec.* (document), 2.2

[SK97c] ———, "A video compression scheme with optimal bit allocation among segmentation, motion, and residual error". *IEEE Transactions on Image Processing*, vol. 6, pp. 1487–1502, November 1997. *Cited in Sec.* 2.2.2

[SMK99] G. M. Schuster, G. Melnikov, and A. K. Katsaggelos, "A review of the minimum maximum criterion for optimal bit allocation among dependent quantizers". vol. 1 (1), pp. 3–17, 1999. *Cited in Sec.* (document)

[SOHW12a] G. Sullivan, J.-R. Ohm, W.-J. Han, and T. Wiegand, "Overview of the high efficiency video coding (HEVC) standard". vol. 22 (12), pp. 1649–1668, 2012. *Cited in Sec.* (document), 2.3.1

[SOHW12b] G. J. Sullivan, J.-R. Ohm, W.-J. Han, and T. Wiegand, "Overview of the high efficiency video coding (HEVC) standard". *IEEE Transactions on Circuits and Systems for Video Technology*, vol. 22 (12), pp. 1649–1668, 2012. *Cited in Sec.* 1.3

[SS08] Y. Q. Shi and H. Sun, *Image and Video Compression for Multimedia Engineering*, CRC Press, 2008. *Cited in Sec.* 1.1.1

[SSB14] V. Sze, G. J. Sullivan, and M. Budagavi, *High Efficiency Video Coding (HEVC) - Algorithms and architectures*, Springer, 2014. *Cited in Sec.* 1.3

[STL04] G. Sullivan, P. Topiwala, and A. Luthra, "The H.264/AVC advanced video coding standard: Overview and introduction to the fidelity range extensions", vol. 5558, pp. 454–474, Aug. 2004. *Cited in Sec.* 1.4

[SW98a] G. Sullivan and T. Wiegand, "Rate-distortion optimization for video compression". vol. 15 (6), pp. 74–90, 1998. *Cited in Sec.* (document), 2.1.1, 3.2.1

[SW98b] G. J. Sullivan and T. Wiegand, "Rate-distortion optimization for video compression". *IEEE Signal Processing Magazine*, vol. 15, pp. 74–90, Nov. 1998. *Cited in Sec.* 2.2.2

[SWL03] G. Sullivan, T. Wiegand, and K. Lim, "Joint model reference encoding methods and decoding concealment methods; section 2.6: Rate control". *JVT-I049*, Sep. 2003. *Cited in Sec.* (document), 3.2.3, 3.2.5

[Tse01] P. Tseng, "Convergence of a block coordinate descent method for nondifferentiable minimization". vol. 109 (3), pp. 475–494, Jun. 2001. *Cited in Sec.* (document), 3.1

[TZS12] L. Tian, Y. Zhou, and Y. Sun, "Novel rate control scheme for intra frame video coding with exponential rate-distortion model on H.264/AVC". *Elsevier Journal of Visual Communication and Image Representation*, vol. 23 (6), pp. 873–882, Aug. 2012. *Cited in Sec.* 2.1.1

[USC93] K. Uz, J. Shapiro, and M. Czigler, "Optimal bit allocation in the presence of quantizer feedback", 1993. *Cited in Sec.* (document), 2.2.3, 3.2, 3.2.2, 4, 4.3

[VNB67] F. Van Ness and M. Bouman, "Spatial modulation transfer in the human eye". *Journal of Optical Society of America*, vol. 57 (3), pp. 401–406, March 1967. *Cited in Sec.* 1.1.2

[VO10] G. Valenzise and A. Ortega, "Improved video coding efficiency exploiting tree-based pixelwise coding dependencies", in *SPIE Visual Information Processing and Communication*, San Jose, USA, Jan. 2010. *Cited in Sec.* (document)

[Vu13] B. C. Vũ, "A splitting algorithm for dual monotone inclusions involving cocoercive operators". vol. 38 (3), pp. 667–681, Apr. 2013. *Cited in Sec.* (document), 3.1.2, 3

[Wal23] J. Walsh, "A closed set of normal orthogonal functions". *American Journal of Mathematics*, vol. 45 (1), pp. 5–24, 1923. *Cited in Sec.* 1.2.3

[Wat87] A. Watson, "Efficiency of a model human image code". *Journal of Optical Society of America A*, vol. 4 (12), pp. 2401–2417, December 1987. *Cited in Sec.* 1.1.2

[WG91] S.-W. Wu and A. Gersho, "Rate-constrained optimal block-adaptive coding for digital tape recording of hdtv". *IEEE Transactions on Circuits and Systems For Video Technology*, vol. 1, pp. 100–12, 1991. *Cited in Sec.* (document), 2.2.1, 2.2.2

[Wri97] S. J. Wright, *Primal-dual interior-point methods*, SIAM, 1997. *Cited in Sec.* (document), 3.1

[WSBL03] T. Wiegand, G. Sullivan, G. Bjontegaard, and A. Luthra, "Overview of the H.264/AVC video coding standard". vol. 13 (7), pp. 560–576, 2003. *Cited in Sec.* (document), 1.4.1

[WSJ+03] T. Wiegand, H. Schwarz, A. Joch, F. Kossentini, and G. J. Sullivan, "Rate-constrained coder control and comparison of video coding standards". *IEEE Transactions on Circuits and Systems for Video Technology*, vol. 13 (7), pp. 688–703, Jul. 2003. *Cited in Sec.* (document), 1.4, 2.1.1

[WTO90] T. Watanabe, Y. Tsukuhara, and K. Ohzcki, "Ratc-adaptive dct coding for color picture", in *Picture Coding Symposium*, 1990. *Cited in Sec.* 2.2.2

[XCL06] J. Xie, L.-t. Chia, and B.-s. Lee, "An Improved Distortion Model for rate control of DCT-based Video Coding", in *International Multi-Media Modelling Conference*, pp. 88–95, Ieee, 2006. *Cited in Sec.* (document)

[YA02] S. Yu and I. Ahmad, "A new rate control algorithm for MPEG-4 Video Coding", in *Proc. SPIE*, 2002. *Cited in Sec.* 2.1.1

[YH00] Y. Yang and S. S. Hemami, "Generalized rate-distortion optimization for motion-compensated video coders". vol. 10 (6), pp. 942–955, 2000. *Cited in Sec.* (document)

[YW82] D. C. Youla and H. Webb, "Image restoration by the method of convex projections. Part I - theory". vol. 1 (2), pp. 81–94, Oct. 1982. *Cited in Sec.* (document), 3.1

[ZL77] J. Ziv and A. Lempel, "A universal algorithm for sequential data compression". *IEEE Transactions on Information Theory*, vol. 23 (3), pp. 337–343, May 1977. *Cited in Sec.* 1.2.4